Rapid Oscillations in Cataclysmic Variable Stars

Submitted in fulfillment of the
requirements for the degree M.Sc.
in the Department of Astronomy
UNIVERSITY OF CAPE TOWN

M.L. Pretorius

August 2004

Abstract

Rapid quasi-coherent oscillations were detected in the optical light curves of 24 cataclysmic variable stars (CVs). In 12 of these systems (TU Men, WW Cet, HX Peg, BP CrA, BR Lup, HP Nor, AG Hya, TW Vir, PU CMa, V426 Oph, V1193 Ori, and CR Boo) for the first time. The results contribute to the observational record of the phenomenology of dwarf nova oscillations (DNOs), quasi-periodic oscillations (QPOs), and longer period dwarf nova oscillations (lpDNOs), strengthen the correlation, valid over nearly six orders of magnitude in frequency, between the ratio of time scales of different classes of oscillations in white dwarf, neutron star, and black hole binaries, and show that the recently recognized lpDNOs occur fairly commonly in high mass transfer rate CVs. Observations of the AM CVn star CR Boo show that the double degenerate binaries are, where rapid oscillations are concerned, similar to hydrogen rich CVs. The period of a QPO in RU Peg is seen to change by 84% over ten nights of outburst—the largest evolution of a QPO period observed to date. A period-luminosity relation is found for lpDNOs in X Leo; this is the first clear case of lpDNO frequency scaling with accretion luminosity. Rapid oscillations are detected in the dwarf novae WX Hyi and V893 Sco in quiescence.

Acknowledgments

I acknowledge and thank my supervisors, Brian Warner and Patrick Woudt, for their support during the pursuit of this degree. It occurred to me many times over the past two years that some students learn astronomy without Brian Warner on hand to answer all their questions; I don't know how they manage. The South African Astronomical Observatory allowed me a large amount of telescope time, and provided me with office space. My thanks to Darragh O'Donoghue for assistance, encouragement, advice, and for the use of his programs EAGLE and DuPhot. Financial support for my studies came from the National Research Foundation and the Department of Labour.

Contents

Chapter 1

Introduction

Accretion is an important and prevalent, but poorly understood, astrophysical process; this is probably the best justification for the study of cataclysmic variable stars (CVs). Accretion is also the most powerful source of energy in the universe: Frank, King & Raine (1985) point out that, compared to fusing hydrogen into helium, accretion onto a neutron star (of, say, mass 1.4 $M_\odot$ and radius 10 km) is more efficient by a factor of $\sim$30. In many cases accretion takes place via a thin disc of material orbiting, and falling onto, a compact object at its centre. Such accretion discs are very commonly occurring structures and therefore relevant in many branches of astronomy. Circumstellar accretion discs around young stellar objects allow for gravitational collapse while conserving angular momentum, it is from these discs that planets form. Gravitational potential energy released by the infall of material from an accretion disc is known to be the principal source of energy in several types of close binary systems, and many more binary stars form discs at some stage of their evolution. Active galactic nuclei are amongst the most energetic objects in the universe and are believed to be powered by accretion of matter from the inner galactic disc onto a supermassive black hole.

However, it is CVs, consisting usually of a K or M type dwarf and a white dwarf in a short period binary system, which offer the best opportunity to observe and understand accretion discs. The discs in dwarf novae, for example, flip from being quasi-stable and optically thin to unstable and optically thick every few weeks or so, allowing for the study of both states and the transitions between them. Furthermore, the luminosity of the high mass transfer rate systems is dominated by emission from the disc. Because a disc is almost two dimensional, the observational appearance of a CV depends quite strongly on the orbital inclination, so that different facets of these stars are revealed by different inclinations. Since the orbital periods are typically of the order of hours, it takes very little telescope time to unravel the geometry of the eclipsing systems. Interactions between plasma and magnetic fields

are displayed in all CVs, in some cases the accretion flow is entirely altered by a strong white dwarf magnetic field, but even where only weak fields are present, they play a role in creating the viscosity that drives disc accretion. What is learned about accretion discs from studying CVs should apply more generally and shed some light on accretion in systems that are not as readily observed.

CVs are of course also very interesting in their own right: they emit radiation at all wavelengths from radio waves to gamma rays, and they vary on time scales ranging from seconds to millions of years as the result of a fascinating assortment of physical mechanisms. Their exciting and often dramatic variability holds the attention of amateur observers, so that the long term behaviour of many CVs has been very well documented. There are hundreds of CVs known and although some global properties unite the various types, so many parameters contribute to determining the observed properties of individual systems, that no two CVs are really alike. This is part of the challenge and interest of CVs and it is often the most extreme or unusual systems that provide general insight.

With the development of high speed photometry came the discovery of variability on time scales of minutes to seconds. This includes irregular flickering, but also highly coherent signals in some systems (namely the DQ Her stars) and quasi-coherent oscillations in the high mass transfer rate systems. We now distinguish between three classes of rapid, quasi-coherent oscillations. Discovered around 30 years ago, dwarf nova oscillations (DNOs) and quasi-periodic oscillations (QPOs) remain two of the unsolved mysteries of CVs. More recently, longer period dwarf nova oscillations (lpDNOs) were recognized as a separate class of oscillation, illustrating that more observations or reinterpretation of existing data can still uncover new features of the phenomenology of the rapid oscillations. Judging by the time scale and coherence of these oscillations, DNOs and lpDNOs most likely originate in the inner disc or on the white dwarf itself, while the accretion disc is believed to be the source of the QPOs. The most viable model of DNOs ascribes them to the interaction of a weak white dwarf magnetic field with the inner accretion flow. The rapid oscillations can thus serve as probes into the accretion process and the interaction between discs and magnetic fields.

Separate classes of rapid oscillations are seen also in low-mass X-ray binaries (LMXBs), in which a neutron star or black hole accretes from a main sequence star. The study of accreting neutron stars and black holes is motivated mainly by the fact that these objects provide a unique window on the physics of strong gravity and dense matter. It was noticed recently that there is a simple relation between the periods of different classes of oscillations which holds for white dwarf, neutron star, and black hole binaries, and perhaps extends also to young stellar objects. In the case of CVs, the relation is that, for a given system, the QPO period (P_{QPO}) is

roughly equal to 16 times the DNO period (P_{DNO}) in that system. The correlation between the ratio of time scales in CVs and LMXBs suggests that similar mechanisms may be responsible for the rapid oscillations in the different systems. Of all these objects, CVs are by far the easiest to observe, since the oscillations in CVs occur at accessible time scales and are present in the optical.

Many challenges concerning rapid oscillations remain. Among them are obtaining polarimetry at high enough time resolution to confirm the magnetic nature of DNOs and lpDNOs, and using an indirect imaging technique such as eclipse mapping to identify the location in the disc where QPOs originate. Even just photometry of much higher quality is sure to reveal ever more aspects. With signs hinting at the possibility that the easily observed rapid oscillations in CVs may elucidate the QPOs in LMXBs and disc accretion more generally, DNOs, lpDNOs and QPOs promise to be of interest for some time to come.

These rapid oscillations are the subject of this dissertation. A high speed photometric survey of high mass transfer rate CVs was conducted with the aim of investigating how generally the relation $P_{QPO} \approx 16 \times P_{DNO}$ holds, finding out how common lpDNOs are, and further studying the phenomenology of DNOs, QPOs, and lpDNOs. I present here the results of the observations (Chapter 5) before discussing the implications of the new results in Chapter 6. First, however, I introduce some of the necessary theory of CVs in Chapter 2, and describe the phenomenology of the rapid oscillations (Chapter 3) and the models that have been proposed to explain them (Chapter 4).

Chapter 2

Cataclysmic Variable Stars

This chapter starts by introducing CVs in terms of Roche geometry, and gives a brief overview of some of the physical processes that play important roles in accretion discs. I then discuss only those classes of CVs that are relevant in later chapters.

2.1 Roche Geometry and Mass Transfer

In a binary star system where the orbits are circular, the orbital angular velocity in an inertial frame is given by Newton's generalization of Kepler's third law

$$\Omega_{orb} = \sqrt{\frac{G(M_1 + M_2)}{a^3}}\ \hat{z}\ , \tag{2.1}$$

where $\hat{z}$ is a unit vector perpendicular to the orbital plane, a is the orbital separation, and M_1 and M_2 are the masses of the stars—here, and in every thing that follows, M_1 denotes the mass of the more massive star (primary), and M_2 the mass of the less massive companion (secondary). The orbital period is $P_{orb} = 2\pi/\Omega_{orb}$. Assuming that both stars can be approximated as point masses, the sum of the gravitational and centrifugal potential in a reference frame rotating with the binary is (e.g. Frank et al. 1985)

$$\Phi_R(\boldsymbol{r}) = -\frac{GM_1}{|\boldsymbol{r} - \boldsymbol{r}_1|} - \frac{GM_2}{|\boldsymbol{r} - \boldsymbol{r}_2|} - \frac{1}{2}(\boldsymbol{\Omega}_{orb} \times \boldsymbol{r})^2\ , \tag{2.2}$$

where $\boldsymbol{r}_1$ and $\boldsymbol{r}_2$ are the positions of the centres of the stars. $\Phi_R(\boldsymbol{r})$ is called the Roche potential. It is easy to show (e.g. Warner 1995a) that the shapes of the Roche equipotential surfaces $\Phi_R = const$ depend only on the mass ratio $q = M_2/M_1$, while the scale is a function of a only. The intersection of a few equipotential surfaces with the orbital plane is shown in Fig. 2.1. Φ_R has five stationary points (known as Lagrangian points): L_1, L_2, and L_3 are saddle points; L_4 and L_5 are maxima. Of particular interest is the double lobed surface which contains the inner Lagrangian point L_1 (shown in Fig 2.1 as a heavier curve). The two lobes of this equipotential surface are called the Roche lobes of the two stars.

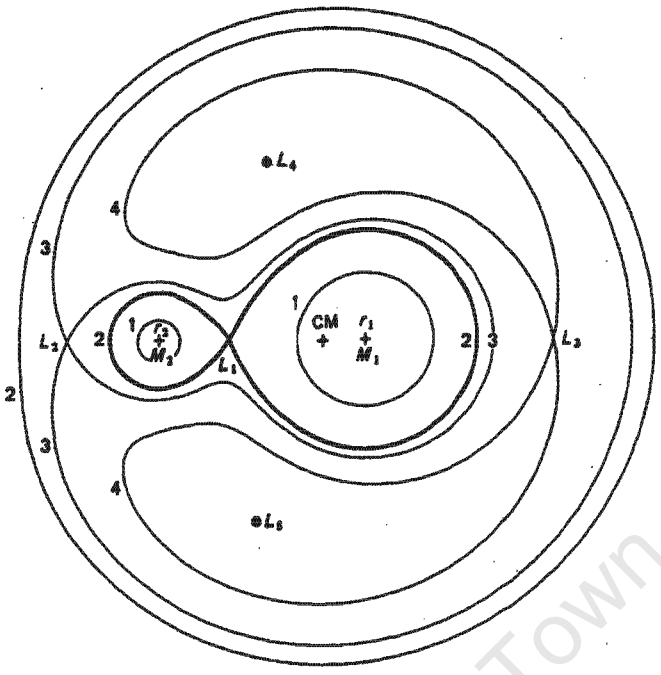

Figure 2.1: The intersection of Roche equipotential surfaces with the orbital plane, for a binary with $q = 0.25$. The equipotentials are numbered 1–4 in order of increasing Φ_r. The centre of mass as well as the Lagrangian points are shown. From Frank et al. (1985).

The Roche lobe of the primary (secondary) is the largest closed equipotential that can contain the mass of the primary (secondary). Clearly, the stellar surface must coincide with an equipotential, then, if the secondary has a radius that is small relative to its Roche lobe, it will be close to spherical. An increasingly larger secondary will have a more and more distorted shape, until it fills its Roche lobe.

A binary in which both stars lie within their Roche lobes is called a detached system; contact binaries are systems where both stars fill or exceed their Roche lobes. In a semi-detached binary, only one star fills its Roche lobe; any outward perturbation of the secondary star envelope in the region of the L_1 point (e.g. by pressure in the atmosphere) causes mass to be transferred into the Roche lobe of the primary, where it ultimately accretes onto the star. Accretion by this process is called Roche lobe overflow. CVs are short period semi-detached binary stars in which a white dwarf (primary) accretes matter from a less massive companion (usually a K or M type dwarf; the secondary) through Roche lobe overflow. Fig. 2.2 is a schematic representation of the structure of a non-magnetic CV.

The assumption that the stars can be approximated as point masses holds for CVs because the secondaries are similar to single main sequence stars, or to giants, in which the mass is centrally condensed, and the primaries are very small compared to the size of their Roche lobes. Furthermore, tidal interaction in a CV locks the

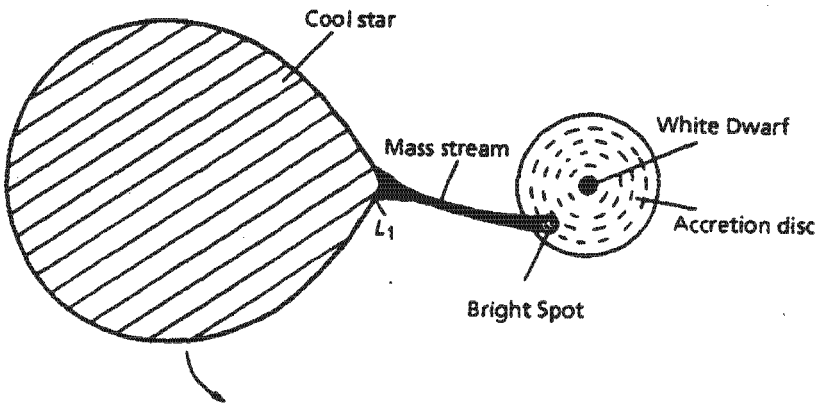

Figure 2.2: The structure of a non-magnetic CV, viewed at an orbital inclination of zero. The arrow at the bottom indicates the direction of orbital motion. From Warner (1995a).

secondary's rotation to its orbital motion, and removes any eccentricity that may initially exist in the orbit. This happens on a time scale that is very short compared to the life time of a CV (e.g. Tassoul 1988). This means that equation 2.1 and 2.2 are valid[1].

Conservation of mass and angular momentum require that a and P_{orb} change when mass is transferred between the stars, since q changes. It can be shown (e.g. Frank et al. 1985) that if $q \gtrsim 5/6$, the secondary's Roche lobe shrinks in response to mass transfer. Unless the secondary contracts very rapidly, the Roche lobe overflow results in a runaway feedback process which continues until the mass ratio is reversed. If $q \lesssim 5/6$ (this is a requirement for a fully-fledged CV) mass loss from the secondary causes its Roche lobe to expand, because material moves closer to the centre of mass, i.e. a (and therefore P_{orb}) must increase to conserve angular momentum. This cuts off mass transfer, since the secondary is now no longer in contact with its Roche lobe[2]. It is clear then that for steady mass transfer in a CV, either mass or angular momentum must be lost from the system. Rates at which mass is lost from CVs through stellar winds are too low to account for the mass transfer rates observed (Warner 1995a). This implies that there must be a mechanism whereby angular momentum is lost from the system to keep the secondary in contact with its Roche lobe and hence to drive mass transfer.

All binary stars lose angular momentum through gravitational quadrupole radiation, in the case of a CV with $P_{orb} \lesssim 9$ h, this drives mass transfer from

[1]The equipotential surfaces in the reference frame rotating with the binary are time dependent for an elliptical orbit.

[2]Unless the secondary is evolving off the main sequence, and therefore expanding. In almost all CVs, however, the secondaries are low-mass stars with life times longer than a Hubble time.

the secondary ($\dot{M}_2$) at a rate (Warner 1995a)

$$\dot{M}_2 = -2.4 \times 10^{15} \frac{(M_1/\mathrm{M}_\odot)^{2/3}(P_{orb}/\mathrm{h})^{-1/6}}{(1-15q/19)(1+q)^{1/3}} \quad \mathrm{g/s}. \tag{2.3}$$

This is just sufficient to account for the mass transfer rates ($\dot{M}$) observed in short period ($P_{orb} \lesssim 2$ h) and very low $\dot{M}$ CVs (like polars). In other CVs, the dominant mechanism of angular momentum loss is believed to be magnetic braking. An ionized stellar wind from a magnetic star is forced to corotate on magnetic field lines out to the Alfvén radius, thereby exerting a braking torque on the rotation of the star. If the secondary loses rotational angular momentum, the angular momentum actually drains from the orbit, since tidal locking keeps it in synchronous rotation. This mechanism drives mass transfer in CVs with $P_{orb} > 2.7$ h at a rate (McDermott & Taam 1989)

$$\dot{M}_2 = 2.00 \times 10^{-11} (P_{orb}/\mathrm{h})^{3.7} \quad \mathrm{M}_\odot/\mathrm{y}. \tag{2.4}$$

Note that, unlike the theory of gravitational radiation, magnetic braking is not properly understood; equation 2.4 is only an approximation—see Ivanova & Taam (2003) for recent results on magnetic braking.

2.2 Accretion Discs

When mass transfer first begins, material enters the Roche lobe of the primary at the L_1 point with initial velocity (perpendicular to the orbital motion) close to the isothermal sound speed in the gas (c_s). It is then accelerated to highly supersonic speed as it falls towards the primary. The Coriolis force deflects the stream so that it follows a trajectory which takes it around the primary, its distance of closest approach to the centre of the primary is denoted by r_{min}. Flannery (1975) gives initial stream trajectories, they lie entirely inside the Roche lobe of the primary. The stream collides with itself at supersonic speed, shocking the gas to high temperatures so that the relative kinetic energy of the collision is radiated away. While only a very small fraction of the angular momentum of the stream is lost to the secondary in this process, a significant amount of energy is dissipated. Therefore, since a circular orbit has the lowest energy for a given angular momentum, this leads to the formation of a ring of gas orbiting the primary at the circularization radius (r_r). This is very close to the radius at which material in Keplerian orbit around the primary has the same specific angular momentum as it had at the L_1 point (Hessman & Hopp 1990).

The Keplerian velocity of a particle in a circular orbit around the primary is

$$v_K(r) = \sqrt{\frac{GM_1}{r}} \; ; \tag{2.5}$$

since the ring has finite radial thickness, equation 2.5 implies that it rotates differentially. Viscosity in the gas then leads to dissipation of energy as heat is generated by the shearing flow and radiated. The loss of energy causes most of the gas particles to spiral to smaller radii through a series of approximately circular orbits at a radial drift velocity $v_{rad} \sim \nu_k/r$, where ν_k is the coefficient of effective kinematic viscosity of the gas. This inward drift requires a loss of angular momentum which, in the absence of external torques, must occur by transfer of angular momentum outwards by internal torques. Thus the outermost particles gain angular momentum and spiral outwards, in this manner the the ring spreads into a disc (this process was first illustrated by Lynden-Bell & Pringle 1974; disc formation is reviewed by Pringle 1981).

The disc material has momentum primarily in the orbital plane, the thickness of the disc perpendicular to this plane is therefore determined by hydrostatic equilibrium (radiation pressure and self gravitation are not important in CV discs; Frank et al. 1985). Assuming that the disc is isothermal in the direction perpendicular to the orbital plane, the scale height is given by $H(r) = rv_s/v_K$, i.e. the disc is geometrically thin if and only if the local Keplerian velocity is highly supersonic; this is the case in CV discs.

From the discussion of disc formation, it is clear that some form of viscosity is required to transport angular momentum, and hence drive accretion through the disc. Discs are so tenuous that ordinary molecular viscosity is too small to be of any consequence (e.g. Pringle 1981). Therefore the term viscosity, in this context, has nothing to do with kinematic viscosity as defined in fluid hydrodynamics; it simply refers to whatever processes transport angular momentum. High observed accretion luminosities, and the fact that some CVs are able to adjust to radical changes in the mass transfer rate through the disc ($\dot{M}_d$) in only days, indicate that angular momentum is efficiently transported. Angular momentum could be transfered between adjacent annuli of a disc through turbulence of some kind (but purely hydrodynamic turbulence does not seem to be a viable mechanism; e.g. Ryu & Goodman 1992). The effective kinematic viscosity of a turbulent process has the form $\nu_k \sim \ell v_t$, where ℓ is the size of the largest turbulent eddies, and v_t is their turnover speed. The viscosity can then be parametrized as (Shakura & Sunyaev 1973)

$$\nu_k = \alpha c_s H \ , \tag{2.6}$$

and since the largest eddies are smaller than the scale height, and the turbulence is probably subsonic, one expects $\alpha \leq 1$. Equation 2.6 is the α-prescription for disc viscosity; note that it offers no insight into the physical nature of the processes involved.

The most plausible cause for viscosity is magnetic turbulence (e.g. Lynden-Bell

1969); this can be accommodated within the α-prescription (Shakura & Sunyaev 1973). Any magnetic field present in the disc will be sheared by the differential rotation, so that radial components are transformed into azimuthal components, and amplified. The energy required to amplify the field comes from the kinetic energy of the disc material. When the magnetic pressure becomes comparable to the central disc pressure, the Parker instability (Parker 1970) leads to a dynamo action in the disc (Tout & Pringle 1992b). The dynamical instability in accretion disc flow discovered by Balbus & Hawley (1991) implies that there is no need for the existence of a strong equilibrium magnetic field.

Another mechanism whereby angular momentum may be transported in a disc results from the influence of the secondary on the disc: Sawada, Matsuda & Hachisu (1986) found tidally induced spiral shock waves in 2D numerical simulations of accretion discs. It is thought that these shocks may provide an angular momentum transport mechanism, since gas passing through the shocks will lose energy and angular momentum without requiring turbulent or magnetic viscosity. Subsequently, two arch-like structures were seen in Doppler tomograms of the emission lines of hydrogen and helium (e.g. Steeghs, Harlaftis & Horne 1997; Morales-Rueda, Marsh & Billington 2000), and interpreted as observational confirmation of the presence of tidally induced spiral shock waves in CV discs. Godon, Livio & Lubow (1998) threw doubt on this interpretation by pointing out that a two-armed spiral pattern would require the disc to be unrealistically hot. Furthermore, model calculations predict spiral structure in the surface density of the disc, whereas the observations reflect the distribution of the emissivity in specific spectral lines. Another problem is that the 2D hydrodynamic spiral wave models predict perfect axial symmetry while the observed arch-like structures have unequal intensities. Smak (2001) shows that a simple model, based on a mechanical, restricted three body approximation explains the presence, as well as the asymmetry of the structures seen in the Doppler tomograms. It is therefore not certain what role, if any, spiral shocks play; the accepted cause of viscosity is magnetic turbulence.

The luminosity of the disc is roughly half the gravitational potential energy lost as the disc material spirals down to the white dwarf surface

$$L_d \approx \frac{1}{2}\frac{GM_1\dot{M}_d}{R_1} \quad , \tag{2.7}$$

(where R_1 is the radius of the white dwarf) the other half goes into kinetic energy of the disc material's Keplerian motion and is radiated when the disc material is close to the white dwarf surface, just before finally accreting.

In the absence of a strong magnetic field, the inner disc extends down to the surface of the white dwarf. Since the white dwarf's angular velocity (Ω_1) is much lower than the Keplerian angular velocity, $\Omega_K(r) = \sqrt{GM_1/r^3}$, at its surface, the

disc material must be decelerated to match Ω_1 in the innermost annulus of the disc. This boundary layer is expected to have a very small radial extent (much less than R_1), and radiation pressure becomes significant in this region (e.g. Frank et al. 1985). The luminosity released in the boundary layer is (Kley 1991)

$$L_{BL} = L_d \left(1 - \frac{\Omega_1}{\Omega_K(R_1)}\right)^2 . \tag{2.8}$$

Therefore, unless Ω_1 is close to break-up velocity, almost half of the accretion luminosity is radiated in the boundary layer (as can be seen from equation 2.7 and 2.8). If the boundary layer is optically thick, most of the radiation is emitted at soft X-ray and EUV wavelengths; an optically thin boundary layer radiates mostly hard X-rays (see the discussion in Section 2.4.1). It seems that the boundary layer (or at least the inner disc) is the source of flickering in some CVs (e.g. HT Cas; Patterson 1981). For recent results concerning flickering, see Baptista & Bortoletto (2004).

For the most part, the disc is sufficiently close to the primary that the gravitational influence of the secondary is negligible. The outer disc, however, is affected by the tidal influence of the secondary (e.g. Osaki, Hirose & Ichikawa 1993). This interaction transfers the angular momentum transported outwards through the disc back into the binary orbit. The outer disc radius (r_d) is determined by tidal dissipation, as well as disc viscosity and effects of the mass transfer stream. More extreme tidal interaction can occur, see Section 2.4.2.

The stream makes a turbulent, supersonic impact with the outer rim of the disc, forming a shock front in which the energy of the impact is radiated. This 'bright spot' can dominate the system luminosity at optical wavelengths. It is possible for part of the stream to flow over the disc rim, but if the bulk of the stream impacts in the bright spot, its luminosity is not much less than the upper limit given by

$$L_{sp} \lesssim \frac{GM_1\dot{M}_2}{r_d} . \tag{2.9}$$

The bright spot is responsible for orbital humps (e.g. Krzeminski 1965), which are a prominent feature of many CV light curves, and in some systems the origin of flickering (e.g. U Gem; Warner & Nather 1971, but see also Bruch 1992, who finds that in most cases the bright spot plays only a minor role in flickering). Livio (1993) reviews the interaction between the accretion stream and the disc.

2.3 The Period Gap

The most remarkable feature of the P_{orb} distribution of non-magnetic CVs, is the orbital period gap: a very noticeable scarcity of systems with 2.2 h $\lesssim P_{orb} \lesssim$ 2.8 h

(see e.g. fig. 2.1 of Warner 1995a). The conventional explanation for this—disrupted magnetic braking—was first proposed by Robinson et al. (1981) who noticed that the masses of secondaries in the period gap fall in the same range as those of low-mass main sequence stars that are changing their internal structure from a deep convective envelope to total convection.

When the secondary becomes fully convective its magnetic field structure was thought to change, causing the magnetic braking mechanism to become less efficient. Angular momentum is then no longer lost at the high rate appropriate to magnetic braking, and mass transfer proceeds at a much lower rate (Rappaport, Joss & Verbunt 1983; Spruit & Ritter 1983). Its history of high $\dot{M}$ will have driven the secondary out of equilibrium, but it now has time to shrink in radius to regain equilibrium, thereby losing contact with its Roche lobe. The system is left as a faint detached binary; angular momentum loss takes place from then on via the much slower mechanism of gravitational radiation. The secondary is thought to come back into contact with its Roche lobe at the time when P_{orb} has decreased to ~ 2 h, at which point mass transfer resumes.

That magnetic braking is inefficient in a fully convective secondary is called into question by Tout & Pringle (1992a). Irradiation-driven mass transfer, coupled with shielding of the secondary by the disc may prove to be a better explanation for the period gap (Wu, Wickramasinghe & Warner 1995a,b).

The period gap does not exist for strongly magnetic CVs (Wickramasinghe & Wu 1994).

2.4 Dwarf Novae

Dwarf novae (I will abbreviate dwarf nova(e) to DN) are characterized by outbursts during which their luminosity increases by typically 2–5 mag; the outburst amplitude is larger for some systems. The (normal) outbursts last for about 2–20 days and the recurrence interval ranges from tens of days to tens of years, but is fairly well defined for any given object. Based on their long term photometric behaviour, DN are divided into three distinct subtypes:

SU UMa stars, in addition to normal outbursts, also undergo superoutbursts which last ~5 times longer than normal outbursts and have maxima ~0.7 mag brighter. A large fraction of the additional superoutburst light (0.3–0.4 mag) is modulated as periodic humps (called superhumps) with periods a few percent longer than P_{orb}.

Z Cam stars show rapid successions of outbursts interspersed with standstills, lasting tens of days to years, during which the star stays at ~0.7 mag below maximum.

U Gem stars are DN that do not belong to either of the two other subtypes.

2.4.1 The Dwarf Nova Outburst

Bath (1969, 1972) proposed that the cause of a DN outburst was a large and sudden increase in $\dot{M}_2$. Among the many things wrong with this model (see e.g. Warner 1995a), it predicts that the bright spot luminosity increases, and r_d decreases on the rise to outburst—predictions that were quickly contradicted by observations (Smak 1971). In fact, these observations indicated that the component of the system that brightens during outburst is the disc; changing eclipse profiles showed this more clearly (Warner 1974).

It is now generally accepted that a DN outburst results from the release of gravitational potential energy during a temporary phase of much higher than usual $\dot{M}_d$, in accordance with the disc instability model of Osaki (1974). By the disc instability model, $\dot{M}_2$ is roughly constant, and higher than viscous interactions in the quiescent disc allow $\dot{M}_d$ to be. Matter therefore builds up in the disc until an instability (the nature of which was unknown at the time) triggers an outburst by making the viscosity rise sharply, so that angular momentum transport is greatly enhanced. The resulting much higher $\dot{M}_d$ increases the system luminosity and drains the disc of material until it drops back into the quiescent, low viscosity state. Since viscosity by magnetic turbulence requires that the disc material couples to the magnetic field, the viscosity is high when the disc is hot and thus ionized, and low when the disc is cool.

Hoshi (1979) discovered the physical mechanism responsible for the disc (or thermal) instability; his work was further developed by e.g. Meyer & Meyer-Hofmeister (1981), and Cannizzo, Gosh & Wheeler (1982); Osaki (1996) is a recent review of the disc instability model, dealing also with superoutbursts (Section 2.4.2).

The ionization of hydrogen at $\sim 10^4$ K lies at the heart of the disc instability. The opacity of hydrogen, as it is becoming ionized, is significantly higher than that of neutral hydrogen; furthermore, it is a very sensitive function of temperature ($\kappa \sim T^{10}$). This leads to the existence of a range of surface densities ($\Sigma = 2 \int \rho dz$, where ρ is volume density, and z is the direction perpendicular to the orbital plane) where each value of Σ corresponds to three thermal equilibrium values of the effective temperature (T_{eff}), in any given region of the disc, depending on its ionization state. In other words, if the locus of models for which heating through viscous interactions equals energy radiated from the surface, is plotted in the Σ–T_{eff} plane, they form an S-shaped curve. The S-curve of thermal equilibrium models is shown schematically in Fig. 2.3. A disc annulus with (Σ, T_{eff}) to the left of the curve cools to the lower branch of the curve, while a (Σ, T_{eff}) to the right of the curve will cause it to heat until it reaches thermal equilibrium on the upper branch.

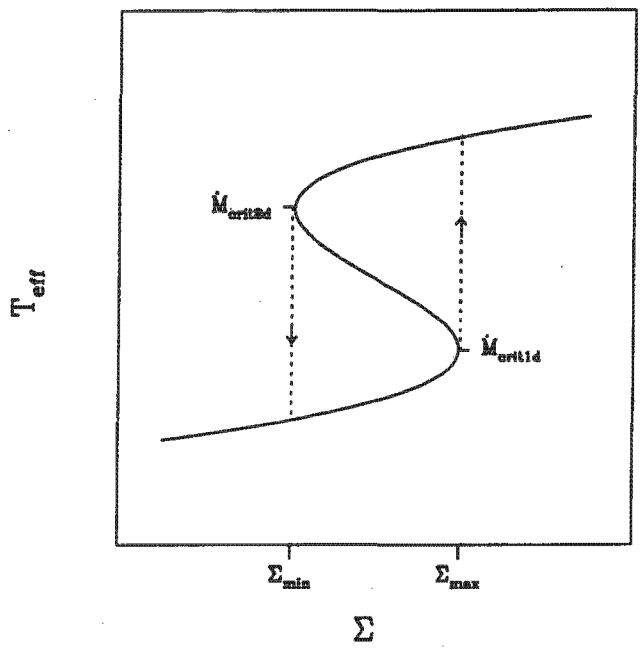

Figure 2.3: A schematic representation of the thermal equilibrium S-curve in the Σ–T_{eff} plane. The upper (lower) branch of the curve corresponds to outburst (quiescence). An annulus on the middle branch is in unstable thermal equilibrium. In realistic models, the shape of the S-curve depends on α (e.g. Pojmanski 1986). The thermal cycle of heating and cooling is illustrated by dashed lines and arrows.

The relation between the midplane disc temperature and T_{eff} is sensitively dependent on the fraction of the energy that is transported in the z (or vertical) direction by convection, since convective energy transport lowers the vertical temperature gradient. This fraction is increased by greater opacity; therefore, in the presence of partially ionized hydrogen, a convective instability occurs. Koen (1976) constructed the first models of convective accretion discs. The relations between Σ, $\dot{M}_d$, and T_{eff} have the form

$$\dot{M}_d \propto \alpha \Sigma T \propto T_{eff}^4 \ . \tag{2.10}$$

Thus for $T \propto T_{eff}^N$, with $N \geq 5$, $\partial T_{eff}/\partial \Sigma < 0$ (middle branch of Fig. 2.3), which implies an unstable disc structure, since, in such a region, the local $\dot{M}_d$ increases in response to a decrease in Σ, decreasing Σ even further. The transition from optically thin to optically thick solutions, where convection sets in, occurs at a critical density, Σ_{max}; the onset of the inverse process is marked by Σ_{min}. These two values of Σ correspond to mass transfer rates $\dot{M}_{crit1d}$ and $\dot{M}_{crit2d}$, and are increasing functions of radius (e.g. Mineshige & Osaki 1985).

If the mass transfer rate into some annulus, with T_{eff} on the lower branch of the S-curve, is between $\dot{M}_{crit1d}$ and $\dot{M}_{crit2d}$, its surface density increases until it reaches Σ_{max}. At this point the instability is triggered, and the annulus heats until it enters the high state, where energy transport is fully convective. Material spreads to adjacent annuli, pushing their surface densities over the critical value, and in this manner a heating wave propagates through the disc, and switches the whole disc to

outburst. The outburst rise time depends on both the distribution of material in the disc, and the radius of the first annulus to enter the high state. The larger the radius of this annulus, the shorter the interval before the whole disc reaches the high state, i.e. the faster the rise to maximum. The instability that flips the disc back to the low state is again triggered locally when the drain of material out of the disc causes the surface density of some annulus to drop below Σ_{min}. This is always an annulus in the outer disc, since Σ_{min} is highest there, explaining why, whereas outburst rise times differ, the rate of decay from maximum is similar for all outbursts. A cooling wave propagates inwards, and returns the whole disc to quiescence. In outbursts with a fast optical rise the system brightens at longer wavelengths first, with the rise at shorter wavelengths progressively delayed; this is called the UV delay. An almost simultaneous rise at all wavelengths occurs for outbursts with a slow optical rise (e.g. Bailey 1980; Hassall et al. 1983; Smak 1987). The EUV flux only rises when the heating wave reaches the inner edge of the disc; the rate of accretion onto the primary ($\dot{M}_1$)—and with it the EUV flux—is enhanced only during the time between the arrival of the heating and cooling fronts at the inner disc edge (e.g. Cannizzo 1993). The disc instability model predicts a smaller than observed UV delay; the correct UV delay may be achieved if the inner disc is truncated by a weak white dwarf magnetic field (Livio & Pringle 1992).

Whereas a DN brightens also at soft X-ray and EUV wavelengths during outburst, the hard X-ray flux falls (e.g. Jones & Watson 1992). Changing vertical optical depth of the boundary layer is thought to cause this: at low accretion rates the boundary layer is optically thin and cools inefficiently, so that it reaches very high temperatures and emits hard X-rays; when $\dot{M}_d$ increases, the boundary layer becomes optically thick, cools more efficiently, and radiates at EUV and soft X-ray wavelengths (see e.g. Pringle 1977; Pringle & Savonije 1979; Tylenda 1981; Patterson & Raymond 1985).

2.4.2 Superoutbursts

Superoutbursts, accompanied by superhumps, are the defining property of the SU UMa stars. Superhumps have periods (P_{sh}) a few percent longer than P_{orb}, they were first observed by Vogt (1974) and Warner (1975a) in a superoutburst of VW Hyi, and most often have highly non-sinusoidal pulse profiles. The fact that superhumps appear at roughly the same amplitude in all SU UMa stars, independent of binary inclination, implies that they represent an intrinsic flux variation, rather than a geometric effect.

Superoutbursts are explained as resulting from tidal resonance between the disc and the secondary, which drives the disc into an elliptical shape (Whitehurst 1988b; the presence of an elliptical disc in superoutburst was already proposed by Vogt 1982). A superoutburst is always triggered by a normal outburst (e.g. Vogt 1982,

1983). As the disc radius expands during outburst, the outer edge of the disc can, under the right conditions, reach a region where particles in the outer disc are in a 3 : 1 tidal resonance with the secondary (i.e. the particles orbit three times per binary orbital cycle). This causes the disc to become elliptical, and strong tidal dissipation in the eccentric disc maintains the high viscosity required for a DN outburst. The elliptical disc precesses progradely, and viscous dissipation—caused by tidal stresses—produces the superhump modulation at a frequency

$$\frac{1}{P_{sh}} = \frac{1}{P_{orb}} - \frac{1}{P_{prec}} ,$$

where P_{prec} is the precession period of the disc (e.g. Whitehurst 1988a). A recent discussion of an alternative mechanism for superoutbursts (the enhanced mass transfer model) can be found in Schreiber, Hameury & Lasota (2004).

For a disc in equilibrium with the mass transfer stream, the 3 : 1 resonance radius is smaller than the tidal radius (at which the disc is truncated by the influence of the secondary) only if $q \lesssim 0.25$ (Paczynski 1977; Hirose & Osaki 1990)[3]. Since the secondary is Roche lobe-filling, q and P_{orb} are closely related for a system where the primary has a typical white dwarf mass (Warner 1995a); in such a system $q \lesssim 0.25$ implies $P_{orb} \lesssim 3$ h. Just about all the SU UMa stars do have P_{orb} below the period gap, conversely, all DN below the gap are expected to be SU UMa stars.

Any CV with $q \lesssim 0.25$ and $\dot{M}_d$ high enough to lead to a disc radius in the tidal resonance region could produce superhumps by this mechanism. A few nova-like variables and AM CVn stars meet the requirements and have superhumps, in some cases permanent superhumps are seen (see Section 2.5 and 2.7).

Superhumps usually appear early in superoutburst and fade away towards the end of the outburst plateau, when they are sometimes replaced by late superhumps—a modulation of similar period, but which is roughly antiphased with the superhumps (e.g. Vogt 1983). A variation in bright spot brightness, resulting from the varying depth in the white dwarf potential well at which the stream impacts the disc, was initially proposed as a model for superhumps (Vogt 1982), but has since been used to explain late superhumps (e.g. Whitehurst 1988a; Murray 1996; Rolfe, Haswell & Patterson 2001), but see also Hessman et al. (1992). Hellier (2001a) proposes an alteration to the tidal thermal instability model (Osaki 1989), namely that the tidal and thermal instabilities are uncoupled. The tidal eccentricity can persist after the disc has come down from the thermal high state at the end of the outburst. The viscous dissipation, which causes the superhumps, then decreases because the disc viscosity is now much lower. At this point the late superhumps become detectable above the superoutburst light.

[3]It is possible for r_d to reach the 3 : 1 resonance radius in systems with q as large as 0.33, if a drop in $\dot{M}_2$ causes the disc and stream to be out of equilibrium (Murray, Warner & Wickramasinghe 2000).

Another variation on the theme of superhumps is negative superhumps, which are photometric modulations with periods less than P_{orb}. Negative superhumps may be caused by nodal precession of a disc that is tilted out of the orbital plane (Harvey et al. 1995). When observed in DN, negative superhumps appear to be independent of the state of outburst (e.g. Patterson 1999; Fu et al. 2004).

2.5 Nova-like Variables

A CV with $\dot{M}_2 > \dot{M}_{crit2d}$ will appear like a DN permanently in outburst. These high $\dot{M}$ systems are called nova-like variables (NLs), and have absolute magnitudes similar to those of DN at maximum (e.g. Patterson 1984; Warner 1987a). There are only very few NLs below the period gap; this is compatible with the belief that high $\dot{M}$ is driven by magnetic braking, which does not operate below the gap.

In contrast to DN at quiescence, NLs never show prominent orbital humps. This is because, in NLs, $\dot{M}_d = \dot{M}_2$, whereas, for quiescent DN, $\dot{M}_d \ll \dot{M}_2$ (e.g. Paczynski 1978) which means that the bright spot luminosity relative to the disc luminosity in a NL is less important than in a quiescent DN.

Udalski (1988) first suggested (in connection with TT Ari, which happens to be a rather confused case) that NLs may have permanent superhumps, and therefore appear observationally like SU UMa stars in permanent superoutburst. In fact, all NLs with $P_{orb} \lesssim 2$ h may be expected to show superhumps.

Two spectroscopically defined NL subtypes are UX UMa stars—with persistent broad Balmer absorption lines in addition to the emission lines usually present in NLs—and RW Tri stars—which have pure emission line spectra, sometimes with sharp absorption cores. The distinction between these two subtypes is (at least in part) a matter of binary inclination. All NLs (except VY Scl stars in low state; see below) have optically thick discs, so that the contribution from the absorption line spectrum decreases with increasing inclination. This is evident in RW Tri stars, where the relative strengths of the optical emission lines are seen to be greater for higher inclination systems (Warner 1995a).

VY Scl stars are a photometrically defined NL subtype (Wade & Ward 1985) characterized by occasional low states (at least 1 mag fainter than the average brightness, lasting for weeks to years) in their longterm light curves. While faint, VY Scl stars have the spectroscopic appearance of DN in quiescence. These low states are believed to be caused by changes in $\dot{M}_2$—in terms of the disc instability model (Section 2.4.1) VY Scl stars have $\dot{M}_2 > \dot{M}_{crit2d}$, with occasionally $\dot{M}_2 < \dot{M}_{crit2d}$.

It has been proposed that VY Scl stars are in effect Z Cam stars in permanent standstill (e.g. Warner & van Citters 1974), but there is a fair amount of evidence indicating that this is not the case. Z Cam stars in standstill often show $\sim$0.2 mag

fluctuations in brightness on timescales of 10–20 d; this is not seen in VY Scl stars (Warner 1995a). VY Scl stars in low state have been observed to brighten for short times to high state brightness, but with usually very long rise and descent times. Z Cam stars, on the other hand, soon start undergoing outbursts, with maxima 0.5–1 mag brighter than standstill brightness, when they descend from standstill (Warner 1995a). Also, the absolute magnitude of a Z Cam star at a given P_{orb} is fainter than that of a NL at the same P_{orb} (see fig. 4.16 of Warner 1995a). At maximum light VY Scl stars are UX UMa, RW Tri, or SW Sex stars.

SW Sex stars were defined by Thorstensen et al. (1991); most of them are high inclination systems with significant radial velocity phase shifts relative to the expected radial velocity of the white dwarf. They typically have 3 h $< P_{orb} <$ 4 h; some show VY Scl low states and superhumps. It was at first thought that the SW Sex properties may result purely from very high inclination (e.g. Dhillon et al. 1992), but since then low inclination SW Sex stars have been found (e.g. V442 Oph; Hoard, Thornstensen & Szkody 2000).

Amongst the explanations offered for the properties of SW Sex stars is a flared accretion disc, in which the optically thick rim of the disc blocks the view of the white dwarf (Knigge et al. 2000). Hellier (2000) proposes that SW Sex behavior can be explained by the combination of accretion stream overflow (over the disc) and an accretion wind, caused by episodes of very high $\dot{M}$, which are balanced by VY Scl low states. The range 3 h $< P_{orb} <$ 4 h contains most of the VY Scl stars (e.g. Warner 1995a). If irradiation in a high $\dot{M}$ NL leads to even higher $\dot{M}$, the system may become an SW Sex star. When the feed-back cycle breaks (e.g. Wu et al. 1995a) a VY Scl low state results. This mechanism works preferentially just above the period gap, since the orbital separation is less than in other NLs, explaining the P_{orb} distribution of SW Sex stars and VY Scl stars.

Horne (1999) proposes that a magnetic propeller, similar to that in AE Aqr (Wynn, King & Horne 1997), explains most of the peculiar SW Sex properties. Patterson et al. (2002) also favour strong white dwarf magnetic fields in SW Sex stars, and claim that both negative superhumps and QPOs (which are quite common features of SW Sex stars) can be explained by strong white dwarf magnetism; this is further discussed in Section 4.2.2.

2.6 Intermediate Polars

In almost one quarter of all CVs, the white dwarf has a magnetic field sufficiently strong to disrupt the formation of an accretion disc to a significant extent. These are the Polars (or AM Her stars) and Intermediate Polars (IPs). Defining characteristics of Polars are spin-orbit synchronism, and the presence of strong circular polarization.

IPs are characterized by very stable (non-orbital) pulsations in their optical and X-ray light curves; the period stability parameter $Q = |\dot{P}|^{-1}$, where $\dot{P}$ is the time rate of change of the period, for the IP X-ray modulations is greater than 10^{10}. Other widely shared properties of IPs (although no single system has all of these attributes) are: high excitation spectra, pulsations in the HeII emission lines, circular polarization, presence of orbital side bands, strong X-ray emission and a very hard X-ray spectrum.

Magnetically channeled accretion from the inner edge of a truncated disc onto a rapidly rotating white dwarf explains most of the properties of IPs. The white dwarf spin cycle produces the photometric modulation that characterizes an IP as the rotating 'beam', originating from the almost radially infalling accretion, periodically sweeps across the line of sight. This model was constructed to explain observations of DQ Her, which was the first IP to be discovered, and remained for 24 years the only member of its class. DQ Her has a 71 s modulation in its optical light curve (Walker 1956), which is very stable, having $Q > 10^{12}$ (e.g. Herbst, Hesser & Ostriker 1974). Between the start of eclipse and mideclipse the phase of the 71 s oscillation increases by about 90°, it then rapidly decreases by around 180° near mideclipse, and recovers smoothly to the out-of-eclipse ephemeris during egress (Warner et al. 1972). More precise observations of the eclipse-related phase shift were made by Patterson, Robinson & Nather (1978b), who in addition showed that the oscillation has the same colour as the system; Chanan, Nelson & Margon (1978) found that the pulse phase increases with increasing wavelength across the HeII 4686 emission line. All these observations can be explained in terms of magnetic accretion: DQ Her has high orbital inclination, so that the outer rim of the disc obscures the white dwarf, as well as most of the near side face of the disc, while a larger part of the far side disc surface is visible. The optical pulse maximum occurs when an EUV or X-ray beam from the accreting magnetic pole sweeps azimuthally across the far side disc face, where it is absorbed and emitted in the optical (this model took some time to develop—see Bath, Evans & Pringle 1974a; Lamb 1974; Katz 1975; Patterson et al. 1978b; Chanan et al. 1978; Chester 1979; Petterson 1979, 1980).

The most direct evidence supporting the magnetic rotator model of IPs is the detection of circular polarization in four of these systems: BG CMi (Penning, Schmidt & Liebert 1986), PQ Gem (Stockman et al. 1992), V2400 Oph (Buckley et al. 1995), and RR Cha (Rodríguez-Gil & Potter 2003); Cropper (1986) report marginal detections in other IPs. For DQ Her, both linear and circular polarization modulated at a period of 142 s (implying that the 71 s signal is the first harmonic of the white dwarf spin frequency; see also Zhang et al. 1995) has been observed (Swedlund, Kemp & Wolstencroft 1974; Kemp, Swedlund & Wolstencroft 1974).

However, the DQ Her results were of low statistical significance and have never been confirmed. Primaries in IPs have magnetic moments $\mu_1 = BR^3$ in the range 10^{32}–10^{34} G cm^3, corresponding to magnetic fields of 1–10 MG. This is slightly weaker than the fields in Polars, but the lack of spin-orbit synchronism in IPs is also a matter of higher $\dot{M}$ and greater orbital separation (Patterson 1994).

A star's magnetosphere is defined as the volume around it within which the magnetic field strongly affects the flow of mass and angular momentum; its radius is r_μ. The conditions that determine whether a disc forms are not precisely known, but if $r_\mu < r_{min}$, a disc will definitely form; if the radius at which the material in the stream attaches to the magnetic field lines (r_A) is greater than r_r, no disc can form (Warner 1995a). V2400 Oph is an example of a discless IP (Buckley et al. 1997).

The theory of disc-fed accretion onto a compact magnetic star was developed by Elsner & Lamb (1977) and Ghosh & Lamb (1978, 1979a,b). The corotation radius (r_{co}) is the point where Ω_1 (and hence also the angular velocity of the magnetosphere) matches the the Keplerian angular velocity, $r_{co} = (GM_1/\Omega_1^2)^{1/3}$, the field is normally not strong enough at r_{co} to exert much influence on the motion of disc material, and the flow remains very nearly Keplerian up to the radius r_0 (which is usually called the radius of the inner edge of the disc, despite the fact that a thin annulus of disc material exists inside of r_0, and taken to be equal to r_μ). This radius is given by

$$r_0 \approx 5.15 \times 10^{10} \left(\frac{M_1}{\mathrm{M}_\odot}\right)^{-1/7} \left(\frac{\mu_1}{10^{34}\ \mathrm{G\,cm^3}}\right)^{4/7} \left(\frac{\dot{M}_d}{10^{16}\ \mathrm{g/s}}\right)^{-2/7} \mathrm{cm}. \qquad (2.11)$$

(Ghosh & Lamb 1979b). At the radius denoted r_A, the disc flow has been decelerated to again match the magnetospheric rotational velocity, and disc material is entirely threaded onto the field lines. The annulus corresponding to $r_A \leq r \leq r_0$ is called the deceleration zone, and is normally assumed to be narrow in radial extent. The fastness parameter $\omega_s = \Omega_1/\Omega_K(r_0) = (r_0/r_{co})^{3/2}$ is defined by Ghosh & Lamb; for $\omega_s > 1$ no accretion can take place, and the disc exerts a spin-down torque on the primary. There exists a critical value of ω_s, denoted ω_c, for which there is no net torque on the primary, even though it is accreting; this value of the fastness parameter is given by $\omega_c \approx 0.95$ (e.g. Wang 1996).

The above discussion applies to a dipole field with its axis aligned to the white dwarf spin axis; IPs are probably all oblique rotators—see Fig. 2.4. Three dimensional magnetohydrodynamic simulations of accretion from a disc onto an inclined dipole field are presented by Romanova et al. (2003, 2004).

Some fraction of the rotating beam from the accreting magnetic pole falls on structures that are fixed in the reference frame rotating with the binary (e.g. the secondary or the vertical thickening on the outer edge of the disc where the stream impacts). This light is reprocessed and observed, in some systems, as a signal—

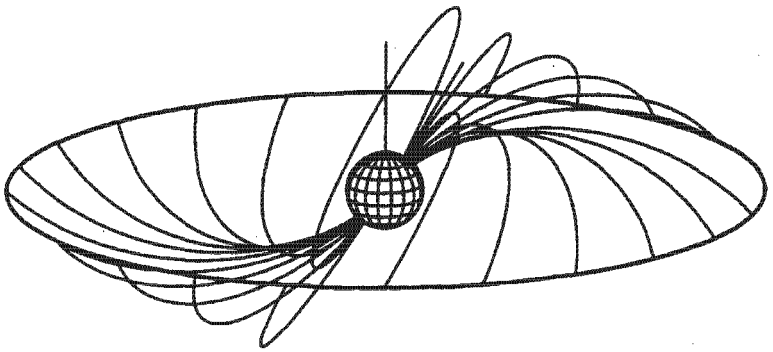

Figure 2.4: An oblique magnetic rotator. The vertical line at the top represents the spin axis. A few field lines and the inner edge of the disc are shown; the regions of the accretion flow outside the orbital plane, from the inner disc edge to the white dwarf, are called accretion curtains (reproduced out of Hellier 2001b).

called an orbital side band—at the beat frequency $\omega_{reproc} = \omega_1 - \Omega$ between the white dwarf spin frequency (ω_1) and the orbital frequency ($\Omega = 1/P_{orb}$). More complex interactions between the spin and orbital cycles give rise to additional side bands e.g. $\omega_1 + \Omega$ and $\omega_1 - 2\Omega$ (Warner 1986).

The existence of orbital side bands also indicates that much of the radiation we observe has been reprocessed. White & Marshall (1981) point out that the amplitude of the $\omega_1 - \Omega$ optical signal in AO Psc is too large to be powered by the observed pulsed X-ray flux. This implies that the rotating beam must be powerful at wavelengths that are not detected, probably EUV.

From r_A inward, the accretion flow is completely controlled by the magnetic field and so it falls along almost radial trajectories onto the white dwarf at highly supersonic velocity. This results in the formation of a shock front above the stellar surface. The kinetic energy of the diffuse plasma in the accretion column is converted to hard X-rays in the shock. Most IPs are very hard X-ray sources, which imply that they must be powered by radial accretion. However, the hard X-ray flux from IPs is $\sim 4\times$ less than expected for a radially accreting white dwarf, suggesting that $\sim 80\%$ of the accretion energy does not get dissipated in the shock. Patterson (1994) proposes that this is because most of the accreting material consists of denser blobs which have sufficient momentum to penetrate through the shock front and impact deep in the white dwarf atmosphere, where their kinetic energy is absorbed by the white dwarf and radiated at soft X-ray or EUV wavelengths (this was first suggested, in a more general context, by Kuijpers & Pringle 1982). This flux is not usually detected because of, e.g., interstellar absorption. However, we know that the observed pulsations in the HeII emission lines are most likely produced by photoionization, and are an order of magnitude too strong to be ascribed to

photoionization by hard X-rays. This means that there must be a source of soft X-rays.

Several IPs have photometric high states which resemble DN outbursts to some extent. In some cases, these can be caused by the disc instability which operates in DN (e.g. in GK Per; Kim, Wheeler & Mineshige 1992) but in other systems the outbursts are due to different instabilities; see e.g. Warner (1995a, 1997), and Hellier, Mukai & Beardmore (1997).

2.6.1 DQ Her Stars

DQ Her stars are a subset of the IPs consisting of the four[4] systems DQ Her, V533 Her, AE Aqr, and WZ Sge (many authors do not recognize the distinction and regard the terms 'IP' and 'DQ Her star' as synonymous). They are distinguished from other IPs by their shorter white dwarf spin periods ($P_1 = 1/\omega_1 < 200$ s), and by weaker and softer X-ray emission. A shorter P_1 means that r_0 is smaller than in other IPs. The magnetically controlled accretion thus falls into a shallower potential well, and the infall trajectory is not quite radial; also, the accretion shock can be as high as r_0 above the white dwarf surface (Wickramasinghe, Wu & Ferrario 1991). These factors imply that the X-ray emission is softer than in IPs with longer white dwarf spin periods. In fact, no X-ray flux is observed from DQ Her itself, which is probably a result of complete obscuration of the white dwarf by the disc (e.g. Petterson 1980).

The properties of DQ Her stars are reviewed by Warner (1995a) and Warner (1995b). DQ Her and V533 Her are both nova remnants; AE Aqr is a NL; WZ Sge is an SU UMa type DN, but there is no model that accounts for all of WZ Sge's properties; Warner (2004) is the latest on this issue. It was for long argued that non-radial g-mode pulsations of the white dwarf may explain the behaviour of WZ Sge, but it has now been conclusively shown that stellar pulsations are not the cause of the rapid brightness modulations in this star (Welsh et al. 2003).

2.7 AM CVn Stars

There are now twelve members of the AM CVn class of CVs known (Downes et al. 2001). These systems are characterized by a complete absence of hydrogen in their spectra, see Warner (1995a) and Warner (1995c) for reviews. Other common properties of the AM CVn stars are very short period variability (orbital periods of the order of 10^3 s) and broad helium absorption or emission lines. Evidence for mass transfer comes from the presence of flickering in the light curves of some members of the class e.g. AM CVn (Warner & Robinson 1972b), and the fact that a few AM CVn

[4]V373 Sct may be another member of the class (Woudt & Warner 2003).

stars have distinct high and low photometric states, e.g. V803 Cen (O'Donoghue & Kilkenny 1989) and CR Boo (Patterson et al. 1997).

The most generally accepted model for the AM CVn stars is that they are semi-detached binaries consisting of a low-mass degenerate helium secondary transferring mass via an accretion disc to a DB white dwarf primary (Faulkner, Flannery & Warner 1972; see also Smak 1967). O'Donoghue & Kilkenny (1989) first suggested that the $\sim 10^3$ s photometric periods observed in most of the AM CVn stars are superhump rather than orbital periods. The superhumps have highly non-sinusoidal profiles and are expected to form by the same mechanism as in the SU UMa stars.

Helium accretion discs have lower opacity and sound velocity and higher ionization temperature than hydrogen rich ones. Comparing the properties of the AM CVn stars to those of hydrogen rich CVs should provide a valuable test of our understanding of accretion discs.

Chapter 3

Phenomenology of the Rapid Oscillations

Arguably the most remarkable discovery of early high speed photoelectric photometry was the strictly periodic modulation in DQ Her, at an amplitude of 0.035 mag in U, and with the startlingly short period of 71 s (Walker 1956). Searches for similar periodicities in other CVs, carried out in the 1950s and 60s, were unsuccessful (Walker 1957; Mumford 1966, 1967), despite including observations of objects that are now known to posses short time scale oscillation (e.g. WZ Sge and AE Aqr). These efforts failed not only as a result of low time resolution and signal-to-noise, but also because periodic modulations with amplitudes less than about 0.01 mag are not likely to be detected by visual inspection of light curves[1].

Technological advances in the 1970s (see e.g. Nather & Warner 1971), which included the ever increasing quantum efficiency of detectors, but also digital manipulation of data, revealed oscillations at similar time scales to that in DQ Her, but of much lower coherence, and usually at lower amplitude. This phenomenon—now called dwarf nova oscillations, or DNOs—was first observed in three outbursting DN, and in the NL UX UMa (Warner & Robinson 1972a); the DNOs had periods of the order of 10 s, and amplitudes of a few millimagnitudes (mmag). DNOs are now known to be a fairly common feature of high $\dot{M}$ CVs. Patterson, Robinson & Nather (1977) discovered a second class of oscillation (which is known as quasi-periodic oscillations, or QPOs) when they noticed a modulation with a period near 50 s, and much lower coherence than had up until then been displayed by DNOs, in outburst light curves of RU Peg; a DNO at higher frequency and of much higher stability was present at the same time, implying that the 50 s oscillation was a

[1]Mumford (1966) did perform a periodogram analysis of some of his observations, but this was, at the time, a very inefficient technique because it involved manually digitizing light curves, and calculating periodograms with analogue computers.

distinct phenomenon. Recently, motivated by the conjecture that the ratio of QPO period to DNO period ($R = P_{QPO}/P_{DNO}$) in a given star is generally close to 16, a third class of oscillations was introduced (Warner, Woudt & Pretorius 2003, hereafter WWP03); these are called longer period dwarf nova oscillations (lpDNOs), and have, for a given system, periods (P_{lpDNO}) around 4 times the DNO period, which is equivalent to $\sim$1/4 times the QPO period.

Although DNOs, lpDNOs, and QPOs are all quasi-periodic, it initially seemed as though there was a clear dividing line in terms of coherence between DNOs and QPOs, but it soon became evident that this is not the case (e.g. Robinson & Warner 1984). The distinction between the three types of rapid oscillation is therefore primarily based on period, rather than coherence, and in most cases this still leads to QPOs having orders of magnitude lower coherence than DNOs and lpDNOs. The most complete and recent listing and classification of DNOs, lpDNOs, and QPOs is that by Warner (2004, hereafter W04).

Aperiodic brightness variations on time scales of tens of seconds to minutes (flickering) are present in most CV light curves. Flickering is associated with the turbulent mass transfer and accretion processes and has greater amplitude at lower frequency—i.e. it is red noise (e.g. Bruch 1992). Flickering is easily recognized in an amplitude spectrum as a smooth rise in amplitude of the mean noise level towards the lower frequency end (note that a smooth rise in amplitude at decreasing frequency is also characteristic of data taken under a slightly non-photometric sky). Since QPOs generally have lower frequency, and usually lower coherence, their study is more seriously impeded by flickering activity than that of DNOs and lpDNOs. The intrinsically noisy nature of CVs (and all mass transferring binaries) thus places a limit on the benefit that can be derived from obtaining photometry with larger telescopes.

Quasi-coherent oscillations with periods of the order of seconds are observed in Polars (e.g. Middleditch 1982), they have a physical origin that is fairly well understood (e.g. Langer, Chanmugam & Shaviv 1981), and quite different from that of the rapid oscillations discussed here.

3.1 Dwarf Nova Oscillations

DNOs are associated with high $\dot{M}$, non-magnetic CVs; they occur in all subtypes of outbursting DN, are intermittently present in some NLs, and have been observed in two AM CVn stars (see table 1 of W04). No IP has ever been observed to have a DNO, although the DQ Her stars WZ Sge and AE Aqr, and the IP GK Per, have modulations which may be compared to DNOs or lpDNOs (see e.g. Patterson 1978, 1979b, 1980, 1991; Mazeh et al. 1985; Patterson, Richman & Kemp 1998; Morales-

Rueda, Still & Roche 1999; WWP03; W04; Hellier, Harmer & Beardmore 2004).

In DN, DNOs typically appear about half way up the rising branch of outburst (but this is deduced from fairly sparse coverage of this phase of outburst), and disappear at about the same brightness on the descending branch after having been present through maximum. Different behaviour is seen in AH Her, where DNOs are present before and after, but not at maximum (Stiening, Hildebrand & Spillar 1979; Hildebrand et al. 1980; Patterson 1981), and in VW Hyi, where DNOs are rarely seen near maximum, but are very frequently present during the late decay from outburst (Robinson & Warner 1984; Warner & Brickhill 1974, 1978; Schoembs & Vogt 1980[2]; van der Woerd et al. 1987; Woudt & Warner 2002a, hereafter WW02a). In some outbursts of DN known occasionally to have DNOs none are observed, e.g. an outburst of KT Per was extensively observed by Robinson & Nather (1979) and Nevo & Sadeh (1978) with no DNOs found, while the system has shown DNOs in similar outbursts (Nevo & Sadeh 1976; Robinson 1973b). Furthermore, there are DN that have been well observed in outburst in which DNOs have never been detected; e.g. over 40 h of photometry of YZ Cnc during outbursts failed to produce any DNO detections (Patterson 1981). Similarly, there are NLs in which DNOs do not seem to occur; RW Sex, e.g., is a well studied NL with no DNOs ever observed.

Although almost exclusively associated with outburst, DNOs have been observed in a few quiescent DN; examples are OY Car (WWP03), V893 Sco (see Section 5.8), and possible detections in HT Cas and SU UMa in hard X-rays (Córdova & Mason 1984; Eracleous, Patterson & Halpern 1991).

DNO periods are shorter than those of QPOs and lpDNOs, falling in the range 2.8 s to ~100 s, with individual systems displaying a much smaller range of periods; the minimum observed values of P_{DNO} for individual systems cluster strongly in the range 19–20 s. DNOs are oscillations of moderate coherence: variations in P_{DNO} of up to 19% have been observed in a single outburst of SY Cnc, while in AH Her period variations of as much as 38% occur between different outbursts (Hildebrand et al. 1980; Patterson 1981); a DNO in VW Hyi has been seen to change its period from about 26 s to about 40 s in only ~4.5 h (WW02a). However, stable phasing is sometimes maintained for an hour or more, e.g., a DNO in SY Cnc showed no detectable deviation in either phase or period over a 3 h run (Robinson 1973b). This leads to optical DNOs having $10^3 < Q < 10^7$; note that Q is a measure of period, and not phase, stability. It has been shown that the coherence of optical DNOs in SS Cyg and AH Her is a function of outburst phase, being highest near maximum

[2]Schoembs & Vogt (1980) report the possible detection of a DNO with a period of 33.9 s near maximum light in VW Hyi. At such high luminosity, this period does not fit in with the dependence of DNO periods on luminosity described by WW02a; they argue that the signal was probably a beat between a DNO at 14.18 s and the 10 s sampling time used by Schoembs & Vogt.

light—in the case of SS Cyg the coherence decreases by more than a factor of 7 during outburst, with DNOs becoming unobservable towards the end of outburst (Hildebrand, Spillar & Steining 1981a,b; Córdova et al. 1984); see also fig. 13 of Warner, O'Donoghue & Wargau (1989) where it appears that increased frequency of phase or period changes produces a decline in coherence late in outburst.

In optical light, DNO amplitudes are typically a few times 0.001 mmag, which equates to a fraction of 1%. Only in a few rare observations do DNOs attain large enough amplitude to be seen directly in the light curve (e.g. in VW Hyi, Warner & Harwood 1973, WW02a; TY PsA, Warner et al. 1989, Section 5.5; KT Per, Robinson 1973b; OY Car, Marsh & Horne 1998, WWP03; V2051 Oph, Steeghs et al. 2001). Fourier analysis makes it possible to detect DNOs at amplitudes as low as 0.2 mmag (Patterson, Robinson & Kiplinger 1978a); in this case the signal was detectable only because it was uncommonly coherent, remaining strictly periodic for 3.5 h[3]. DNO amplitudes usually change on time scales of hours or less, these changes often include disappearance and reappearance, e.g. in Z Cha a DNO was seen to develop and disappear in a single run (Warner & Brickhill 1978); in IX Vel, the DNO amplitude grows and decays on a time scale of hours (Warner, O'Donoghue & Allen 1985); a DNO in KT Per grew from being undetectable to an amplitude of 6 mmag in less than 15 min. (Robinson 1973b). The amplitudes seem to be independent of binary inclination, with optical DNOs appearing at amplitudes of a few mmag in low inclination systems, e.g. V3885 Sgr (Warner 1973), IX Vel (Warner et al. 1985), and HP Nor (Section 5.11), as well as in high inclination systems, e.g. UX UMa (e.g. Warner & Robinson 1972a), and OY Car (e.g. WWP03); the largest amplitudes known for optical DNOs are seen in the intermediate inclination systems VW Hyi and TY PsA.

The short periods of optical DNOs imply an origin near the white dwarf, so that it was expected that high energy oscillations were the ultimate source of optical DNOs (e.g. Bath 1973; Warner & Brickhill 1978; Paczynski 1978). Pringle (1977) further predicted that DNOs would be much more prominent in soft X-rays than in the optical flux. This expectation was fulfilled when Córdova (1979) and Córdova et al. (1980) observed high amplitude soft X-ray pulsations from U Gem and SS Cyg.

The amplitude of X-ray DNOs is generally 20–100%; coherence can change by a factor of 3 within 1 h, and by a factor of 10 between different outbursts (Córdova et al. 1984), usually being lower than that of optical DNOs. X-ray DNOs originate in the inner disc where high energy flux is produced, and the large amplitudes mean that the DNOs must be an intrinsic feature of the X-ray production mechanism,

[3]This oscillation (seen in SS Cyg) had a period of 9.735 s, and was probably a beat between a DNO at 6.970 s and the 4 s integration time, hence the low observed amplitude (see the discussion in W04).

rather than just a small perturbation of the X-ray source. Córdova et al. (1980) find that the DNO source in SS Cyg is considerably smaller than the white dwarf.

DNOs are not often seen in hard X-rays (e.g. Swank 1979; Nousek et al. 1994; Ponman et al. 1995; Wheatley, Mauche & Mattei 2003); where hard X-ray DNOs have been detected in DN, it was in quiescence (Córdova & Mason 1984; Eracleous et al. 1991), but see also Jensen et al. (1983).

Córdova & Mason (1982) were first to point out that the higher coherence of optical DNOs is probably a selection effect: because of their much lower amplitudes, optical DNOs are only detectable when their coherence is high, and their disappearance towards the end of outburst may be the result of reduced coherence. There is an implicit assumption here that optical, EUV, and X-ray DNOs represent the same phenomenon, and this has always been the belief: Hildebrand et al. (1981a) state that both the amplitude and period of DNOs observed in the UV suggest that they have the same source as the the pulsed soft X-rays; Warner et al. (1989) show that the appearance of the phase variability of optical and X-ray DNOs is almost identical. Mauche & Robinson (2001) finally showed by simultaneous observations in the two wavebands that optical and EUV DNOs are identical in period and phase (the lack of phase delay implies that, if optical DNOs are reprocessed EUV oscillations, the reprocessing site must be in the inner disc). More generally, the time scale of DNOs observed in the EUV or soft X-ray flux is the same as in the optical for any given CV.

Already in the earliest observations of DNOs in DN, a variation of P_{DNO} on an outburst time scale was recognized, this was seen in Z Cam, where P_{DNO} decreased as the system brightened, and increased as it faded (Warner & Robinson 1972a). The period-luminosity relation is a universal feature of DNOs: when present in DN, DNOs have $dP_{DNO}/dt < 0$ on the rise to outburst, and $dP_{DNO}/dt > 0$ on the decline, with a minimum DNO period being reached roughly 1 d after maximum optical luminosity. P_{DNO} is a double valued function of optical luminosity (I), having different values at equal luminosity on the rising and falling branch of outburst; therefore, in the P_{DNO}–I plane, a loop is traced out during outburst. This is true of all well studied DN; for a given system, the location and shape of the loop varies from outburst to outburst (Patterson 1981; Hildebrand et al. 1981a). The slope of the P_{DNO}–I relation, derived mostly from observations made on the decline from outburst, is

$$s \equiv \frac{d\log(P_{DNO}/\mathrm{s})}{d\log(I/I_{ref})} = -0.25 \pm 0.15 \tag{3.1}$$

(Warner & Robinson 1972a; Robinson 1973a,b; Nevo & Sadeh 1976, 1978; Hildebrand et al. 1980; Patterson 1981; Schoembs 1986; Patterson et al. 1995). Jones & Watson (1992), Mauche (1996), and Mauche & Robinson (2001) give a

very similar dependence of DNO period on soft X-ray and EUV luminosity. On the decline from an outburst of VW Hyi, WW02a measure $s = -0.15$, as the system fades through $V = 12.5$, however, the relation becomes as sensitive as $s \approx -2$. There is also some evidence that a similar relation holds for NLs; values of $s = -0.2$ and $s = -1.4$ are found for UX UMa and IX Vel respectively (Warner & Nather 1972; Warner et al. 1985), but these values result from measuring P_{DNO} over only a small range in brightness.

It was long assumed (e.g. Patterson 1981) that P_{DNO} is a single valued function of $\dot{M}_1$ (and thus also bolometric accretion luminosity), and that the double valued nature of the P_{DNO}–I relation reflects a changing bolometric correction over outburst (see Section 2.4.1), i.e. the dependence of I on $\dot{M}_1$ differs on the rising and falling branch of outburst. Mauche (1996) finally demonstrated that there is a single valued relationship between P_{DNO} and EUV luminosity, with P_{DNO} a minimum at maximum EUV flux.

Superimposed on the systematic period-luminosity variation are abrupt changes in period, phase, and amplitude (which occur independently of each other) in optical as well as X-ray observations; this can be seen in, e.g., fig. 13 of Warner et al. (1989), fig. 6 of Córdova et al. (1980), and fig. 11 of Jones & Watson (1992). The rapid changes in period, which interrupt intervals of comparative stability lasting ~1000 s, can be as large as 0.05 s, occur in less than 100 s, and (as first pointed out by Warner 1995b) are not accompanied by any significant changes in system luminosity. Furthermore, these period changes can take place in either direction relative to the systematic variation of P_{DNO} with changing luminosity. This behaviour places probably the most severe constraint on physical explanations for DNOs (Warner & Woudt 2002, hereafter WW02b).

Phase and amplitude changes of optical DNOs during eclipse have been tracked in a few eclipsing systems where above average DNO phase and period coherence allow it. In UX UMa the amplitude is greatest before eclipse[4], and a $-360°$ phase shift (i.e. the oscillation loses one cycle) occurs, beginning and ending at the same orbital phases as eclipse of the disc (Nather & Robinson 1974; Knigge et al. 1998). A continuous $-360°$ shift in DNO phase through eclipse is also observed in HT Cas; again, the DNO amplitude is lowered in eclipse (Patterson 1981). DNOs in Z Cha are slightly reduced in amplitude during eclipse; the phase slowly decreases during ingress, and rapidly increases after mid eclipse (Warner & Brickhill 1978). Because of the rapidity of eclipse in Z Cha, as well as low DNO amplitude, this

[4]Warner & Robinson (1972a) and Warner & Nather (1972) stated that the DNOs were absent just after eclipse, and so must originate from the white dwarf. However, Nather & Robinson (1974) showed that they are in fact present throughout the orbital cycle, although the DNO amplitude is reduced in eclipse.

result is not as clean as those found for UX UMa and HT Cas. DNOs observed in OY Car, late in superoutburst, were eclipsed but showed no phase shift during eclipse (Schoembs 1986).

The eclipse-related phase and amplitude changes imply that DNOs at optical wavelengths result from a rotating X-ray or EUV beam that is reprocessed off the disc, in a similar manner as the oscillation in DQ Her, but with the details depending on geometrical effects such as inclination. Petterson (1980) shows that for UX UMa, the direction of the phase shift does not require retrograde rotation of the white dwarf, instead light reflected off the far side of the disc makes a smaller contribution to the DNO modulation than light received from the near side or directly from the white dwarf (requiring that only ~0.1% of the pulsed light is observed in the optical without reflection). The model of Petterson (1980) also fits the HT Cas data very well for $i = 77°$, which is the inclination independently deduced from eclipse analysis (Patterson 1981).

Further evidence that optical DNOs originate from reprocessing of a higher energy rotating beam comes from time resolved spectroscopy of V2051 Oph, where the pulse phase of the QPO sideband (the meaning of QPO sideband is explained in Section 3.3) in the emission lines is wavelength dependent, with the pulse in the red wing leading the pulse in the blue wing—i.e. the pulse phase has the opposite dependence on wavelength to that in DQ Her. The direction of the phase dependence requires that in V2051 Oph the oscillation maximum occurs when the rotating beam sweeps over the near side of the disc, or some structure on it; a greater contribution from reprocessing off the near side is understandable, since the smaller magnetosphere of a DN implies that the white dwarf obscures much of the far side of the inner disc (see Section 4.1.5).

Multicolour optical observations of AH Her, SY Cnc, and EM Cyg (Hildebrand et al. 1981b; Middleditch & Córdova 1982; Stiening, Dragovan & Hildebrand 1982) indicate that the optical DNO spectrum is much bluer than the disc continuum. Middleditch & Córdova (1982) find that no single blackbody or free-free spectrum, or combination of blackbody spectra, modulated in intensity or temperature, can fit the colours of the DNO in SY Cnc, and that a thermal spectrum added to a small amount of recombination radiation from HI, HeI, and HeII is required; they therefore suggest that emission lines may also be pulsed—Steeghs et al. (2001) found that this is indeed the case in V2051 Oph. Marsh & Horne (1998) find also in OY Car a DNO spectrum which is bluer than the mean spectrum. In UX UMa, the DNO spectrum is extremely blue at pre- and posteclipse orbital phases, but much redder near mideclipse, suggesting a more extended source. This supports the two component model of Petterson (1980), where DNOs originate from a small hot region, with both a direct and reprocessed component observed. Mauche (1997a)

finds that the spectrum of the EUV DNOs in SS Cyg is neither blue nor red nor gray relative to the net (phase integrated) spectrum. This means that the DNOs are not caused by variations in effective temperature, column density, or effective area, since these variations would result in a blue, red, or gray oscillation spectrum respectively. The data can be explained by variations in the emission line flux atop a constant underlying continuum, or by variations in the optical depth of overlapping absorption lines.

Only very rarely is significant power present in the harmonics or subharmonics of the DNO frequency, i.e. in most cases DNOs are pure sine functions to within the limits of measurement. This result is not surprising, since a modulation at $\sim$1 mmag has to be remarkably non-sinusoidal for harmonics to appear above the noise level in a typical CV amplitude spectrum; furthermore, the time resolution is usually not high enough to sample the higher harmonics adequately. Nevertheless, there are a few observations of DNOs that are measurably non-sinusoidal. Mauche (1997b) detected a DNO with significant first harmonic in SS Cyg at the peak of outburst; on a different occasion a DNO in this system (while systematically drifting to shorter period) very rapidly changed its period from 6.59 to 2.91 s, suggesting that the oscillation frequency made a transition from fundamental to first harmonic, with the P_{DNO}–I relation being less sensitive after the frequency doubling (Mauche & Robinson 2001). van Teeseling (1997) observed a 2.8 s DNO in the next outburst of SS Cyg; it seems likely that this was also a first harmonic. A 28.06 s DNO in V2051 Oph has been reported to have a significant subharmonic in the continuum light curve (Steeghs et al. 2001).

Early claims of multiperiodic DNOs were based on very weak evidence: Warner & Robinson (1972a) stated that a DNO in CN Ori underwent transitions between discrete periods, with two periods simultaneously present at times; Robinson (1973b) presents some evidence of four periods simultaneously present in KT Per. However, Warner & Brickhill (1978) reanalysed the CN Ori data and concluded that there was no evidence of multiple periods simultaneously present or of transitions between discrete periods; they point out that because of the identity $\sin\omega_a t \sin\omega_b t = \frac{1}{2}(\cos(\omega_a-\omega_b)t-\cos(\omega_a+\omega_b)t)$, an amplitude modulated sine function $\sin\omega_a t \sin\omega_b t$ appears in a Fourier transform as two peaks separated by $2\omega_a$. Therefore, if in a section of light curve of duration T, the envelope of a sine function at frequency ω happens to have a systematic variation, power appears in the Fourier transform on either side of the peak at ω, and separated from it by $1/T$. The few observations where DNOs are definitely not singly periodic are discussed in Section 3.3.

A dependence of DNO phase on orbital phase in UX UMa has been seen but not modeled (Nather & Robinson 1974). In OY Car Schoembs (1986) finds that the superhump modulates the amplitude of the DNOs, with DNO amplitude being

greatest at superhump maximum. Warner & Brickhill (1978) present evidence that P_{DNO} varies with orbital phase in V436 Cen and VW Hyi.

Because of the low amplitudes of DNOs, the rapid changes in their periods and amplitudes are very difficult to analyse, and it is seems likely that the detailed characteristics deduced for the oscillations depend, at least to some extent, on the method of analysis used.

3.2 Quasi-periodic Oscillations

Unfortunately, there is quite a bit of art involved in the detection of QPOs; with no generally agreed upon definition of what constitutes a QPO, it is impossible to determine objectively and consistently whether one is present in a light curve or not. In fact, QPOs are probably often mistaken for flickering: WW02a remark in connection with early light curves of VW Hyi that rapid variability, which was initially dismissed as flickering, is in hindsight clearly recognizable as QPOs. Perhaps because it is so difficult to quantify their properties, QPOs received less attention, in the past, than DNOs.

QPOs often have coherence times as short as a few cycles (typically $5 \lesssim Q \lesssim 20$), so that one train of oscillations usually soon disappears to be replaced by another with slightly different period, or shifted in phase. This behaviour is illustrated in fig. 14 of WW02a, where an oscillation grows and then decays over about 5 cycles, followed by growth and decay over a few cycles of another QPO with similar period, but phase shifted by $\sim$0.4 cycles relative to the first. Even for very prominent QPOs, the power is normally distributed over such a broad band of frequencies, that it is not conspicuous in a Fourier transform, and thus cannot be detected unless the modulation is readily seen in the light curve (e.g. fig. 3 of Patterson et al. 1977). Examples of exceptionally coherent QPOs are found in light curves of WX Hyi and RU Peg—see fig. 3 of WWP03, and Fig. 5.8.

Fourier analysis—like most analysis techniques used to search for modulations in light curves—determines what strictly periodic terms a light curve consists of. A technique more suited to detecting quasi-periodic components may reveal that QPOs are more common than currently thought; essentially, however, this would only imply moving back the dividing line between QPOs and flickering. Robinson & Nather (1979), e.g., state that in some (but not all) cases, an autocorrelation function is more sensitively able to detect low Q modulations than Fourier analysis. The usual practice is to accept only QPOs that are obvious to the eye in the light curve.

QPOs occur in all subtypes of DN and NLs, and also in the high $\dot{M}$ state of the AM CVn star CR Boo. Only the two DN VW Hyi and WX Hyi have been observed

to display QPOs in quiescence; see WW02a and Section 5.13 (the ~100 s oscillation in HT Cas reported by Patterson 1981 is now classified as an lpDNO). QPOs exist independently of DNOs, W04 lists several detections of QPOs in DN and NLs that have never been observed to have DNOs; it can also happen that DNOs and QPOs appear at different phases of the same outburst (Warner et al. 1989).

QPO pulse profiles usually appear to be sinusoidal, but note that the low coherence and signal-to-noise means that this will necessarily be the case, unless the profile is highly non-sinusoidal; exceptions are noted by WW02a and Kato, Hirata & Mineshige (1992).

As pointed out by W04, there are two distinct timescales for QPOs: many systems have QPOs with periods of the order of 1000 s, in some cases (e.g. WX Hyi, VZ Pyx, HX Peg, and OY Car) these kilosecond QPOs are observed in addition to QPOs with periods an order of magnitude shorter. The observational properties of the DNO-related QPOs (i.e. QPOs with $P_{QPO} \approx 16 P_{DNO}$), and kilosecond QPOs are separately discussed below.

3.2.1 DNO-related QPOs

The discovery observations of QPOs (Patterson et al. 1977) showed the oscillation present on five consecutive nights of outburst, starting just before maximum, but not covering a very large range in system luminosity. In addition to erratic variations on time scales of several minutes, there was a systematic decrease in amplitude over the five nights; P_{QPO} varied between 48 s and 55 s, but with no systematic trend.

Robinson & Nather (1979) and Patterson (1981) later found QPOs in other outbursting DN, and in NLs. Ironically, none of the additional QPO detections of Robinson & Nather (1979) has survived reclassification by W04; of all the QPOs listed by Patterson (1981), only a 413 s signal in VW Hyi and a ~1000 s signal in TT Ari are still considered to be QPOs (the QPO in TT Ari belongs with the kilosecond QPOs discussed in the next section). Nevertheless, the observational data base of QPOs has grown, and many general properties have emerged.

The amplitudes of DNO-related QPOs are usually a few times 0.01 mag (low Q modulations with significantly lower amplitudes are not detectable), but can get as large as 0.12 mag (Warner & Brickhill 1978); light curves where individual QPO cycles have amplitudes of 0.2 mag are shown by WW02a.

QPO periods are longer than DNO and lpDNO periods, falling in the range 50 s to several hundreds of seconds. In systems that have both DNOs and DNO-related QPOs, the relation $P_{QPO} \approx 16 P_{DNO}$ holds (by definition of DNO-related QPO; note that the ~380 s and ~5000 s oscillations in GK Per are related in this way, so that, despite the long period, the ~5000 s QPOs are included with the DNO-related QPOs). In a few cases, QPOs have been seen to follow a period luminosity relation,

similar to that for DNOs: the average QPO period in GK Per decreased over three nights of the rise to maximum (Morales-Rueda et al. 1999); WW02a report a QPO in VW Hyi with a period evolving from about 400 s to roughly 600 s during a decline of 0.45 mag (at 0.09 mag/h); evolution of P_{QPO} over 10 nights of an outburst of RU Peg is described in Section 5.2. The systematic increase of QPO period in VW Hyi was followed by frequency doubling, with some evidence that the first harmonic grows in, rather than the modulation suddenly changing from fundamental to first harmonic (WW02a). Frequency doubling of a QPO seems to occur also in EF Peg (Kato 2002).

It is not often that QPOs are detected at high energies, and then usually only in hard X-rays; detections of X-ray oscillations are listed in table 2 of W04. It is clear that the time scale of X-ray QPOs in any given system is the same as in the optical, implying that probably the same phenomenon is observed in the two wavebands. The most noteworthy examples of X-ray QPOs are those in VW Hyi, where the hard X-rays were 100% modulated at ~200 s when they returned at the end of outburst (Wheatley et al. 1996), and in SS Cyg during the time of suppression of hard X-rays after the start of outburst, and again when they recover at the end of outburst (Wheatley et al. 2003). Temperature or absorption column density variations cannot explain the X-ray QPOs in SS Cyg, since no change in hardness ratio is seen over the QPO cycle; quasi-periodic obscuration of the X-ray source by a structure that is opaque at X-ray wavelengths is not ruled out (Wheatley et al. 2003; W04).

The observation that ~100 s oscillations persist through eclipse in U Gem was used to prove that QPOs do not originate in the bright spot (Robinson & Nather 1979). These oscillations are now classified as lpDNOs and therefore the argument is invalid, but the conclusion still holds: in VW Hyi, e.g., the QPOs appear to be quite unaffected by the orbital hump modulation—see fig. 1 of WW02a.

The minima of large amplitude QPOs occasionally comprise deep dips in luminosity (see e.g. fig. 2 of WW02b, and fig. 9 of Wheatley et al. 2003). A more extreme display is seen in SW UMa, where the minima of the ~370 s QPO are deepened by what looks like shallow eclipses lasting about 60 s (Kato et al. 1992).

3.2.2 Kilosecond QPOs

The second set of QPOs have periods ranging from 750 s (in SS Cyg) to ~3000 s (in MV Lyr). As noted before, kilosecond QPOs occur in some systems which also have QPOs with periods an order of magnitude shorter, as well as DNOs and/or lpDNOs, while in many NLs and DN only kilosecond QPOs have been observed. It is perhaps significant that no NL has been found to have both sets of QPOs. In one case (HX Peg; see Fig. 5.26), a kilosecond QPO has been seen to coexist with

a QPO at higher frequency.

The amplitudes can be as large as 0.3 mag (greater than what is seen for the largest amplitude ~100 s QPOs); periods change on time scales $\ll$1 d (Patterson et al. 2002). An example of exceptionally large coherence in kilosecond QPOs is furnished by V1193 Ori (see Section 5.22). The oscillations have profiles that sometimes appear to be flare-like, rather than sinusoidal (see e.g. fig. 10 of Patterson et al. 2002, and Fig. 5.26).

Kilosecond QPOs have been observed in several DN, but the NLs that display this phenomenon are almost all SW Sex stars (exceptions being RW Sex, V842 Cen, BB Dor, and V1193 Ori). With the very large data base of the Center for Backyard Astrophysics, Patterson et al. (2002) state that kilosecond QPOs are found in more than one half of SW Sex stars, and are not seen to be prominent in other classes of CVs.

3.3 Interaction between DNOs and QPOs

In discussing their discovery observations of QPOs, Patterson et al. (1977) remark that no correlation could be found between the QPO and a DNO which was present at the same time. Despite the fact that DNOs and QPOs exist independently of each other there is, in many cases, clear evidence of interaction between DNOs and (DNO-related) QPOs.

Robinson & Warner (1984) observed a QPO in VW Hyi which not only modulated the system luminosity, but also the amplitude of a DNO present at the same time, the DNO amplitude being greatest at the maxima of the QPO. This behaviour has twice more been seen in VW Hyi (Warner & Brickhill 1978; WW02a).

Another remarkable correlation in behaviour of a DNO and QPO was seen in VW Hyi at the end of an outburst, where both P_{DNO} and P_{QPO} steadily increased as the system faded by a factor of about 2. The ratio P_{QPO}/P_{DNO} remained at a nearly constant value of about 15 throughout the evolution of P_{DNO} from about 26 s to roughly 40 s and P_{QPO} from ~400 s to ~600 s (WW02a); the value of R is also roughly 15 in older VW Hyi observations that were reanalysed. The authors furthermore find in one observation a quasi-periodic variation in the phase of a DNO, which is correlated with a QPO present at the same time. Something similar is seen in the phase of the DNOs detected by Nather & Robinson (1974) and Knigge et al. (1998), this is discussed by WW02b. In one light curve of OY Car, a correlation is seen between the phase behaviour of a DNO and QPO which are simultaneously present; this is illustrated in fig. 4 of WWP03.

Perhaps the most informative interaction between the two classes of oscillation is a few observations of double DNOs, or QPO side bands: a second modulation

at slightly lower frequency accompanying the true DNO, similar to an orbital side band in IPs. This has been observed in V3885 Sgr (Hesser, Lasker & Osmer 1974), OY Car (in the UV; Marsh & Horne 1998), V2051 Oph (Steeghs et al. 2001), VW Hyi (WW02a,b), V436 Cen, and EC 21178-5417 (WWP03), and possibly in SS Cyg (in the EUV; Mauche 2002). In the case of VW Hyi, as well as in V436 Cen, SS Cyg, and some of the EC 21178-5417 observations, the beat period between the two components of the double DNO corresponds to the period of a QPO present in the same light curve. The OY Car and VW Hyi QPO sidebands have significant first harmonics (Marsh & Horne 1998; WW02a).

3.4 Longer Period Dwarf Nova Oscillations

WWP03 first drew attention to a class of rapid oscillations separate from DNOs and QPOs—the longer period DNOs or lpDNOs. They list 12 systems in which lpDNOs have been observed; a number of these are from published observations where the oscillations were mentioned, but without explanation. W04 gives a more up to date list of lpDNO detections.

lpDNOs have coherence similar to DNOs (an example of an lpDNO with very poor coherence is furnished by the ~32 s oscillation in SS Cyg; Robinson & Nather 1979), but seem to have, on average, slightly larger amplitudes. They are often present at the same time as DNOs and/or QPOs, in these cases the relations $P_{lpDNO} \approx 4 \times P_{DNO}$ and $P_{lpDNO} \approx 1/4 \times P_{QPO}$ hold. When only one set of oscillations is observed in a system, it can be difficult (or impossible) to decide to which class it belongs (see e.g. the discussion V426 Oph in Section 5.16).

Most lpDNO detections are in optical light, but they have been observed in X-ray light curves as well: in VW Hyi in outburst and quiescence (van der Woerd et al. 1987; Pandel, Córdova & Howell 2003), and in U Gem in quiescence (Córdova & Mason 1984). There is only one example of an optical lpDNO observed in a quiescent DN (in HT Cas; Patterson 1981).

Like DNOs, lpDNOs are not observed in all high $\dot{M}$ CVs. Furthermore, DN that occasionally have lpDNOs do not show them in every outburst, and in NLs that are known to have lpDNOs, they are not always present; see WWP03.

In contrast to the DNOs in AH Her and SY Cnc, a 160 s oscillation, now recognized as an lpDNO, was found to be very red relative to the disc; however, this was a single short observation and the result needs to be confirmed, as stated by the authors at the time (the data were taken with the same equipment that showed DNOs in SY Cnc to be bluer than the disc; Middleditch & Córdova 1982).

When lpDNOs and DNOs are present simultaneously, comparison of the amplitude and phase changes in the two types of oscillation indicates that they behave

independently of each other (see fig. 12 and 15 of WWP03, and Fig. 5.13 and 5.16 in Chapter 5).

Double lpDNOs separated by the frequency of a simultaneously present QPO have been seen in AQ Eri and HX Peg; in VW Hyi the beat period between two components of a double lpDNO was similar to P_{orb} (WWP03). An lpDNO in EC2117 was once observed to double its period (WWP03); in VZ Pyx and possibly KT Per frequency doubling of an lpDNO is seen (Section 5.18; Robinson & Nather 1979).

The most distinctive property of lpDNOs is that, in contrast to DNOs, there is in most cases (but see Section 5.4) no evidence that P_{lpDNO} scales with accretion luminosity. The lpDNO in HT Cas, e.g., has a period of about 100 s in outburst as well as in quiescence; in VW Hyi the mean value of P_{lpDNO} stayed unchanged on seven nights while the system faded from 10.6 to 13.7 mag (Haefner, Schoembs & Vogt 1977, 1979; Schoembs 1977); WWP03 gives more examples.

As stated in Chapter 2, Warner & Nather (1971) displayed eclipse light curves of U Gem that showed that the flickering disappears during eclipse (which, in this system, is of the bright spot) to prove that the bright spot is the source of flickering. Robinson & Nather (1979) reported QPOs at around 100 s in U Gem, these persisted through eclipse, which led them to conclude that the bright spot is not the source of QPOs; these QPOs were reclassified as lpDNOs by WWP03 and W04. Warner (1976) shows another eclipse light curve of U Gem, which supposedly again illustrates flickering present before, but not during eclipse. In this light curve, however, the flickering looks very much like a $\sim$100 s quasi-periodic modulation, at least as clear and coherent as the oscillations shown in fig. 14 and 15 of Robinson & Nather (1979). Why the oscillations should be eclipsed in one case, and not in the other is not clear.

lpDNOs being a very recently recognized phenomenon, there are bound to be many aspects of the phenomenology still to be uncovered. Specifically, no study of amplitude and phase behaviour of lpDNOs through eclipse has yet been made.

Chapter 4

Models of the Rapid Oscillations

Several mathematical models have been constructed with the aim of quantifying the coherence of DNOs and QPOs. The models describe the oscillations as, e.g., a second order autoregressive process (Robinson & Nather 1979; Hildebrand et al. 1981a; Robinson & Warner 1984), or a strictly periodic function of which the phase, or the higher order time derivatives of phase, is randomly disturbed (Córdova et al. 1980, 1984; Horne & Gomer 1980). Any of these models can produce variability that is indistinguishable from most of the available observations[1]. Although a quantitative characterization or definition of QPOs will be valuable, there does not seem to be much promise of mathematical models leading to understanding of the physical nature of the rapid oscillations; for this reason only models that have a physical basis are described in the rest of this chapter.

4.1 Dwarf Nova Oscillations

A model of DNOs must be consistent with $P_{DNO} \sim 10$ s; all models appeal to the gravitationally determined time scale of the white dwarf ($\tau_G \sim 1/\sqrt{G\overline{\rho}}$, where $\overline{\rho}$ is the mean density of the star) to achieve the correct periods (Warner 1995a). Furthermore, both the systematical period-luminosity relation and the rapid changes in phase or period must be accounted for. The short time scale instability of the period, phase, and amplitude of DNOs reflects equally rapid changes in the structure that produces them.

The very high stability of the photometric modulation of an IP is attributed to the large rotational inertia of a white dwarf. Simple IP type rotation of the primary cannot explain DNOs, since the periods vary by ~10% on time scales of hours to days during outburst; the rotational kinetic energy of a rapidly rotating white dwarf

[1] Jones & Watson (1992), however, show that the phase behaviour of DNOs in their data is poorly represented by models in which random variability of the phase is described by a single parameter.

is $\sim 10^{49}$ ergs, while a DN outburst involves only about 10^{40} ergs.

The eclipse-related phase shifts of DNOs indicate a rotating beam origin, however, the source of the beam need not be a spot on the surface of the white dwarf; equally good fits may be obtained if the source of the oscillations were an orbiting bright spot in the inner disc, or a progradely moving non-radial oscillation of the white dwarf (Petterson 1980).

Because EUV and X-ray flux provides a more direct view of the site where DNOs originate from, observations at high energy have contributed to restricting viable models.

I describe in the following sections most of the models that have at one time or other been proposed for DNOs, although only the last (the low inertia magnetic accretor model discussed in Section 4.1.5) at this point seems to be reconcilable with all the observations.

4.1.1 White Dwarf Pulsations

The first explanation offered for DNOs was non-radial g-mode white dwarf pulsations (Warner & Robinson 1972a). Because radial as well as non-radial p-mode pulsations of a ~ 1 $M_\odot$ white dwarf have periods in the range 1–10 s (e.g. Chanmugam 1972), only g-modes hold any promise of explaining DNOs. Osaki & Hansen (1974) find g-mode pulsation periods of 50–200 s, as well as a period-luminosity relation (see also Brickhill 1975). Nather & Robinson (1974) calculate phase shifts for a non-radially pulsating white dwarf, which give satisfactory fits to their eclipse-related phase shift data of UX UMa. However, Bath et al. (1974c) point out that Brickhill (1975) had applied the results of Osaki & Hansen (1974) where they really are not valid; furthermore, the model requires slow rotation, whereas estimates of the accretion rates of DN imply that they contain rapidly rotating primaries, and to fit DNO periods, the model of Osaki & Hansen (1974) and Brickhill (1975) requires unrealistically high temperatures (Papaloizou & Pringle 1978).

Pulsations in a thin surface layer of a rapidly rotating white dwarf can be excited through e.g. interaction with the disc; periods and coherence times of both DNOs and QPOs can be produced in this manner (Papaloizou & Pringle 1978, 1980). Since only the outermost layer is involved in the pulsation (in order to account for the time scales of period variation), it is only the angular velocity of a thin layer that produces the DNOs. Thus period changes may not be directly related to temperature changes occurring in the oscillating region. If the mean rotation rate of the outer layer is determined during outburst by a balance between $\dot{M}_1$ and the rate at which these layers can transfer their angular momentum to the rest of the star, it may lead to the observed period-luminosity relation. The phase instability of DNOs may be achieved in this model through the superposition of a number of oscillations with

closely spaced periods.

It does not seem as though this model can account for the large amplitude of X-ray DNOs, especially not if many different modes are excited. Furthermore, virtually all DNOs are singly periodic; non-radial pulsations are expected to be multiperiodic (unless a specific excitation mechanism favours the creation of a single periodicity). Warner & Robinson (1972a) cited transitions between discrete periods in CN Ori as the strongest evidence for g-mode pulsations; however, Warner & Brickhill (1978) showed that the discrete periods were not real, and no credible evidence of transitions between oscillation modes has since been found. The small size of the oscillating object inferred from X-ray observations is also inconsistent with white dwarf pulsations.

4.1.2 Disc Pulsations

Several authors have considered pulsations of the accretion disc as the cause of DNOs or QPOs. Disc pulsations can modulate the system luminosity either by obscuration and reflection, or as intrinsic brightness variations.

van Horn, Wesemael & Winget (1980) show that non-radial oscillation modes of the disc can produce oscillation periods in the range 10–150 s, and speculate that interaction between the white dwarf and inner disc may drive the oscillations.

Adiabatic oscillations of an annulus of the disc (out of the orbital plane) have periods of the order of the Keplerian period of that annulus, independent of the detailed structure of the disc (Cox 1981), and so the time scale can fit both DNOs and QPOs. Adjacent annuli will act independently, and with slightly different frequencies, to produce a quasi-periodic brightness modulation. Cox & Everson (1982, 1983) include the effects of nonadiabaticity and viscosity in similar calculations, and show that the expected decay time of such an oscillation can be reconciled with QPOs, or the more incoherent DNOs.

The energy dissipated in the boundary layer is about equal to that dissipated in the entire rest of the disc, and potentially provides a powerful driving mechanism for oscillations. Córdova et al. (1980) first suggested instabilities of the accretion flow may exist at the inner disc edge; these oscillations are intrinsic luminosity variations. Papaloizou & Stanley (1986) find that the boundary between disc and star can be subject to oscillations driven by viscous instabilities. The amplitudes of such oscillations are too low to account for the X-ray observations of DNOs, and so the model is untenable. Note further that these mechanisms cannot operate in systems where the boundary layer is disrupted by a strong magnetic field.

Pulsational instabilities in accretion discs are also investigated by e.g. Kato (1978), Lubow & Pringle (1993); Carrol et al. (1985); Collins, Helfer & van Horn (2000b), see also Collins, Helfer & van Horn (2000a).

Since disc pulsations are not confined to a particular annulus, the oscillation power is spread over too great a range of frequencies to account for the more coherent DNOs.

4.1.3 Hot Spots in Keplerian Orbit

Bath (1973) was the first to remark that the range of DNO periods coincide with that of Keplerian periods just above the surface of a white dwarf. Inhomogeneities (or hot spots) may be produced in the inner disc by e.g. a turbulent instability or interaction of the accretion flow with a weak white dwarf magnetic field. The hot spot then orbits the white dwarf at the local Keplerian frequency, and modulates the luminosity as it is periodically eclipsed by the primary, or obscured by the disc. The spot fades because of cooling and differential rotation and is replaced by a new one, perhaps at a different radius, which leads to a phase and/or period change. If the hot spots are created at the magnetospheric radius (as proposed by Bath 1973), the period-luminosity relation can be ascribed to changing $\dot{M}_1$, and hence magnetospheric radius. It is estimated that the shearing time for such a blob is $\sim$1000 s (Bath 1973; Bath, Evans & Papaloizou 1974b), which is short compared to the life time of some DNOs. Furthermore, the mechanism is not able to produce DNOs in very low inclination systems like SS Cyg and RU Peg, experiences difficulty in accounting for the largest amplitude DNOs, and offers no reason why it appears that there is almost always only one hot spot present.

A variation on the theme is a model proposed by Popham (1999), which includes no magnetic field; the disc extends all the way to the white dwarf. An (again unknown) instability causes a non-axisymmetric bulge at the transition radius between the optically thick inner disc and optically thin boundary layer; the bulge rotates at Keplerian velocity, and the period-luminosity relation is explained as the transition radius varying in response to systematic changes in $\dot{M}_d$. The model predicts that DNOs will not be present in hard X-rays, which is contradicted by observations (Córdova & Mason 1984; Eracleous et al. 1991; Jensen et al. 1983), and that EUV/soft X-ray DNOs should be non-sinusoidal in high inclination systems (at least UV DNOs in the high inclination NL UX UMa are found to be sinusoidal to a high degree; Knigge et al. 1998).

4.1.4 Magnetically Channeled Accretion

Warner (1983) proposed that the primaries in DN may be slow magnetic rotators (like primaries in IPs); inhomogeneities near the magnetospheric radius modulate the accretion flow onto the magnetic poles, producing DNOs at the beat period between Keplerian rotation at r_0, given by $P_K(r_0) = 2\pi r_0^{3/2}(GM_1)^{-1/2}$, and the

white dwarf spin period: $P_{DNO} = [1/P_K(r_0) - 1/P_1]^{-1}$. Using equation 2.11, one obtains

$$P_K(r_0) = 6.3 \left(\frac{M_1}{M_\odot}\right)^{-5/7} \left(\frac{\mu_1}{10^{31}\ \mathrm{G\,cm^3}}\right)^{6/7} \left(\frac{\dot{M}}{10^{17}\ \mathrm{g/s}}\right)^{-3/7} \mathrm{s},$$

so that variations in $\dot{M}$ during outburst account qualitatively for the period-luminosity relation. Optical DNOs are then reprocessed X-ray emission from the accretion column of the white dwarf. Warner (1987b) further suggests that if e.g. the angular size of the beam varies in response to the noisy variations in $\dot{M}$, an amplitude modulated component at the beat period between P_1 and P_{orb} may produce a QPO. This beat frequency model fails when applied to DNOs, since it does not account for eclipse-related phase shifts, and it is not really clear why P_1 should not be observed, but it has been more successfully applied to X-ray binaries (e.g. Lamb et al. 1985).

King (1985) proposes a model very similar to the one described in Section 4.1.5: differential rotation of the white dwarf envelope during a DN outburst amplifies existing small magnetic fields, and electrons from a hot corona are channeled onto the white dwarf surface through magnetic flux tubes, producing accretion hot spots. Even a magnetic field too weak to disrupt the disc may destroy axial symmetry of the boundary layer and produce DNOs in this manner. Since only a small fraction of the accreting material is magnetically channeled (the corona has by definition very low density), and since many coronal tubes—leading to many accretion zones—are expected to form, the intensity modulation resulting from this mechanism should be very small.

4.1.5 The Low Inertia Magnetic Accretor Model

Paczynski (1978) was first to qualitatively describe what is now called the low inertia magnetic accretor (LIMA) model; his work was developed by Warner (1995b) and WW02b. During a DN outburst, a surface layer of accreted material forms at the equator of the white dwarf; this equatorial belt has a mass $M_b \sim 10^{-10} M_\odot$, which is about the mass accreted in an outburst. Because it consists of high angular momentum material, and will be, in a low magnetic field system, decoupled from the core, the equatorial belt rotates at higher angular velocity (Ω_b) than the body of the white dwarf. Rotation relative to the core results (through fiction) in a dynamo action which amplifies any seed magnetic field present to the point where it is strong enough to control the inner accretion flow (e.g. King 1985; WW02b). Disc material that is magnetically channeled onto the equatorial belt will form accretion curtains and shocks in the same manner as in IPs; these are observed as DNOs, which in this model represent the spin cycle of the equatorial belt. There is observational evidence for the existence of a hot equatorial accretion belt, spinning more rapidly than the

body of the white dwarf, in VW Hyi after outburst (Sion et al. 1996; Godon et al. 2004). A similar result is found for U Gem (Long et al. 1993; Cheng et al. 1997), as well as WZ Sge and AL Com (Szkody et al. 1998), and possibly for RU Peg (Sion & Urban 2002).

A permanent magnetic field $B \gtrsim 10^5$ G permeating the bulk of a white dwarf is required to enforce solid body rotation (e.g. Katz 1975; WW02b); a field generated by friction in the white dwarf envelope will not significantly contribute to the transport of angular momentum to the core. WW02b show that even at the highest mass transfer rates seen during DN outbursts, a multipole field of $B \gtrsim 2 \times 10^4$ G is sufficient to control the inner accretion flow. Variation in P_{DNO} on an outburst time scale is attributed to the relatively low rotational inertia of the equatorial belt; its angular velocity (and hence P_{DNO}) is governed by the magnetic accretion torque (viscous torques linking the envelope to the core are very low; e.g. Durisen 1973). The LIMA model is thus an extension of the IP pulsation mechanism to systems with lower magnetic field strength; this naturally explains the monoperiodic nature of DNOs, QPO sidebands (like orbital sidebands in IPs) being produced by reprocessing—see Section 4.2.1.

Huang et al. (1996) present spectroscopic observations of the DN VW Hyi in outburst suggesting that the accretion disc is truncated above the white dwarf surface, and that gas flows from the inner edge of the disc onto the white dwarf in a structured manner. More direct evidence of the presence of magnetism in 'non-magnetic' CVs comes from comparison of the eclipse duration and ingress/egress times in X-ray observations of the DN OY Car (made in quiescence, shortly after an outburst) to that in the optical (Wheatley & West 2003). They conclude that the X-ray eclipse is of a small polar region, and that this is the signature of magnetically channeled accretion. Many more clues hint at the presence of weak magnetism in supposedly non-magnetic CVs: the UV delay in DN can be explained if the inner disc is magnetically truncated (Livio & Pringle 1992); Hameury & Lasota (2002) propose that the absence of DN outbursts in VY Scl stars in the low state can be accounted for if the inner disc is eliminated by a weak white dwarf magnetic field (see also Lasota 2004); the recent discovery of magnetic fields of between 2 and 4 kG in a three single DA white dwarfs (Aznar Cuadrado et al. 2004) demonstrates that such low fields are probably common in isolated white dwarfs.

A magnetic field anchored in the equatorial belt is most likely to exist during outburst when greater $\dot{M}_1$ causes high differential rotation. The transience of the magnetic field explains why DNOs are not usually seen in quiescent DN. Systems that do not generate a sufficiently strong field to channel accretion, probably the truly non-magnetic CVs, never have DNOs.

M_b increases during outburst, and the magnetic field strength is variable (these

are not independent effects); if these factors are neglected one obtains $P_{DNO} \propto \mu^{6/7}\dot{M}^{-3/7}$, for a dipole field, and $P_{DNO} \propto \mu^{6/11}\dot{M}^{-3/11}$ for a quadrupole field (Warner 1995b). Using these dependencies together with calculations by Cannizzo (1993), Warner (1995b) obtains loops in the P_{DNO}–I plane that are not unlike those in the diagrams displayed by Patterson (1981). Mauche (1997b) finds from EUV observations $P_{DNO} \propto \dot{M}^{-0.094}$; WW02b shows that the weaker dependence of P_{DNO} on $\dot{M}_1$ is accounted for when variable μ and M_b are included. The inertia of the equatorial belt may cause its rotation period to lag behind that of the inner edge of the disc, but minimum P_{DNO} should still occur near maximum $\dot{M}_1$ (Mauche 1996).

In most DN, DNOs stay present through maximum, implying that the surface layers do not get spun up to the maximum possible angular velocity. The minimum DNO period that can be attained is limited by breakup angular velocity of the primary and is given by

$$P_{DNO_{min}} = 17.2A^{3/2}\left(\frac{R_1}{10^9\ \mathrm{cm}}\right)^{3/2}\left(\frac{M_1}{\mathrm{M}_\odot}\right)^{-1/2}\ \mathrm{s}\ ,$$

where A is the ratio of the equatorial radius of the white dwarf to the volume radius (Warner 1995b); note however that a factor of 1/2 is introduced in the case of two-pole accretion. Using the mass frequency function for isolated white dwarfs (e.g. Bergeron, Saffer & Liebert 1992), it can be shown that the clustering of the observed minimum values of P_{DNO} around 19–29 s is probably a reflection of the mass distribution of the primaries (Warner 1995b; see also fig. 9 of Knigge et al. 1998, and fig. 19 of Patterson 1981). All observed DNO periods are consistent with a model where DNOs result from the rotation cycle of the white dwarf[2] (although of course estimates of M_1 are not available for all the CVs in which DNOs have been detected).

In a DN outburst with fast optical rise, $\dot{M}_1$ only increases about a day after the optical rise. Therefore, in this model, DNOs should not be present during the ascending branch of such outbursts; there are no reports of DNO detections to contradict this expectation.

Warner (1995b) argues that in AH Her the disappearance of DNOs at maximum light is more likely to be the the result of changed accretion geometry, than the magnetosphere being pushed down to the white dwarf surface. Lamb (1988) points out that for $r_0/R_1 < 3$ higher, and less compressible, components of the field geometry (such as a quadrupole component) start dominating the flow. This may

[2]Stiening et al. (1982) detected DNOs on several nights of an outburst of EM Cyg, following the usual period-luminosity relation. The minimum observed DNO period was 14.63 s. With $M_1 = 0.56 \pm 0.05\mathrm{M}_\odot$ (Robinson 1974; Stover, Robinson & Nather 1981), this period is too short to represent Keplerian rotation above the white dwarf surface, or below breakup spin of the white dwarf, even for the case of two accretion zones. However, M_1 for EM Cyg was underestimated; North et al. (2000) find $M_1 = 1.12 \pm 0.08$ $\mathrm{M}_\odot$, which resolves the problem.

explain the reduced sensitivity of P_{DNO} on $\dot{M}_1$ found at maximum of outburst in SS Cyg (Mauche & Robinson 2001).

If the abrupt changes in period seen in phase diagrams reflected changes in Ω_b, they would be accompanied by luminosity changes of

$$\sim 4\pi^2 M_b R_1^2 \frac{\Delta P_{DNO}}{P_{DNO}^3 \Delta t} > 100 \ \mathrm{L}_\odot,$$

(Warner 1995b) where $\Delta t \lesssim 100$ s is the time interval over which the change occurs, and the period changes (ΔP_{DNO}) can be as large as 0.05 s. However, no detectable change in optical or X-ray flux implies that the luminosity involved is $\ll 1$ $\mathrm{L}_\odot$; thus period discontinuities are ascribed to magnetic reconnection events.

Field lines connecting the equatorial belt to a disc annulus that has angular velocity different from Ω_b are wound up. The resulting tension in the field is relieved by reconnection in the magnetosphere (rather than by repositioning of the footpoints of the field in the disc or star, see e.g. Lamb et al. 1983; Livio & Pringle 1992). Ω_b approaches Ω_1 at increasing latitude, therefore reconnection produces accretion curtains feeding disc material to different latitudes on the belt that have angular velocities distributed around the mean angular velocity of the belt. This easily accounts for the period discontinuities seen in phase diagrams, which place the strongest constraints on models of DNOs, and which are not successfully accounted for in other models. WW02b show that the time scale of reconnection is compatible with observations, and that, since $\dot{M}_1$ is most stable near maximum light, the reconnection events, and thus period discontinuities, should occur most infrequently at that time—in agreement with the data.

On the descending branch of outburst, there is a time when r_0 is increasing so rapidly that Ω_b cannot slow down fast enough to maintain near-equilibrium accretion (i.e. r_μ becomes greater than r_{co}). Disc material threaded to the equatorial belt's magnetic field lines is centrifuged outward; the belt thus loses angular momentum to the disc at a higher rate than before, and $\dot{M}_1$ is reduced to almost zero. The rapid increase in P_{DNO} seen in VW Hyi at this stage of outburst (where $s \approx -2$) is accompanied by a complete drop in EUV flux, which supports the propellering scenario (Mauche, Mattei & Bateson 2001; WW02b).

WW02b shows in some detail that the observed properties of DNOs in VW Hyi (P_{DNO}, the interval between discontinuities in P_{DNO}, and the period-luminosity relation) are all compatible with the LIMA model.

The sinusoidal nature of DNOs has been used as evidence in favour of pulsations rather than hot spots on the white dwarf or in the disc (e.g. Robinson 1976); however, if the pulsed light reaches us mainly through reflection, any non-linearity of the intrinsic variation can be smoothed out, independent of the orbital inclination (see e.g. Petterson 1980). Where DNOs are directly observed (e.g. in UX UMa) sinusoidal

pulse profiles are understandable if the accretion zones are long arcs running around the equatorial belt.

The discs of NLs are close to equilibrium, but they do vary in brightness on time scales of days to weeks; these changes are probably mirrored by $\dot{M}_1$. However, changes in accretion rate will not immediately appear as changes in P_{DNO}, there will be a delay of the order of the drift time scale of the disc (Warner 1995b).

Using the approximation $P_{DNO} \propto \mu^{6/7}\dot{M}^{-3/7}$, a value of $s \sim -1.1$ is obtained for high luminosity systems (in which brightness depends on accretion rate as $dM_v/d\log\dot{M} \approx -1$; Smak 1989). This is consistent with the value of s suggested by observations of IX Vel, but more sensitive than what is seen in UX UMa.

Knigge et al. (1998) point out that, in the LIMA model, relatively more DN than NLs should have DNOs, since NLs have on average a higher $\dot{M}$ and so smaller magnetospheres, and many NLs have higher $\dot{M}$ than DN in outburst (Warner 1995a). Table 1 of W04 shows that this is indeed the case.

The frequency doubling seen in SS Cyg and VW Hyi is not yet properly understood (see the discussion in W04). In the case of SS Cyg frequency doubling occurs at the brightest phase of outburst, and one may speculate that it represents a transition from single- to two-pole accretion, since higher polarities increase in importance close to the white dwarf surface. Frequency doubling in the late decline from outburst in VW Hyi may result from a change in viewing geometry: the spin modulation of the IP XY Ari is double peaked in quiescence, but single peaked in outburst; this is interpreted as obscuration of the lower magnetic pole by the inner disc when r_0 decreases during outburst (Hellier et al. 1997). Conversely, when the the inner disc is retreating late in outburst, the second accretion curtain (feeding the lower pole) will become visible beyond the inner disc rim, perhaps explaining frequency doubling in VW Hyi (see also Warner & Woudt 2004). In V2051 Oph, the subharmonic to the 28.06 s DNO may indicate that there are two accretion zones on the equatorial belt which is rotating at 56.12 s (WW02b).

4.2 Quasi-periodic Oscillations

Since the discovery of QPOs, it has been mostly agreed that they originate in the disc; Patterson et al. (1977) and Robinson & Nather (1979) argue that QPO periods are too short to be ascribed to the secondary, while their low coherence rules out the primary, so that the disc must necessarily be the source of the QPOs. Papaloizou & Pringle (1980), however, showed that pulsations in the surface layers of a rapidly rotating white dwarf can in fact reproduce both the time scale and coherence of QPOs. The model of hot spots in Keplerian rotation around the white dwarf (Bath 1973) may produce the correct coherence time of QPOs, but note that the

longer periods of QPOs require spots to be farther out in the disc, where significant obscuration by the white dwarf becomes more difficult to achieve. Several of the disc pulsation mechanisms discussed in Section 4.1.2 are promising explanations for QPOs. If a model like those proposed by Cox & Everson (1982, 1983) holds for QPOs, then you would expect to see a decrease in QPO period at shorter wavelengths (since the periods are proportional to Keplerian period, and the disc temperature increases at decreasing radius; Warner 1995a) this observation has not been made.

Since several mechanisms are capable of producing QPOs, there may well be no single physical cause for the phenomenon. Specifically, QPOs seem to be a natural consequence of accretion onto a magnetic star (see e.g. Goodson & Winglee 1999; Goodson, Böhm & Winglee 1999; Uzdensky 2002; Uzdensky, Königl & Litwin 2002; Romanova et al. 2003, 2004; Spruit & Taam 1993). Goodson & Winglee (1999) find, in the context of young stellar objects that are magnetically accreting from the inner edge of a disc, that r_0 varies quasi-periodically; each inward oscillation results in an innermost ring of disc material being stripped off and quickly accreting, so that the system luminosity is modulated by quasi-periodic accretion events. Their results are of special interest because estimates of the radial infall velocity of the accreting ring (v_r) places it at $\sim 10^{-2} v_K$; if one identifies the Keplerian period at the inner disc edge with P_{DNO}, this is equivalent to $P_{QPO}/P_{DNO} \sim 100/2\pi \approx 16$. Evaluating equation 9 of Goodson & Winglee (1999) with parameters suitable to a high $\dot{M}$ CV gives similar results; e.g., for $M_1 = 0.6$ M$_\odot$ and $\dot{M}_d = 1.0 \times 10^{-9}$ M$_\odot$/y, using the standard α-disc model of Shakura & Sunyaev (1973) with $\alpha = 0.5$ at the inner disc edge, $v_r \approx 10^{-2} v_K$ requires a white dwarf magnetic field $\approx 1 \times 10^5$ G. Quasi-periodic accretion events could produce QPOs with peaked, flare-like profiles, as seen for a few kilosecond QPOs (e.g. Fig. 5.26), but the time scale of such modulations is more in keeping with DNO-related QPOs.

4.2.1 DNO-related QPOs

Motivated by the work of Carrol et al. (1985) and Lubow & Pringle (1993), WW02b propose that QPOs arise from the non-axisymmetric $m = 1$ g-mode disc pulsations, which Lubow & Pringle (1993) conclude have the best propagational properties in the inner disc. This pulsation comprises a vertical thickening of selected annuli of the disc over an extended range of azimuth; the thickening, or bulge, propagates retrogradely in the frame of rotation of the disc, but at less than the Keplerian angular velocity, so that it travels progradely in an inertial frame.

WW02b argue that the perturbation is most likely to be excited in the inner disc by interaction with the white dwarf's magnetic field. A problem with models that ascribe QPOs to disc pulsations is that, since the whole disc is potentially unstable to vertical oscillations, the fact that a QPO often has a definite mean period for hours

on end is hard to explain. However, reconnection of magnetic field lines (which is an inevitable consequence of the twisting and shearing of the field in an accretion disc) may drive oscillations at preferred radii (Tajima & Gilden 1987).

In the deceleration zone (the annulus corresponding to $r_A \leq r \leq r_{co}$, where the corotation radius is now defined as $r_{co} = GM_1/\Omega_b^2$), the angular velocity of the disc material exceeds that of the magnetic field lines, so that the field lines are dragged forward by the plasma, which exerts a spin-up torque on the white dwarf via the equatorial belt. It is here that disc pulsations are most likely to be excited. The magnetic axis is generally inclined with respect to the spin axis of the primary and equatorial belt (an aligned field will produce annular accretion zones round the poles and will not generate the anisotropic radiation pattern observed as DNOs). Thus magnetic field strength varies with azimuth in the deceleration zone; plasma attached to the strongest field lines in this annulus experiences a larger deceleration than plasma at the same radius but threaded by weaker field lines, resulting in material piling up and a shock being created, which heats and thickens the disc around the azimuth where the field is strongest. The twisting of field lines will cause them to bend over, and so provide vertical magnetic pressure support that may assist in lifting plasma out of the orbital plane in this region. The result of these effects is a region where the disc is denser and vertically thicker (a blob). The blob grows until its rotation relative to the magnetosphere of the equatorial belt causes the field lines threading it to reconnect at an energetically more favourable azimuth. Reconnection occurs when the blob has rotated through an angle of about 2π relative to the unstressed position of the field (Lamb et al. 1983). The perturbation resulting from the sudden release of the blob launches a traveling wave (or QPO wall) which propagates at a speed determined by the local conditions in the disc.

Since the magnetosphere is small, the inner disc edge is close to the white dwarf, and a relatively large fraction of the radiation from the central source can be intercepted by the QPO wall. No large intrinsic luminosity variation is needed, instead the system luminosity is modulated as the wall obscures the constant luminosity radiation from the white dwarf, casts a shadow over the disc surface, or presents varying surface area of its illuminated inner face. The relative importance of these effects depends on the inclination, and, in a given system, is also time dependent, since the amplitude and profile of the traveling wave may change on relatively short time scales.

WW02b show that the observed QPO amplitudes are energetically feasible in a model where QPOs are produced in this manner. The role played by obscuration is illustrated in e.g. fig. 2 of WW02b; they also point out that quasi-periodic obscuration of the central source should be seen in the absorption spectrum, and that this may be what caused deep, narrow absorption cores, present in one spectrum of

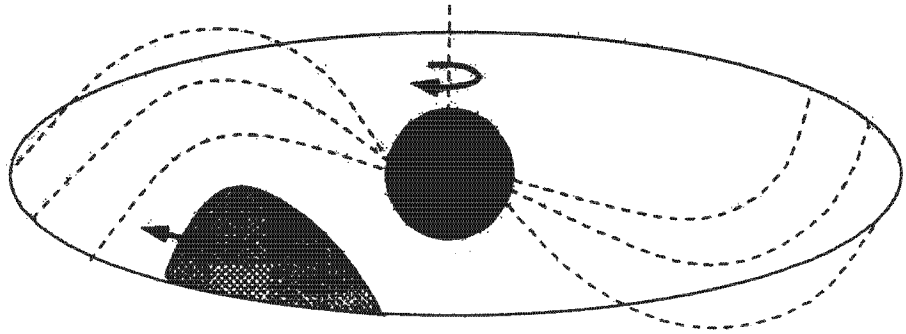

Figure 4.1: A schematic representation of the unified model of DNOs and QPOs. The white dwarf spin axis, equatorial belt, and traveling wave at the inner disc edge are shown. From Hellier (2004).

VW Hyi at supermaximum, but absent in another taken 10 min. later (Huang et al. 1996).

A traveling wave excited in the way described here may damp out quickly, but the next reconnection event regenerates it. WW02b estimate the time scale for reconnection as $T_R = 2\pi/(\Omega_K(r_0) - \Omega_b)$; then assuming a 1 : 1 resonance between reconnection events and the orbit of the blob leads to

$$\frac{P_{QPO}}{P_{DNO}} = \frac{\omega_s}{1-\omega_s} \ . \tag{4.1}$$

Therefore ω_s (which is here defined as $\omega_s = \Omega_b/\Omega_K(r_0)$) in the range 0.91–0.95 is required to account for the observed $10 \lesssim R \lesssim 20$. Equation 4.1 implies that for roughly constant ω_s, P_{QPO} is roughly proportional to P_{DNO}, as observed in VW Hyi, and—by the fact that $R \approx 16$ in all observations—in CVs generally.

All rapid variability in some light curves appears to be QPOs and/or DNOs, with no obvious contribution by flickering (e.g. fig. 1 of WW02a; Fig. 5.38). If flickering is caused in these systems by magnetic instabilities in the inner disc, (see e.g. Bruch 1992), then perhaps when a more organized magnetic structure makes the excitation of QPOs possible, the flickering activity is suppressed. The usual absence of QPOs in quiescence may be understood if a magnetic field strong enough to excite them in the manner described here is generated only in outburst; the rare observations of QPOs in quiescence then implies that some magnetic influence can occur also in the low $\dot{M}$ state.

The model of QPOs discussed here is illustrated in Fig. 4.1, together with the LIMA model of DNOs. Note however that it is not obvious what type of accretion geometry should be expected close to the white dwarf surface.

Reprocessing of the rotating DNO beam by the traveling wave can generate the second set of DNOs, or QPO sidebands, the frequency of the QPO sideband is the

beat between the DNO and QPO periods: $P_{DNO2} = (1/P_{DNO} - 1/P_{QPO})^{-1}$. Several detections of this reprocessed component constitutes the strongest observational support for this model of QPO production; this was first proposed by Patterson (1980) to explain a phenomenon very similar to a double DNO or lpDNO in WZ Sge. The waveform of the QPO sideband is a convolution of the profile of the QPO wall and the DNO beam, and if the traveling wall has an irregular or non-sinusoidal profile, the QPO sideband may be non-sinusoidal, again as seen in a few instances[3]. Note that in most VW Hyi observations the DNO amplitude is not modulated by the QPO, and there is no QPO side band; this is explained by the obvious fact that, even in a given system, the shape and height of the QPO wall is variable. The observed QPO coherence does not limit the coherence of the QPO sideband, since the apparent stability of the QPO wall depends on the viewing geometry, and it may be more robust as seen from near the disc centre; furthermore, even if the traveling wave only lasts for a few orbits, it corresponds to many more DNO cycles.

It may be possible to determine the radial distance of the rotating wall from observations of large amplitude QPOs in a deeply eclipsing system (e.g. V893 Sco). However, studying the effect of eclipse on the phase and amplitude of a QPO will be more complicated than for DNOs, because of the lower coherence and longer periods of QPOs.

4.2.2 Kilosecond QPOs

It is proposed by Patterson et al. (2002) that the kilosecond QPOs in SW Sex stars may represent the rotation of an accreting, strongly magnetic white dwarf (see also Groot, Rutten & van Paradijs 2001; Hoard et al. 2003); in other words these systems are interpreted as IPs in which, for some reason, the stable rotation of the primary is observed as a quasi-periodic modulation. The authors show that the QPO periods are close to the value expected for the white dwarf spin period in these systems, and speculate that a factor such as high $\dot{M}$ may explain why the observed modulations are only quasi-periodic. This effect is seen in the DQ Her star AE Aqr: its strictly periodic 33 s oscillation (identified with the rotation of the primary) appears as a quasi-periodic signal near 35 s in the high $\dot{M}$ state (Patterson 1979b, 1994). Furthermore, there are indications in the photometry of a few SW Sex stars that a periodic signal may underlie the QPOs (Patterson et al. 2002). Additional support for this interpretation comes from the detection of circular polarization weakly modulated at periods close to the QPO periods in two

[3]Marsh & Horne (1998) considered reprocessing as the cause of the double DNO in their observations, but concluded (incorrectly) that a non-linear response of reprocessing efficiency to increasing intensity of the incident beam is required to produce the non-sinusoidal profile of the QPO sideband.

SW Sex stars, V795 Her and LS Peg (Rodríguez-Gil et al. 2001, 2002). However, it remains to be demonstrated that the variability in polarization in these two objects is stable enough to be ascribed to white dwarf rotation.

Patterson et al. (2002) include TT Ari with its very well studied ~20 min. QPO (Smak & Stepien 1969; Mardirossian et al. 1979, 1980; Sztajno 1979; Jensen et al. 1983; Semeniuk et al. 1987; Udalski 1988; Hollander & van Paradijs 1992; Tremko et al. 1996; Kraicheva et al. 1999) in a list of SW Sex stars with kilosecond QPOs, despite the fact that it does not meet all the requirements for classification as an SW Sex star, pointing out that TT Ari is in many respects similar to NLs in this class. However, TT Ari differs from the other objects in this list in that it has been observed (on a few rare occasions) to have DNOs. DNOs with periods in the range 32 to 43 s were detected in TT Ari on two different nights by Mardirossian et al. (1979, 1980); their light curves are of high quality, and the detection was confirmed by Sztajno (1979), so that there is no obvious reason to doubt the result. Jensen et al. (1983) also observed a ~32 s DNO in optical and X-ray light curves of TT Ari (this observation was unusual, because a ~12 s oscillation coexisted with the ~32 s signal, furthermore the oscillations were detected in the waveband 0.15 to 4.5 keV—higher energy than that at which DNOs are usually seen). If the LIMA model applies to these DNOs, TT Ari's white dwarf magnetic field cannot exceed 10^5 G by much.

The same argument applies to all systems in which DNOs have been observed, therefore in e.g. HX Peg, WX Hyi, and VZ Pyx, the kilosecond QPOs must have a different origin. Some speculation on the physical cause of these QPOs may be found in W04.

4.3 Longer Period Dwarf Nova Oscillations

WWP03 interpret lpDNOs as magnetically channeled accretion onto the polar regions of the body of the white dwarf, rather than onto the equatorial belt. In other words, the lpDNO modulation reflects the spin cycle of the primary, which explains why P_{lpDNO} does not usually scale with $\dot{M}$, as well as the independent behaviour of DNOs and lpDNOs.

In a low magnetic field white dwarf, the high angular momentum material accreted at the equator will spread across the stellar surface, resulting in the outer layers rotating differentially in latitude, so that lpDNOs are (unlike the high frequency modulations in IPs) only quasi-periodic.

Assuming two pole accretion, this interpretation is consistent with—admittedly, very uncertain—values of the white dwarf rotation periods for the DN VW Hyi, U Gem, and OY Car; see WWP03 for details. The existence of double lpDNOs also

support a rotating beam model. The period doubling observed in EC2117 may be ascribed to a transition from two- to single-pole accretion; the opposite process may be the cause of frequency doubling of the lpDNO in VZ Pyx; alternatively, the VZ Pyx data may be explained by changing viewing geometry, as proposed for VW Hyi (see Section 4.1.5).

Chapter 5

Observational Results

In a search for DNOs, lpDNOs, and QPOs, high speed photometry of CVs was done at the Sutherland site of the South African Astronomical Observatory using the 30-, 40-, and 74-in. telescopes and the University of Cape Town charge-coupled device (UCT CCD), a frame-transfer CCD. O'Donoghue (1995) describes the UCT CCD, Warner (1988) discusses many aspects of high speed photometry and its application to the study of CVs. Visual magnitudes reported by members of the American Association of Variable Star Observers (AAVSO) and VSNET made it possible to catch DN in outburst and AM CVn stars in their high states.

In almost all cases the observations were made in white light; with the UCT CCD this gives photometry with an effective wavelength similar to Johnson V, but with a very broad bandpass. This, together with the non-standard flux distribution of CVs, means that magnitude calibration (achieved by observing hot subdwarf and white dwarf standard stars) and extinction corrections are only approximate (accurate to about 0.1 mag, for the mean magnitude). Since only short time scale variability is of interest here, absolute calibration is not an important concern. Among the advantages of CCD detectors over photomultiplier and image tubes is that CCDs usually allow for differential photometry, so that high quality data can be obtained even in non-photometric conditions.

The images were reduced with a program called **DuPhot**, which is an adaptation of DoPHOT (Schecter, Mateo & Saha 1993). The program calculates an aperture magnitude and a profile-fitted magnitude for each star it finds in a number of user-defined windows on the CCD frames. The light curves were searched for quasi-coherent signals by calculating Fourier amplitude spectra with Darragh O'Donoghue's program EAGLE. This program computes the discrete Fourier transform (Deeming 1975) of a light curve for a specified number of frequencies. Appendix A gives a brief account of discrete Fourier analysis.

Oscillations were detected in 20 DN, 2 NLs, and 2 AM CVn stars; the rest of this

chapter presents and discusses the results for these objects, Appendix B lists null results.

5.1 TU Men

TU Men is an SU UMa type DN (Stolz & Schoembs 1981) with a trimodal distribution of outburst widths, normal outbursts lasting ~1 d (narrow) or ~8 d (wide), and superoutbursts lasting ~20 d. Supermaximum is brighter than 12.5 mag, and the supercycle is ~196 d; normal outbursts have maxima of $m_v \approx 13.5$ mag, and recur after ~37 d (Bateson 1979a). With $P_{orb} = 2.813$ h (Stolz & Schoembs 1984; Mennickent 1995) TU Men was for a long time the only SU UMa star known with an orbital period above the period gap[1].

The December 2002 outburst of TU Men was remarkable in that, judging by its duration and amplitude (as well as by its position in the supercycle) it may have been a superoutburst, but no superhumps were seen. Perhaps the amplitude given for normal outbursts needs to be revised. High speed photometry was carried out at Sutherland on seven nights of this outburst, and again during the December 2003 outburst; Table 5.1 is a log of the observations.

Rapid oscillations were detected on only one night of each outburst (run S6695

Table 5.1: Log of the observations of TU Men during its December 2002 and 2003 outbursts. A V filter was used in the first four runs; the rest of the observations were made in white light.

Run No.	Date at start of night	Start time HJD = 2450000.0+	Length (h)	t_{int} (s)	Telescope	V (mag)
S6674	17 Dec. 2002	2626.42208	2.65	4, 5	40-in.	11.9[a]
S6677	18 Dec. 2002	2627.33669	1.52	6	40-in.	12.0[a]
S6681	19 Dec. 2002	2628.31750	0.80	6	40-in.	12.0[a]
S6686	22 Dec. 2002	2631.39517	2.83	5, 6	40-in.	12.4:[a]
S6688	23 Dec. 2002	2632.27328	0.90	5, 6	40-in.	12.6
S6695	26 Dec. 2002	2635.27795	4.60	1.5, 5, 6	74-in.	15.0
S6697	27 Dec. 2002	2636.27829	1.08	5	74-in.	16.2
S7186	22 Dec. 2003	2996.36461	1.43	5, 6	40-in.	12.2
S7188	23 Dec. 2003	2997.33832	2.10	5	40-in.	12.3
S7193	24 Dec. 2003	2998.46033	1.62	5	40-in.	12.6
S7196	26 Dec. 2003	3000.33728	3.25	5	40-in.	14.4
S7198	27 Dec. 2003	3001.33262	1.73	6	40-in.	16.0
S7203	28 Dec. 2003	3002.38487	1.03	7	40-in.	16.6
S7207	29 Dec. 2003	3003.36255	1.50	6	40-in.	16.7:

Notes: t_{int} is the integration time; ':' denotes an uncertain value; [a]taken with a V filter.

[1]There are now three more SU UMa stars known with periods above the gap, they are ES Dra, V478 Her and VW Vul (Downes et al. 2001).

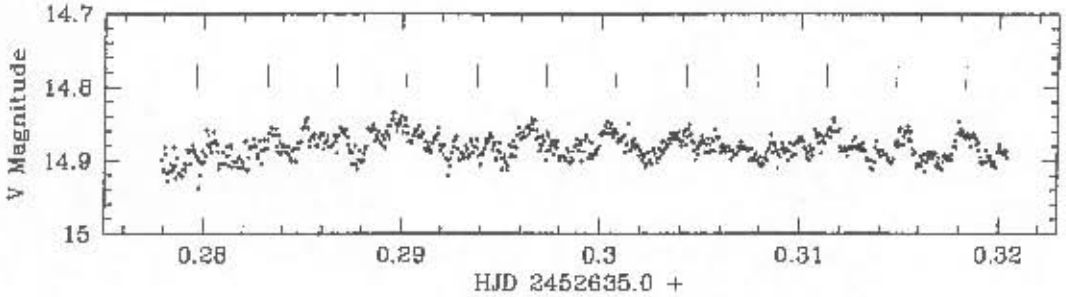

Figure 5.1: The first hour of run S6695, a QPO is clearly visible. The vertical bars at the top of the graph are equally spaced at intervals of 303.6 s, which is the average QPO period. This light curve has been corrected to first order for atmospheric extinction, and a linear trend has been removed.

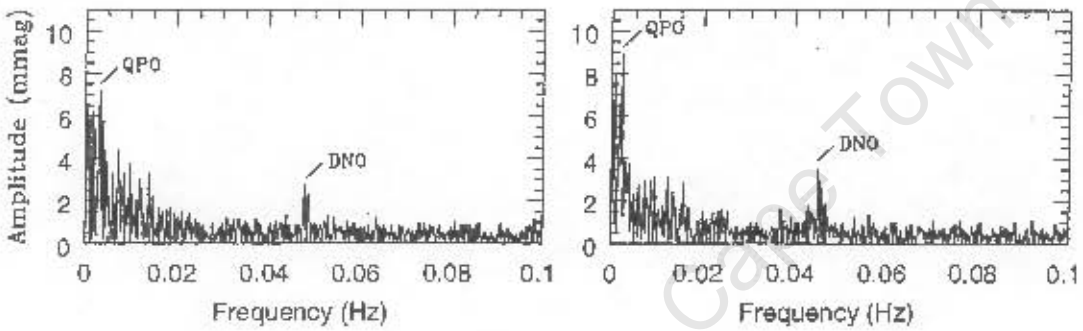

Figure 5.2: Left: the Fourier transform of the light curve shown in Fig. 5.1. A Fourier transform of the same data appeared as fig. 9 of WWP03. The peaks marked QPO and DNO are at 303.6 s and 20.91 s respectively. Right: The Fourier transform of a ~1 h section of run S6695 starting almost 2 h after the end of the part of the light curve shown in Fig. 5.1. The QPO is now at 419.5 s and the DNO at 22.20 s; the DNO amplitude is greater than before.

and S7196), in both cases the system was on the decline from outburst. Fig. 5.1 is the light curve of the first hour of run S6695. A QPO at 304 s can be seen directly in the light curve.

The left hand panel of Fig. 5.2 is the Fourier amplitude spectrum of this section of data, showing a DNO at ~21 s which is not directly visible in the light curve. Apart from the noisy DNO peak, the amplitude spectrum has a flat continuum above ~0.025 Hz, caused by atmospheric scintillation and photon counting noise. The smooth rise in continuum power at frequencies less than 0.025 Hz (on which the excess power attributed to the QPO is superimposed) is the signature of flickering. These two features are shared by the amplitude spectra of most CV light curves. The right hand panel of Fig. 5.2 is the Fourier transform of another 1 h long section of data starting about 2 h after the end of light curve shown in Fig. 5.1. By this time

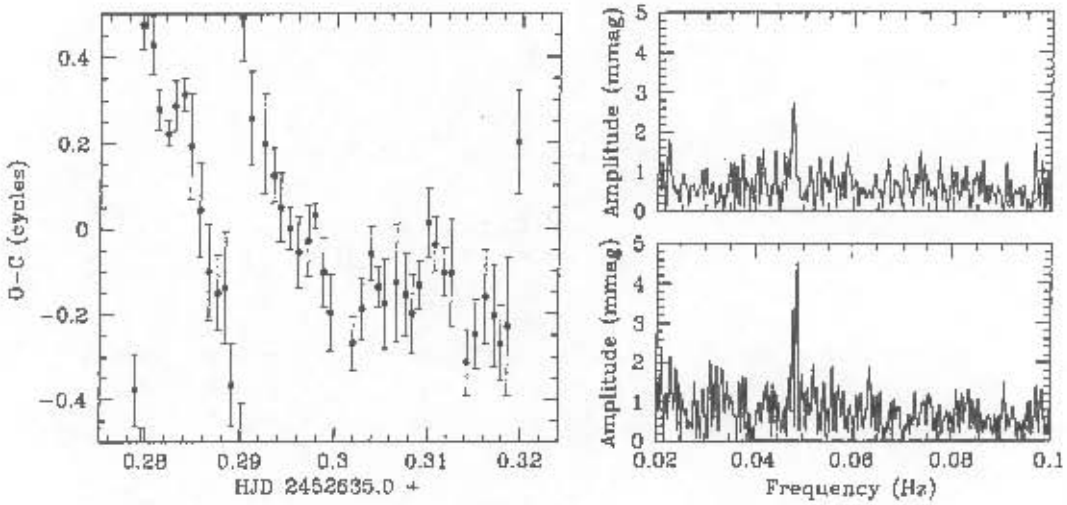

Figure 5.3: Left: The $O-C$ diagram of the DNO in the first hour of run S6695, calculated by comparing ~7 DNO cycles to a sinusoid (period 21.00 *s*) with 50% overlap between consecutive points; 1σ error bars are shown. A few points with very low amplitude (and thus large uncertainty) were omitted. Right: The Fourier transform of the light curve from HJD 2452635.278 up to 2452635.300 (bottom) and from HJD 452635.300 up to 2452635.320 (top). The DNO period changes from 20.55 s to 21.00 s. These periods were determined by fitting a sinusoid to the oscillation by non-linear least squares.

the QPO and DNO periods had increased to 420 s and 22.20 s respectively while TU Men had faded by 0.23 mag. Non-linear least squares fitting gives a DNO amplitude of 3.5 mmag, but note that the true amplitude must be greater (for at least part of the time) since period, amplitude, and phase changes reduce the amplitude of the best-fit fixed period sine function to an oscillation that is only quasi-periodic (see e.g. Fig. 5.11). The DNO disappears (or becomes too incoherent or of too low amplitude to detect) before the end of the run.

Closer inspection of the first 1-h section of light curve shows that the double peaked structure of the DNO feature in the left hand panel of Fig. 5.2 is caused by a changing period, rather than the simultaneous presence of two oscillations. This is evident in the observed minus calculated ($O-C$) phase diagram which is shown on the left hand side of Fig. 5.3. The $O-C$ values were obtained from fitting a sine function with a period of 21.00 s (the test period), with variable amplitude and phase, by least squares to groups of ~7 DNO cycles, and comparing the resulting best-fit observed time with the time calculated from the constant phase sinusoid. In this case an overlap of 50% between consecutive points was allowed. Note that a positive (negative) value of $d(O-C)/dt$ implies a DNO period longer (shorter) than the test period; $d^2(O-C)/dt^2$ greater (less) than 0 implies an increasing (decreasing) DNO period. The negative slope of $O-C$ as a function of time in the first half

of the plot therefore indicates a period that is constant (to within the accuracy of the measurement) and shorter than the test period used (21.00 s) in calculating expected times. At HJD 2462635.3 the period increases to be more consistent with the test period. Fourier transforms calculated separately for the first and second halves of the light curve (right hand side of Fig. 5.3) confirm that the period was increasing. The bottom panel on the right of Fig. 5.3 is a Fourier transform of the data spanning HJD 2452635.278 to 2452635.300; the DNO is at 20.55 s. Taking the observations from HJD 452635.300 up to 2452635.320 gives a single peak at 21.00 s (top panel of the right hand side of Fig. 5.3). Note also that the DNO amplitude is lower in the second half of the first hour of observations.

On the decline from the December 2003 outburst (run S7196) a DNO was again detected, on this night the amplitude was slightly lower than the previous year. The DNO period was 16.57 s (with TU Men at $V = 14.4$). This was the only rapid oscillation seen in the second outburst.

This is the first time that DNOs and QPOs have been observed in TU Men. The increase in P_{DNO} as the system fades is typical; evolution of a QPO period has also been reported before (e.g. in VW Hyi; WW02a).

5.2 RU Peg

RU Peg is a U Gem type DN with outbursts of about 3 mag recurring every 75–85 d and has an orbital period of 8.990 h (Stover 1981). As mentioned in Chapter 3, RU Peg is the CV in which QPOs were first recognized. Patterson et al. (1977) found a QPO with a period near 50 s present at the same time as a signal at ~12 s. The 12 s signal was detected on four nights and was believed to be a DNO. Patterson et al. used integration times of 4 s (with no dead time between integrations) throughout and they can't have had much reason, in 1977, to suspect that their time resolution may have been too low. It is now known, however, that DNOs can have periods as short as 2.8 s (van Teeseling 1997). WWP03 suggest, on the grounds that the value of R for RU Peg is unusual and that the amplitude is uncommonly low (~0.6 mmag), that the 12 s signal seen in RU Peg might have been a beat between a DNO at 2.97 s and the 4 s integration time (see also Section 6.2.1).

The matter can be resolved by observing at very high time resolution or, alternatively, by using different, incommensurate integration times. In the hope of doing this, I observed the July 2003 outburst of RU Peg using the 40-in. reflector at Sutherland, Table 5.2 gives the observing log. All these observations were made under photometric conditions, in Cousins U light (because the system was too bright to observe in white light).

Fig. 5.4 shows the visual AAVSO light curve of this outburst, crosses are the

Table 5.2: Log of the observations of RU Peg.

Run No.	Date at start of night	Start time HJD = 2452000.0+	Length (h)	t_{int} (s)	Telescope	U (mag)
S7009	16 Jul. 2003	837.53233	4.52	5, 4, 2	40-in.	9.0
S7010	18 Jul. 2003	839.56055	3.17	5, 4	40-in.	9.2
S7011	19 Jul. 2003	840.53717	3.93	5, 4, 3, 1	40-in.	9.4
S7012	20 Jul. 2003	841.53055	3.87	5, 4, 2	40-in.	9.5
S7013	21 Jul. 2003	842.53382	1.88	4	40-in.	9.7
S7016	22 Jul. 2003	843.43586	4.13	5, 4	40-in.	9.8
S7021	23 Jul. 2003	844.53042	4.02	6, 5	40-in.	10.1
S7026	25 Jul. 2003	846.46600	1.72	4	40-in.	10.7
S7031	26 Jul. 2003	847.52329	3.57	5	40-in.	11.0

Note: t_{int} is the integration time.

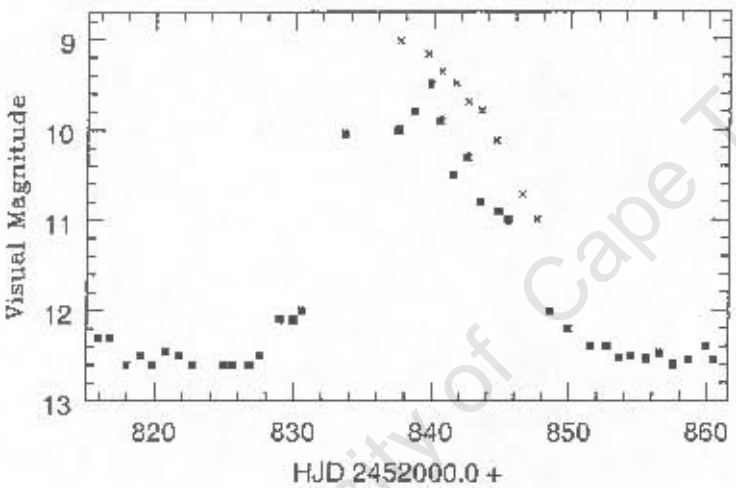

Figure 5.4: The July 2003 outburst light curve of RU Peg based on visual estimates by the AAVSO (squares). Superimposed are the nightly averages of the Sutherland observations (crosses).

nightly averages of my U band observations. The differences between the AAVSO and Sutherland data points are not unexpected, since the observations sample different wavelength bands, and $U - B < 0$.

No DNOs were found in the first night's light curve (the upper limit on the amplitude of a detectable DNO in this run is ~0.7 mmag). The Fourier transform of an 85 min. section is shown as the left hand panel of Fig. 5.5. There appears to be some excess power, probably the result of a QPO, at frequencies between 0.013 and 0.021 Hz (periods between 77 and 48 s). This band of power is not unlike that marked as caused by a QPO in fig. 3 of Patterson et al. (1977).

A shorter section of this part of the observation is displayed in Fig. 5.6. This illustrates the difficulty in detecting low amplitude QPOs—they are not easy to discern in the light curve and Fourier analysis is nearly blind to signals of low coherence, since it represents a light curve as sinusoidal components of constant

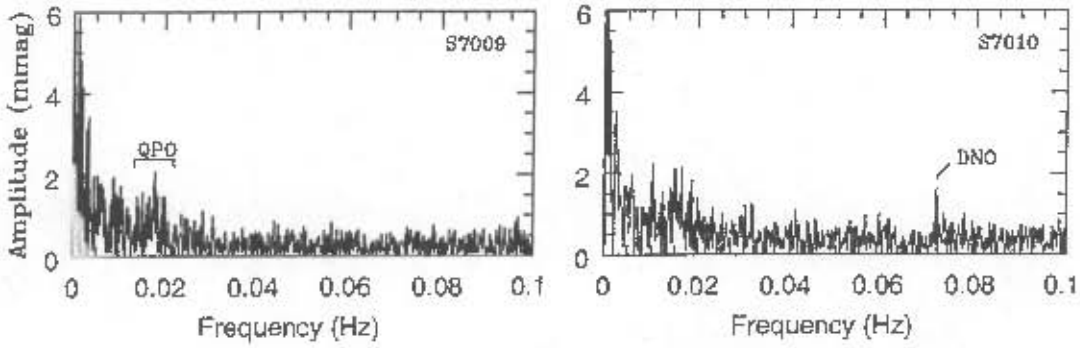

Figure 5.5: Left: The Fourier transform of an 85 min. section of run S7009; it shows some evidence of a QPO, namely a broad band of excess power centred on ~0.017 Hz. Right: The Fourier transform of part of the 18 July (S7010) data. A DNO is (just barely) visible at 13.94 s; the QPO period is near 60 s.

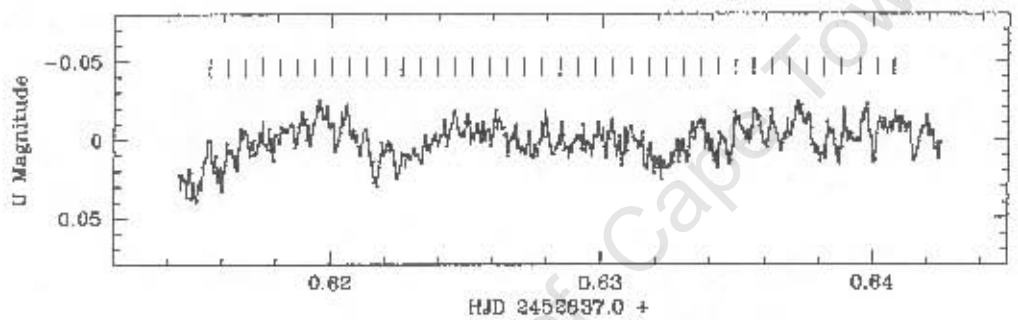

Figure 5.6: A short section of the 16 July light curve (run S7009) of RU Peg after removal of the mean and some low frequency modulations. The points are connected to guide the eye; bars at the top of the graph are equally spaced at intervals of 55.92 s, which is the mean oscillation period in this part of the light curve.

frequency and amplitude. One would be a lot more hesitant to call this a QPO if ~50 s QPOs had not been detected in this system before (Patterson et al. 1977). Of all the QPOs I claim to detect in RU Peg, this one is by far the most questionable.

The right hand panel of Fig. 5.5 is the Fourier transform of a 52 min. section of the 18 July light curve (run S7010). It shows the presence of a DNO at 13.94 s with an amplitude of 1.6 mmag (the period and amplitude were obtained from non-linear sinusoidal least squares fitting). There is also a broad hump of power centred this time on ~0.015 Hz, again indicating the presence of a QPO. The DNO was detected only in this short section of run S7010, which was taken with 5 s time resolution. In the rest of the run the DNO—if it was present—had an amplitude less than 0.8 mmag, so that it was not possible to determine whether the observed period changed when the integration time was changed, i.e. it is not known whether the

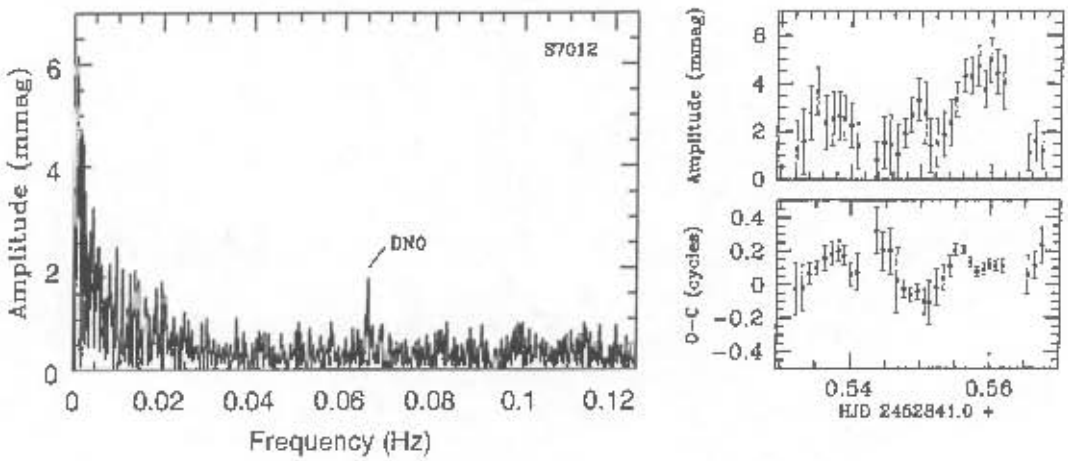

Figure 5.7: Left: The Fourier transform of a 58 min. section of run S7012 after a second order polynomial trend was removed. The DNO period is 15.30 s. There is no evidence of a QPO in these data. Right: The amplitude and $O-C$ diagram of the DNO in run S7012 relative to a fixed period of 15.03 s using ~16 DNO cycles per point, and with 67% overlap between consecutive points. A few points of very low amplitude are not shown. Notice that the amplitude is large for only about 12 min., and that it becomes very low towards the end of this part of the observation.

observed peak is a DNO or a beat between a DNO and the integration time.

A QPO at around 149 s (again of fairly low coherence) was found in the 19 July light curve (run S7011), there was no DNO present. This QPO period is already quite different from what has been seen in RU Peg before.

On the next night (run S7012) no QPO was found, but there was a 15.03 s DNO present in part of the run. The left hand panel of Fig. 5.7 is the Fourier transform of a 58 min. section of this run which was taken with 4 s time resolution. The best-fit DNO amplitude is 1.8 mmag but the amplitude diagram (top right hand panel of Fig. 5.7) shows a much greater amplitude for part of the time. The $O-C$ diagram (lower right hand panel of Fig. 5.7) shows typical DNO variability, but with no large period changes. The DNO was not detected in any other part of the run (Fig. 5.7 shows that the amplitude is already getting very small towards the end of this section of the light curve). So again, it was not possible to see whether the observed peak shifted when the integration time was changed.

The lowest frequency signals that could beat with the integration time to produce the peak seen in run S7010 are at 3.68 s and 7.80 s. For run S7012 these aliases have periods of 3.16 s and 5.45 s. It seems very unlikely that higher frequency DNOs would produce signals below the Nyquist frequency at large enough amplitude to be detected. Note e.g. that if a DNO was present in S7012 at 2.31 s (the alias corresponding to $2/t_{int} - 1/15.03$ s, where t_{int} is the integration time) the observed

amplitude would be a factor of $(\sin x)/x$ smaller than the true amplitude, where $x = \pi t_{int}/P_{DNO}$. The observed amplitude was, for a while, at least as large as 3 mmag (see Fig. 5.7). This would imply, if the observed signal was a beat, that the true amplitude was greater than 22 mmag. DNOs at such large amplitude are rare, but not unheard of (see e.g. Warner et al. 1989; WW02a). Still, the amplitudes of the ∼14 and ∼15 s oscillations are typical of DNOs or lpDNOs whereas that of the 12 s signal seen by Patterson et al. (1977) was unusually low. A further constraint is that, since the observations were made on the decline from outburst, the DNO period should be longer in S7012 than in S7010 (see Section 3.1). This leaves the possibility of a DNO at 3.68 s in S7010 and at 5.45 s in S7012.

Arguing that $P_{QPO}/P_{lpDNO} \approx 4$ one could conclude, for $P_{QPO} \approx 50$ s, that the 12, 14 and 15 s signals are all lpDNOs (WWP03). This argument fails for the QPO periods observed later in the outburst. Assuming that the 14 and 15 s periods are not beats with DNOs above the Nyquist frequency, the period changed by more than 7% while the system faded by 0.32 mag in U. This period change is quite normal for a DNO, but the period of an lpDNOs is usually less sensitively dependent on luminosity (of course, lpDNOs are not yet a very well studied phenomenon; furthermore, in Section 5.4, I present an example of a system in which P_{lpDNO} does depend sensitively on luminosity). It is also possible that, e.g., the observed period

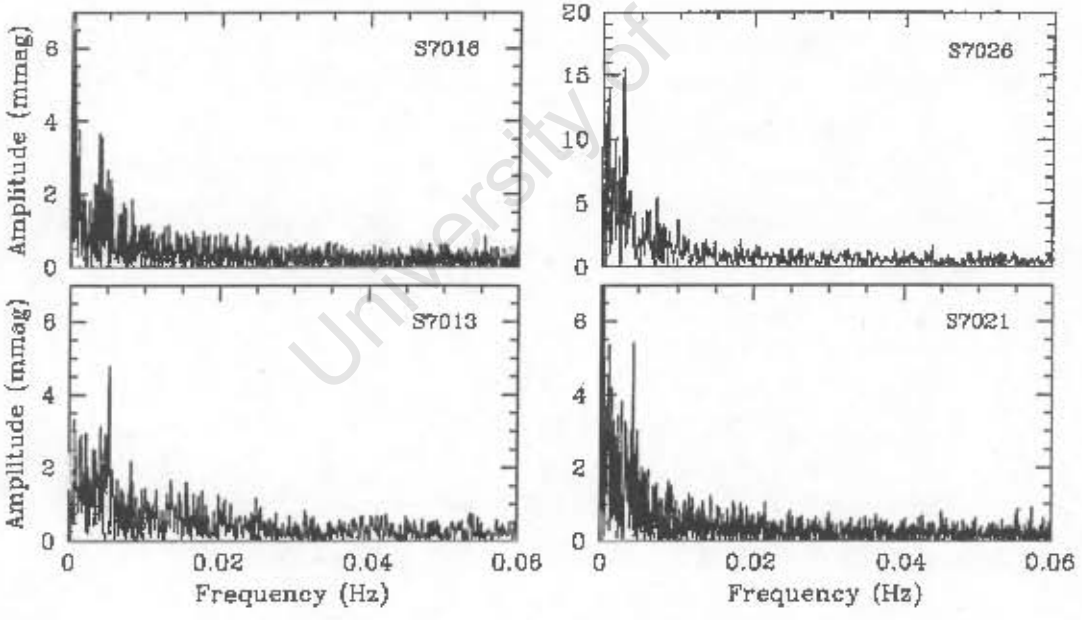

Figure 5.8: Fourier transforms showing QPOs in RU Peg on four nights. The QPOs are much more coherent than before and appear as sharp peaks (or, in the case of S7016, a narrow band) rather than the broad bands of power seen in Fig. 5.5. Notice also how large the QPO amplitude in run S7026 is.

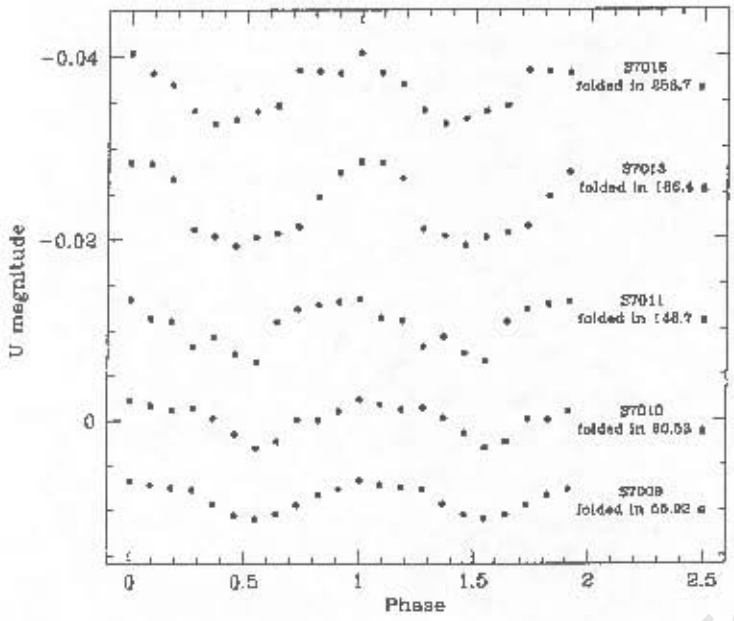

Figure 5.9: The average QPO profiles on five different nights. The profiles have been arbitrarily displaced along the vertical axis. The mean QPO period is given next to each profile.

in S7010 was a beat between a higher frequency signal and the integration time, while that in S7012 was the true oscillation period.

I tentatively classify the 14 and 15 s signals as lpDNOs, but it should be clear from the previous two paragraphs that the question remains open.

No DNOs or lpDNOs were observed during the rest of the outburst. On 21 July (run S7013) the QPO period was 186 s, it now appears in the Fourier transform as a sharp spike, rather than excess power spread over a range of frequencies as seen earlier in the outburst. On the next night (S7016) the QPO shows up in the Fourier transform as a narrow band of power centred on ~257 s, see Fig. 5.8 for the Fourier transforms of these two runs as well as run S7021 and S7026. Fig. 5.9 shows the average QPO profiles for the first five nights during which QPOs were present. The QPO amplitude increases steadily over these five runs. In run S7021 and S7026 the QPOs have much larger amplitudes than those seen earlier in the outburst.

In run S7021 the QPO amplitude is 5.6 mmag and the period is around 223 s. Fig. 5.10 shows part of the light curve for this night, with the QPO clearly present. The Fourier transform for the whole run is shown as the lower right hand panel of Fig. 5.8, the peak caused by the QPO is especially narrow, indicating a relatively stable oscillation.

On 25 July (run S7026) a QPO at ~360 s was present at large amplitude during the entire run, more or less maintaining its coherence for about 14 cycles. This light curve is shown in Fig. 5.11, together with a sine function fitted to the data by non-linear least squares. In terms of coherence and amplitude, there is probably not

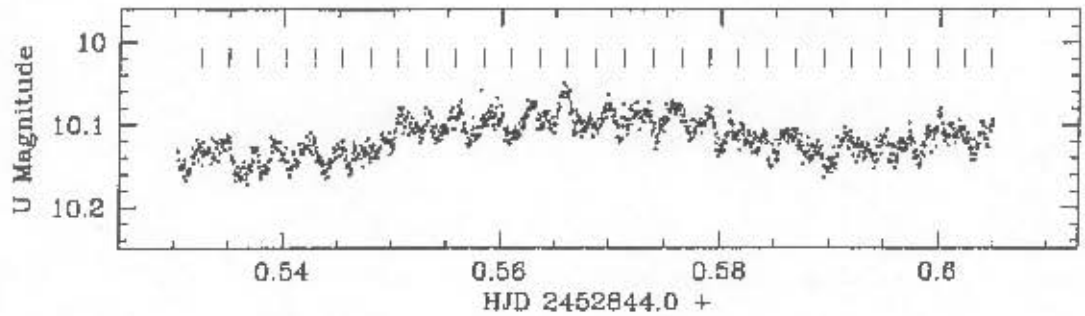

Figure 5.10: The first 107.5 min. of the light curve of RU Peg on 23 July (run S7021). Vertical bars along the top of the graph are at 223.6 s intervals, which is the mean QPO period in this part of the data. Non-linear least squares gives a best-fit amplitude of 5.649 mmag for this QPO.

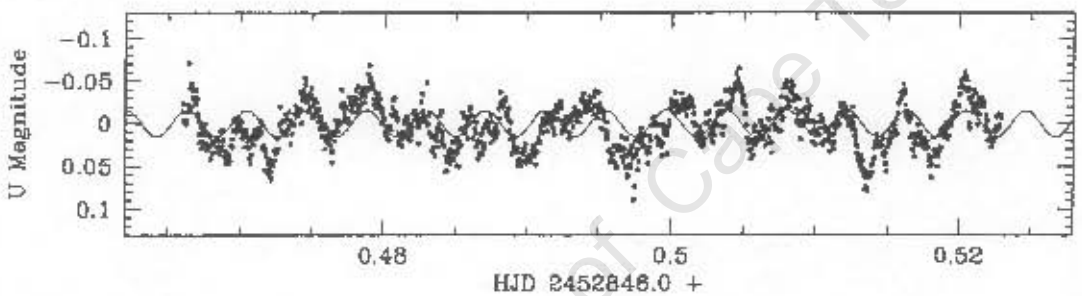

Figure 5.11: The light curve of RU Peg on July 25 (run S7026) after subtraction of the mean and prewhitening to remove a very low frequency variation. The superimposed sine function is a non-linear least squares fit to the data with a period of 360.3 s and an amplitude of 15.39 mmag.

a more spectacular example of a QPO shown anywhere in the literature.

By the next night RU Peg was still above quiescent brightness but only flickering, no quasi-coherent signal was detected.

Evolution of P_{QPO} over many nights of an outburst has not been reported before (Patterson et al. 1977 observed the 50 s QPO in RU Peg over a range in brightness of only ~0.3 mag), and it is not clear whether it is a changing QPO, or whether there are different mechanisms involved. As mentioned in Chapter 3, some systems have kilosecond QPOs in addition to QPOs that follow the relation $P_{QPO} \approx 16 \times P_{DNO}$. RU Peg, however, seems to have a smooth distribution of QPO periods ranging over almost an order of magnitude, and is unique in this regard.

5.3 WW Cet

There is some uncertainty as to what type of DN WW Cet is (e.g. Warner 1987c; Ringwald et al. 1996); it has an orbital period of 4.219 h, a mean quiescent V magnitude of 13.9 (but can get as faint as 15.7 mag) and reaches 9.3 mag in outburst (Ringwald et al. 1996). WW Cet has never before been reported to have DNOs or QPOs; I observed it during two outbursts and, on one occasion, in quiescence (see Table 5.3). With the exception of run S7187, all the observations were made in white light.

Rapid oscillations were detected on only one night. Fig. 5.12 is the light curve for run S7082, it shows WW Cet fading from outburst at an average rate of 0.029 mag/h.

Peaks at ~0.0097 Hz (103 s) and ~0.043 Hz (23.1 s) in the Fourier transform of this light curve (left hand panel of Fig. 5.13) indicate the presence of an lpDNO and DNO. Both the DNO and lpDNO peaks contain some noisy structure. Amplitude and $O-C$ phase diagrams show this to be caused by changing periods and amplitudes, see the right hand side of Fig. 5.13. P_{DNO} shows the usual increase

Table 5.3: Log of the observations of WW Cet.

Run No.	Date at start of night	Start time HJD = 2450000.0+	Length (h)	t_{int} (s)	Telescope	V (mag)
S7070	29 Aug. 2003	2881.62303	1.35	6	36-in.	10.9
S7082	3 Sept. 2003	2886.55197	2.78	5	40-in.	11.8
S7087	5 Sept. 2003	2888.39347	3.88	5	40-in.	13.4
S7163	19 Oct. 2003	2932.51061	0.87	6	40-in.	14.8
S7187	23 Dec. 2003	2997.28335	1.18	6	40-in.	10.4*
S7191	24 Dec. 2003	2998.27296	1.03	5	40-in.	11.5
S7195	26 Dec. 2003	2999.28092	1.32	5	40-in.	12.9
S7197	27 Dec. 2003	3000.27382	1.27	6	40-in.	13.9

Notes: *U magnitude; t_{int} is the integration time.

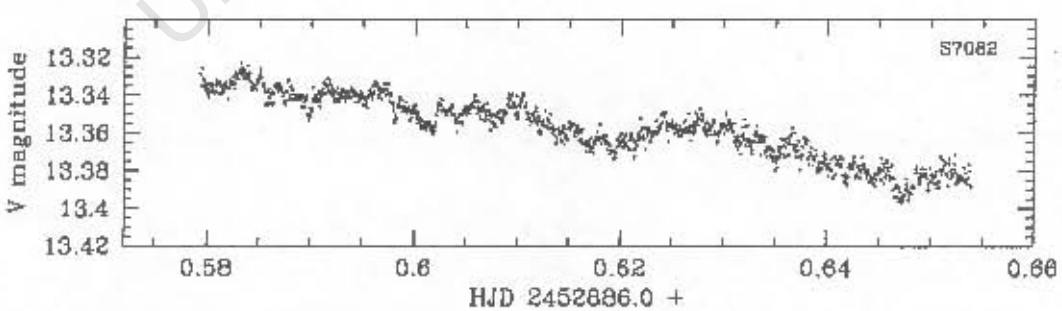

Figure 5.12: Part of the light curve of WW Cet on 3 September 2003, when the system was on the decline from outburst. The data are corrected to first order for atmospheric extinction.

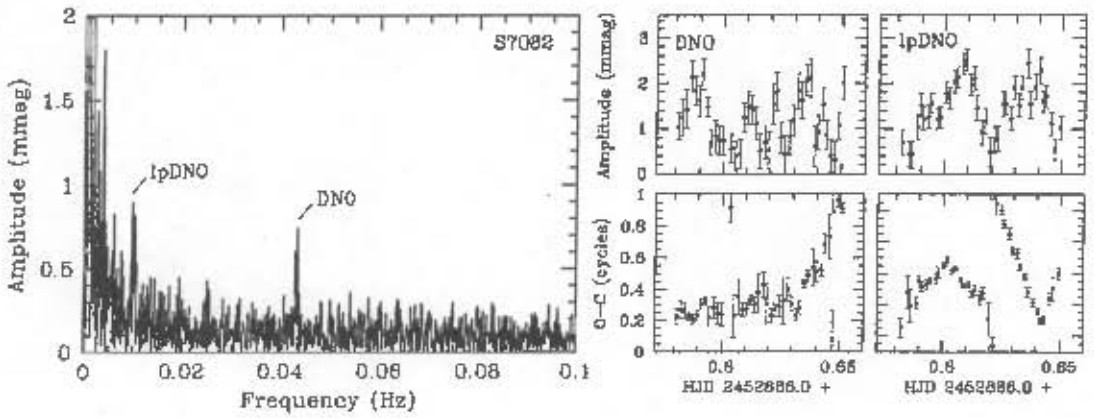

Figure 5.13: Left: The Fourier transform of the light curve shown in Fig. 5.12. An lpDNO at ~0.0097 Hz (103 s) is present at the same time as a DNO at ~0.043 Hz (23.1 s). The light curve was prewhitened to remove a drive error at 40 sidereal seconds, see Fig. A.2 for a Fourier transform of the original data. Right: Amplitude and $O-C$ variation of the DNO (left) and lpDNO (right) in run S7082. The DNO phase is calculated relative to a period of 23.08 s, that of the lpDNO relative to a period of 102.7 s. The DNO period increases systematically, while the lpDNO period changes quite abruptly at around HJD 2452886.603, and again at around HJD 2452886.643.

with decreasing accretion luminosity, while the DNO amplitude varies erratically. The lpDNO period does not change systematically during the observation, rather, it changes abruptly from ~104 s to ~98.6 s at HJD 2452886.603, and increases again at HJD 2452886.643. These changes in period are not accompanied by any remarkable changes in system luminosity (see Fig. 5.12) or oscillation amplitude (see the right most upper panel of Fig. 5.13). There does not appear to be any obvious correlation between the phase and amplitude behaviour of the DNO and lpDNO. The classification of the ~100 s oscillation as an lpDNO, rather than a QPO is based on its period being around 4 times that of the DNO period ($P_{lpDNO}/P_{DNO} = 4.27$).

There is a sharp spike in the Fourier transform at 3.802 mHz (263 s), at larger amplitude than the surrounding noise (see Fig. 5.13). The spike is probably caused by a QPO, but the modulation responsible for it is not obvious in the light curve.

5.4 X Leo

X Leo is a U Gem star with $P_{orb} = 3.946$ h (Shafter & Harkness 1986), a quiescent V magnitude of ~16.5, and outbursts of amplitude ~4 mag roughly every 20 d (Szkody & Mattei 1984). Middleditch & Córdova (1982) report a quasi-coherent oscillation at 160 s in an outburst light curve of X Leo, and note that the oscillation is red compared to the disc.

Table 5.4: Log of the observations of X Leo. All observations were made in white light, using the 40-in. reflector. The last column lists lpDNO periods.

Run No.	Date at start of night	Start time HJD = 2450000.0+	Length (h)	t_{int} (s)	V (mag)	P_{lpDNO} (s)
S6738	4 Feb. 2003	2675.37349	0.18	5	13.4:	—
S6742	5 Feb. 2003	2676.37284	0.78	5	14.0	114
S6921	14 May 2003	2774.19907	1.28	5	12.9	88.7
S6923	14 May 2003	2774.32065	1.50	5	12.9	91.3
S6927	15 May 2003	2775.19494	4.17	4, 5, 6	13.2	126
S6930	16 May 2003	2776.18942	0.97	6	13.8:	—
S6931	17 May 2003	2777.19303	1.92	5	14.5	146
S6932	18 May 2003	2778.19122	2.80	7	14.9	172
S6938	19 May 2003	2779.19300	1.05	6	15.4	—
S7171	16 Dec. 2003	2990.55643	1.23	5	12.6	—
S7175	18 Dec. 2003	2992.50216	2.35	5	13.2:	—
S7179	19 Dec. 2003	3000.27382	1.08	5	13.8:	—
S7293	16 Mar. 2004	3081.24386	1.45	5	12.7	95.6
S7295	17 Mar. 2004	3082.24245	5.58	5, 6	13.2	98.8
S7297	19 Mar. 2004	3083.24244	3.68	6	14.9	219
S7298	20 Mar. 2004	3084.24088	1.37	8	15.8	—

Notes: t_{int} is the integration time; ':' denotes an uncertain value.

I acquired high speed photometry of X Leo during 4 different outbursts with the 40-in. reflector at Sutherland, details of the observations are given in Table 5.4. X Leo was found to have commonly occurring lpDNOs with periods in the order of 100 s (conditions were poor during all three nights of the December 2003 outburst, so that the quality of data was too low to show low amplitude oscillations); the periods are listed in Table 5.4. The lpDNOs can in all cases be seen directly in the light curves, Fig. 5.14 shows three examples.

X Leo is the first CV to show, for an lpDNO, a clear period-luminosity relation; all other observations of lpDNOs seem to indicate that P_{lpDNO} has either no, or only very weak dependence on $\dot{M}$. This relation is plotted in Fig. 5.15 for the May 2003, and March 2004 outbursts, with the single point for February 2003 added. In other systems, lpDNOs have been observed to double in frequency, but that is clearly not the case here. The dashed and dotted lines in Fig 5.15 are least squares fits to the May 2003 and March 2004 period-luminosity functions respectively. These give $s \equiv \frac{d\log(P_{lpDNO}/s)}{d\log(I/I_{min})} = -0.29$ for the May 2003 outburst, and $s = -0.11$ for the March 2004 outburst. Despite the factor of almost 3 difference between the gradients of the period-luminosity relation in the two outbursts, s in both cases falls within the range measured for DNOs (see equation 3.1).

In addition to the lpDNOs, the light curves taken on 14 and 19 March 2004 contained DNOs. In the first of these, the DNO was present at a detectable (but very low) amplitude for only about 35 min.; the period was 12.9 s. The 19 March

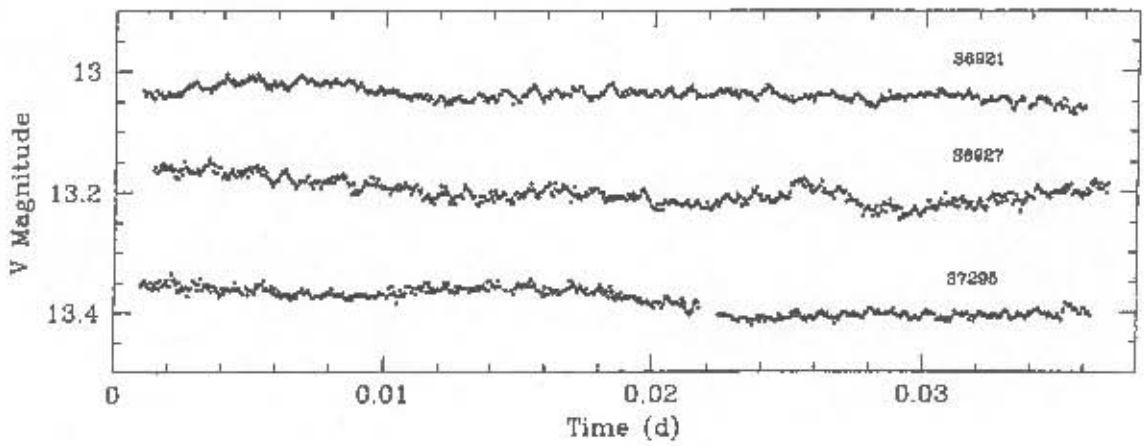

Figure 5.14: A sample of X Leo light curves in which some of the larger amplitude lpDNO cycles can easily be seen. The S6921 and S7295 data are displaced vertically by +0.1 and +0.3 mag respectively, and all three light curves are arbitrarily shifted along the horizontal axis.

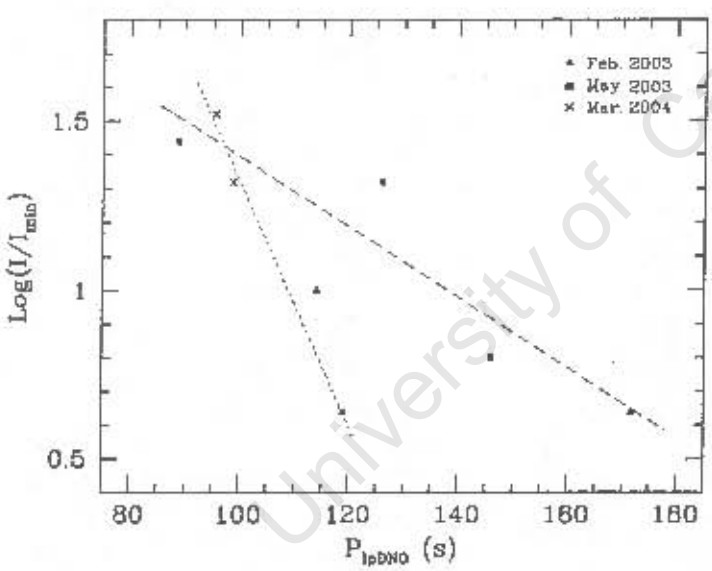

Figure 5.15: $\log(I/I_{min})$ as a function of lpDNO period for the three different outbursts of X Leo. The dashed line is a least squares fit to the four points (squares) of the May 2003 outburst; the dotted line is a fit to the March 2004 data (crosses). A single point (triangle) represents the February 2003 outburst.

2004 light curve, on the other hand, is probably one of the best examples of a simultaneously present DNO and lpDNO. A Fourier transform of part of this run is shown as the left hand panel of Fig. 5.16. The amplitude and $O-C$ diagrams for both oscillations (right hand side of Fig. 5.16) show no correlation between the amplitude and phase variability of the DNO and lpDNO.

Run S6932 contains a modulation on a preferred time scale of around 25 min., and of fairly large amplitude. The light curve, with a best-fit sine function superimposed,

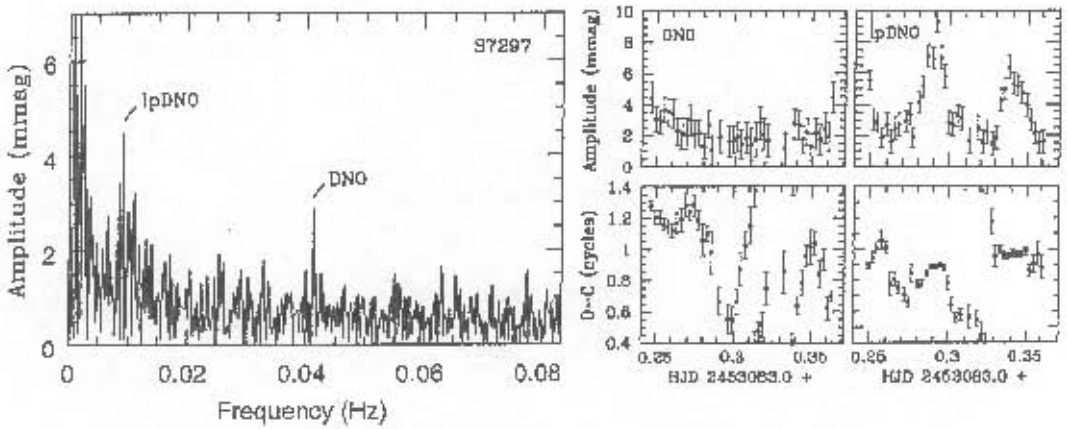

Figure 5.16: Left: The Fourier transform of an hour long section of run S7297, with DNO and lpDNO features marked. Right: Amplitude and $O - C$ phase diagrams for the DNOs and lpDNOs in run S7297. The DNO phase is calculated relative to a fixed period of 24.21 s, and that of the lpDNO relative to a fixed period of 118.5 s.

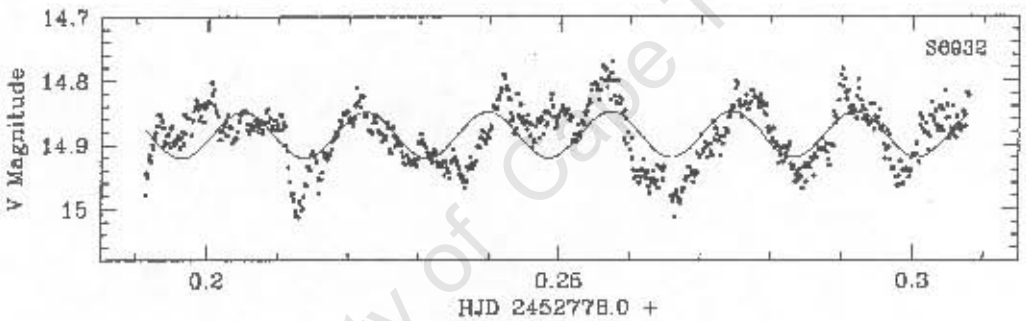

Figure 5.17: The light curve of X Leo on 18 May 2003 (run S6932) after a low amplitude modulation with a period of the order of the run length (probably resulting from changes in transparency) was removed. Non-linear least squares fitting gives an oscillation period of 1501 s; the resulting sine function is superimposed on the data.

is shown in Fig. 5.17. This kind of variability was only observed once, and it is therefore not clear whether it is a QPO.

5.5 TY PsA

Barwig et al. (1982) found TY PsA to be an SU UMa type DN; it has an orbital period of 2.019 h (O'Donoghue & Soltynski 1992; Warner et al. 1989). Warner et al. (1989) detected DNOs at unusually large amplitude in TY PsA, with period evolving from ~25.5 s to ~30 s over 4 nights, while the system faded from $V = 12.4$ to $V = 13.2$, giving a period-luminosity relation $d\log(P/mathrms)/d\log(I/I_{min}) =$

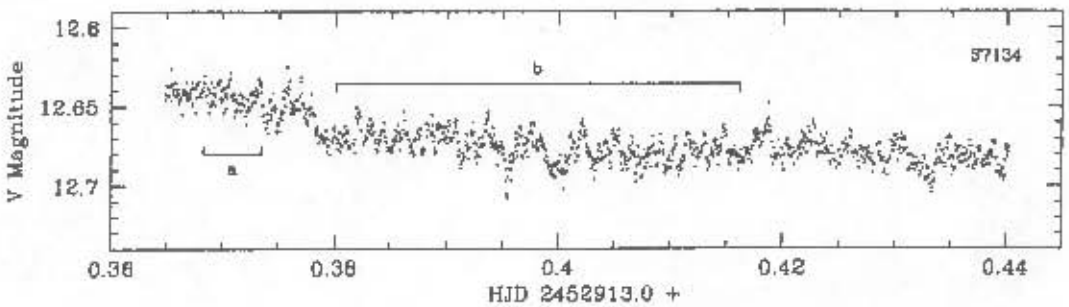

Figure 5.18: Part of the light curve of TY PsA on 30 September 2003. About 12 prominent cycles of a ~357 s can be easily picked out by eye. The sections marked a and b are plotted again in Fig. 5.19.

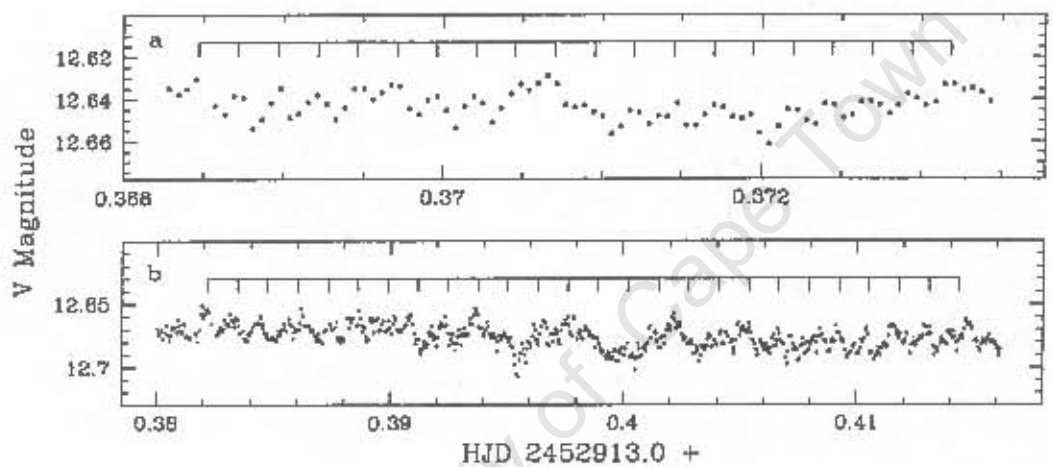

Figure 5.19: Two shorter sections of the data as marked in Fig. 5.18, on scales that make both a DNO and an lpDNO directly visible. The inset scales give the mean period of the DNO (21.43 s, panel a) and lpDNO (111.3 s, panel b) in these sections of light curve.

−0.24. They also report a QPO at 245 s in a run not containing DNOs (this time with TY PsA at $V = 13.9$).

I obtained a single high speed photometry run on this object, in white light, spanning 4.05 h, using the 74-in. reflector on 30 September 2003 (run S7134), while it was on the decline from outburst. Fig. 5.18 shows part of the light curve of this run; directly visible in this observation is a ~357 s QPO. The sections labelled a and b are plotted, in Fig. 5.19, on scales that reveal also two shorter period oscillations.

This light curve is a particularly nice example of the simultaneous presence of all three types of rapid, quasi-coherent oscillations. The Fourier transform (left hand panel of Fig. 5.20) illustrates this more clearly. Integration times of 5 and 6 s were used, which proved that all detected periods were real, rather than beats with signals

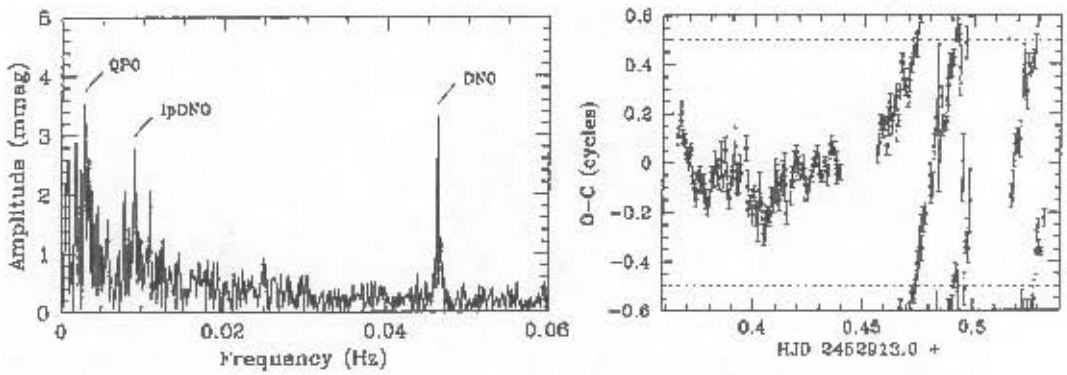

Figure 5.20: Left: The low frequency end of the Fourier transform of the first 1.3 h of run S7134. The QPO (356.7 s), lpDNO (110.4 s), and DNO (21.57 s) peaks are marked. This Fourier transform appeared as fig. 3 of W04. Right: The $O-C$ phase diagram of the DNO in TY PsA, relative to a trial period of 21.59 s. Each point represents a fit to ~ 4.6 DNO cycles, there is 50% overlap between consecutive points. A few points of large uncertainty are omitted; the two long gaps are due to bad weather. Note that (for this kind of oscillation) $O-C$ has a meaningful range of just 1 cycle, so that the data points outside the dotted lines are repeated.

above the Nyquist frequency. Note that, in the Fourier transform, the DNO appears to have larger amplitude than the lpDNO. This is because the DNO has greater coherence; many individual lpDNO cycles actually have larger amplitude than the DNO modulation, see Fig. 5.19. P_{DNO} ranges from 21.43 to 21.90 s (but does not increase monotonically); the QPO power is spread over all frequencies between 2.3 mHz and 3.4 mHz. P_{lpDNO} varies from 89 s to 112 s, but there is no clear trend in the variation.

The instability of the lpDNO period is represented, in the Fourier transform in Fig. 5.20, by spikes on either side of the peak marked lpDNO; phase and amplitude variation are also possible causes of the two lower amplitude peaks. However, these features do not result from simple periodic amplitude modulation of the lpDNO, since this would have led to two spikes of equal amplitude (but note that noise might distort the amplitudes), at equal frequency intervals either side of the lpDNO peak (see e.g. Warner 1986; Warner & Brickhill 1978).

The phase variation of the DNO is illustrated in the right hand panel of Fig. 5.20, which shows a systematic increase in P_{DNO}, upon which is superimposed frequent small phase (or period) changes. This plot is very similar to fig. 13 of Warner et al. (1989). Greater scatter around the roughly linear trend in $O-C$, from about HJD 2452913.48 onwards, indicates that the coherence of the DNO decreases towards the end of the run.

5.6 BP CrA

BP CrA is a Z Cam type DN with visual magnitude varying between 15.9 and 13.5, and an outburst recurrence time of 13.5 d (Bateson 1982a,b); there is no orbital period known for this object.

Observations of BP CrA made during outburst on 4 April 2003 (run S6912) contained a strong DNO. The system was subsequently observed on nine more nights, but the DNO was never detected again—refer to Table 5.5 for details of the observations. Fig. 5.21 displays the Fourier transform of run S6912, which shows that the DNO period is 38.64 s; the amplitude (refined by applying a non-linear least

Table 5.5: Log of the observations of BP CrA. All the observations were made in white light.

Run No.	Date at start of night	Start time HJD = 2452000.0+	Length (h)	t_{int} (s)	Telescope	V (mag)
S6912	4 Apr. 2003	734.55464	2.73	6	30-in.	14.3:
S6915	7 Apr. 2003	737.53081	3.25	6	30-in.	14.1:
S7025	25 Jul. 2003	846.35335	2.55	5, 6	40-in.	13.8
S7029	26 Jul. 2003	847.27017	2.78	6	40-in.	13.7
S7035	28 Jul. 2003	849.31426	1.92	5	40-in.	13.8
S7152	16 Oct. 2003	928.24086	1.33	5	40-in.	14.7
S7154	17 Oct. 2003	930.23288	0.98	5	40-in.	13.8
S7158	18 Oct. 2003	931.24983	1.20	6	40-in.	14.0:
S7161	19 Oct. 2003	932.23729	2.23	5, 6	40-in.	14.0
S7165	20 Oct. 2003	933.24215	1.02	5	40-in.	14.1

Notes: t_{int} is the integration time; ':' denotes an uncertain value.

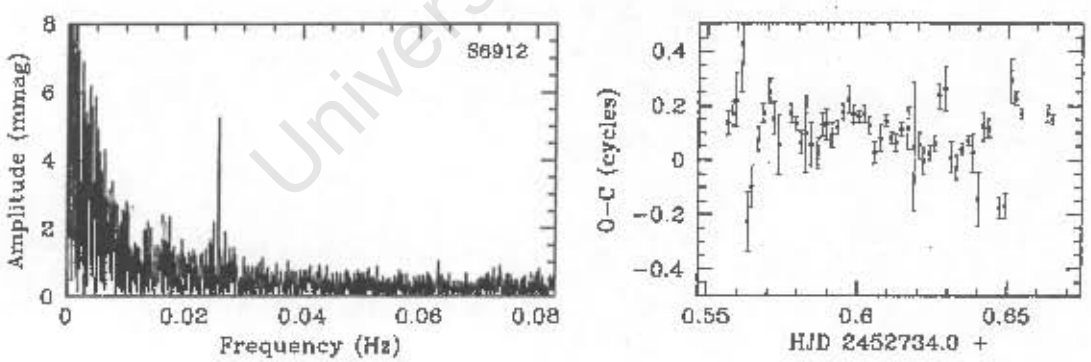

Figure 5.21: The Fourier transform of the light curve of run S6912 (left hand panel), and $O-C$ diagram of the DNO (right hand panel). The DNO period is 38.64 s (0.02588 Hz). The light curve was prewhitened to correct for a prominent drive error—see also Fig. A.2. The $O-C$ values are calculated relative to a fixed period of 38.64 s, using about 8 cycles per point, and 50% overlap between consecutive points, so that every second point is independent.

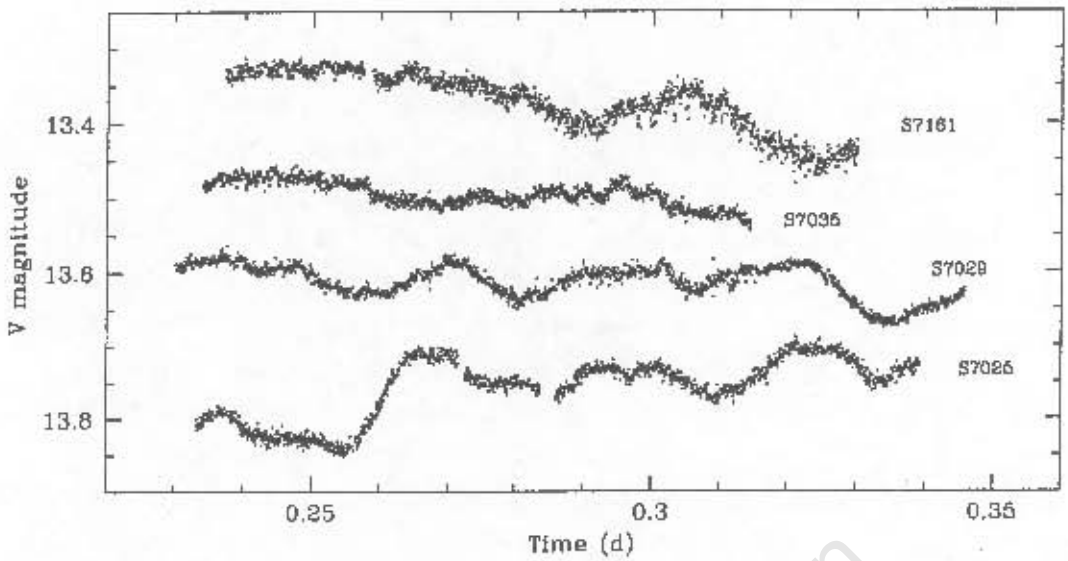

Figure 5.22: Four light curves of BP CrA, arbitrarily displaced along the horizontal axis. The S7029, S7035, and S7161 light curves are shifted vertically by −0.07, −0.35, and −0.63 mag for display purposes.

squares fit) is 5.8 mmag. Also shown in Fig. 5.21 is the $O-C$ phase diagram of the DNO, which shows variability typical of a DNO, with the period initially longer than the test period of 38.64 s (indicated by $O-C$ sharply increasing with time), and then, at around HJD 2452734.575, changing to be more consistent with the test period. No QPOs or lpDNOs could be found in any of my light curves of BP CrA.

Since there is no high speed photometry of BP CrA published, I display a number of light curves in Fig. 5.22. The amplitude of rapid flickering in these light curves is remarkably low. Fourier transforms show mean noise levels at frequencies between ~0.007 Hz (corresponding to ~140 s) and the Nyquist frequency of about 0.8 mmag; the power starts rising only at frequencies lower than ~0.007 Hz. The origin of the longer period variations in these light curves (most evident in run S7025) is not known. The data set did not enable me to find the orbital period.

5.7 HX Peg

HX Peg is a Z Cam type DN with V magnitude varying in the range 16.6 to 12.9, outbursts recurring every 14 to 21 d (Honeycutt et al. 1998), and an orbital period of 4.82 h (Ringwald 1994).

My first observation of HX Peg, made in July 2002 during the late decline from outburst, contained a ~1800 s QPO at impressive amplitude (48.8 mmag). This light curve is shown in Fig. 5.23. In addition to the QPO, there was some evidence of a

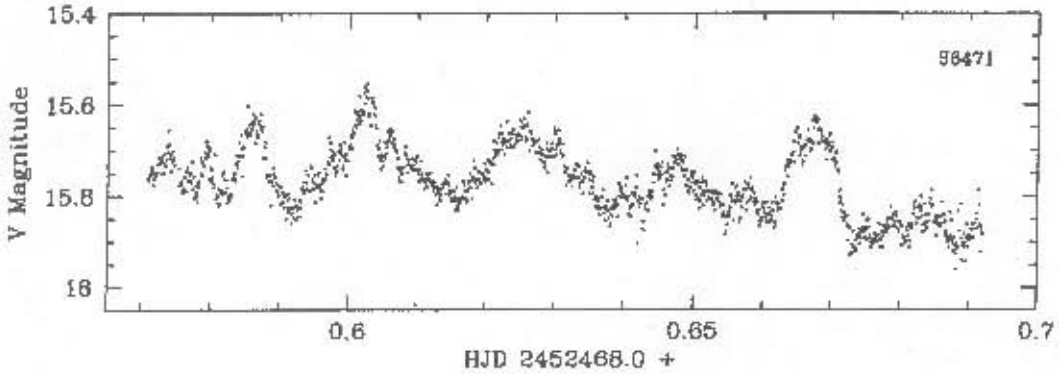

Figure 5.23: The light curve of HX Peg on 12 July 2002 (run S6471). It contains a prominent QPO with a period of 1800 s, and an unusually large amplitude of 48.8 mmag.

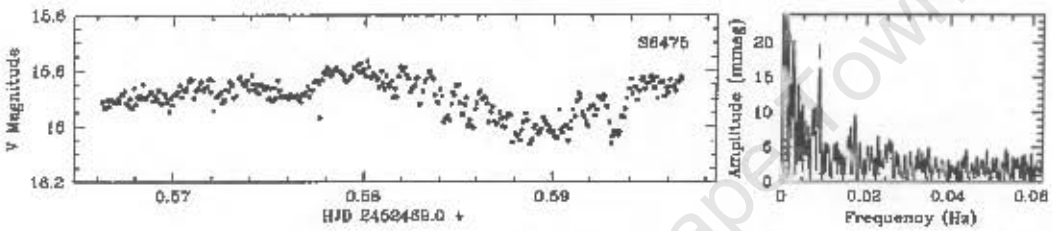

Figure 5.24: Left: the light curve of the last 0.73 h of run S6475 (this was shown as figure 21 of WWP03). Despite the rather poor quality of photometry, about nine prominent cycles of a ~100 s oscillation can easily be seen. Right: the Fourier transform of the light curve on the left, which shows that the period of the oscillation is 111.9 s; this peak is marked by a vertical bar.

~100 s oscillation in the last 0.77 h of this run. On the next night (run S6475) the QPO was still present, and the ~100 s oscillation showed up more clearly—Fig. 5.24 is the light curve and Fourier transform of the last 0.73 h of the S6475 data. A few cycles of the oscillation can be seen directly in the light curve; the Fourier transform shows that the period is 111.9 s. Both of the first two observations were made under very poor sky conditions, as a result, the photometry was not of particularly good quality.

Since HX Peg proved itself an interesting object on these two nights, it was frequently observed during the rest of the 2002 season, and again in 2003 (see Table 5.6), and was seen to have the full set of QPOs, lpDNOs, and DNOs, in addition to the kilosecond QPOs already mentioned.

The ~100 s oscillation was reobserved by Patrick Woudt, this time at a period of 114.8 s, with HX Peg at $V = 13.1$ (run S6584; see WWP03). The similar periods in run S6475 and S6584, despite a 2.8 mag difference in brightness, convinced us that

Table 5.6: Log of the observations of HX Peg; no filters were used.

Run No.	Date at start of night	Start time HJD = 2452000.0+	Length (h)	t_{int} (s)	Telescope	V (mag)
S6471	12 Jul. 2002	468.57089	2.97	8	30-in.	15.8:
S6475	13 Jul. 2002	469.55275	3.22	8	30-in.	15.9:
S6646	25 Nov. 2002	604.26516	2.08	6, 8	40-in.	12.7
S6650	26 Nov. 2002	605.26913	3.05	6	40-in.	12.8
S6654	28 Nov. 2002	607.27506	2.97	5, 6	40-in.	12.9
S6656	29 Nov. 2002	608.26764	1.63	5, 6	40-in.	13.0
S6661	30 Nov. 2002	609.31524	1.77	6	40-in.	13.3
S6667	1 Dec. 2002	610.33857	1.57	4, 5	40-in.	13.6
S7014	21 Jul. 2003	842.61782	1.98	5	40-in.	13.7
S7017	22 Jul. 2003	843.61031	1.95	6	40-in.	13.9
S7090	8 Sept. 2003	890.35176	4.05	5	40-in.	13.1
S7151	14 Oct. 2003	927.37844	2.05	5	40-in.	13.4:
S7156	17 Oct. 2003	930.31122	3.32	5	40-in.	13.9
S7159	18 Oct. 2003	931.31186	4.18	6	40-in.	14.3
S7162	19 Oct. 2003	932.34182	3.68	5	40-in.	14.8
S7166	20 Oct. 2003	933.31166	3.85	6	40-in.	15.2

Notes: t_{int} is the integration time; ':' denotes an uncertain value.

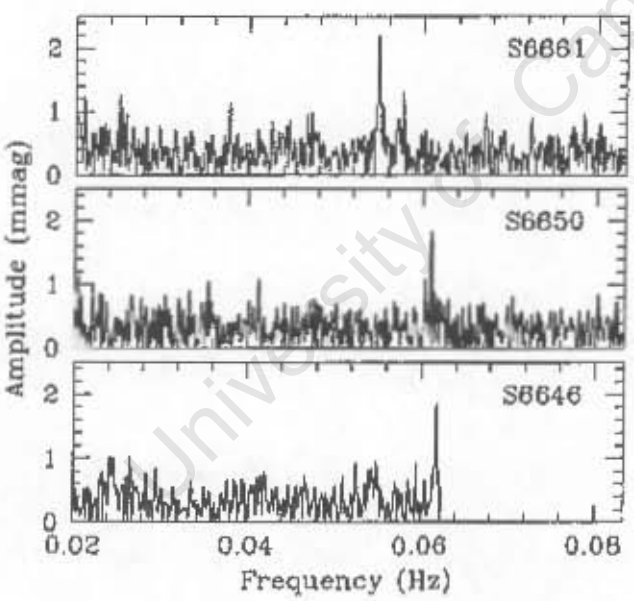

Figure 5.25: Fourier transforms of the light curves of HX Peg taken on 25, 26, and 30 November, showing DNOs at maximum of, and on the decline from the November/December 2002 outburst. The DNO period is 16.19, 16.39, and 18.24 s in run S6646, S6650, and S6661 respectively.

the ~100 s oscillations were lpDNOs rather than DNOs.

Normal DNOs appeared in the November/December 2002 outburst (see Fig. 5.25). These follow the usual, more sensitive, period luminosity relation, changing in period from 16.19 s to 18.24 s, over a time interval of 4 days, while the system faded by 0.6 mag. No DNOs were detected on 28 and 29 November. Run S6656, taken during the same outburst, was particularly interesting, since it contains a double

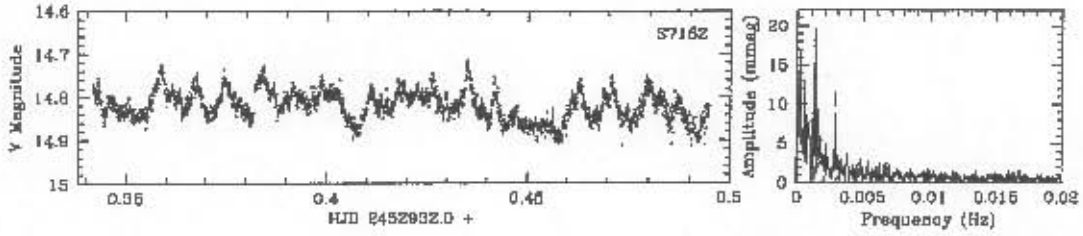

Figure 5.26: Left: The light curve of run S7162, dominated by a QPO with a mean period of 746 s and amplitude of 19.5 mmag. This light curve (binned to a quarter of its original time resolution) appeared as fig. 14 of W04. Right: The low frequency end of the Fourier transform of this light curve, showing, in addition to very large power at 1.34 mHz (746 s), the presence of a normal QPO at a period of 347 s (marked by a vertical bar at 2.88 mHz). The normal QPO, despite an amplitude of 8.78 mmag is almost invisible in the light curve, because it is drowned out by the kilosecond QPO.

lpDNO, with the true lpDNO at 83.4 s, the reprocessed side band at 111.1 s, and some evidence of a QPO near the beat period of 335 s (WWP03). That HX Peg can produce QPOs near this period was confirmed in run S7162, which again shows HX Peg on the decline from outburst. The light curve of run S7162 is also the only example of the coexistence of a normal QPO and a kilosecond QPO, see Fig. 5.26. The normal QPO here is at 347 s, while the much more noticeable kilosecond QPO has a period of 746 s. As mentioned in Section 3.2, several cycles of the kilosecond QPO seem to have flare-like, rather than sinusoidal profiles (despite this, the Fourier transform shows no significant power at the harmonics of the 746 s signal). There were no DNOs or lpDNOs detected in this light curve.

5.8 V893 Sco

Only very few DN below the period gap are not well established SU UMa stars, V893 Sco is the best studied of these[2] (see e.g. Kato, Matsumoto & Uemura 2002). It is an eclipsing DN with an orbital period of 1.823 h (Bruch, Steiner & Gneiding 2000), and outbursts every ~30 d which takes it from a photographic magnitude of 14.5 to 10.6 (Kato et al. 2002).

V893 Sco has been observed to have QPOs at around 350 s (WWP03; Bruch et al. 2000), and DNOs at 25.2 s (WWP03).

I observed V893 Sco in May 2003 on the decline from outburst, and into quiescence; surprisingly, it was again above minimum only two days after reaching quiescence (see Table 5.7 for details). No rapid oscillations were found in any of

[2]V893 Sco is an ecliptic object, and hence unobservable for about two months every year, so that superoutbursts may have been overlooked.

Table 5.7: Log of the observations of V893 Sco; no filters were used. The final column lists the average nightly magnitude outside of eclipse.

Run No.	Date at start of night	Start time HJD = 2452000.0+	Length (h)	t_{int} (s)	Telescope	V (mag)
S6942	19 May 2003	779.47549	1.02	6	40-in.	13.0:
S6945	20 May 2003	780.41393	5.98	7	30-in.	13.9
S6949	21 May 2003	781.39698	3.95	7	30-in.	15.1
S6953	23 May 2003	783.38547	2.97	6	30-in.	14.0

Notes: t_{int} is the integration time; ':' denotes an uncertain value.

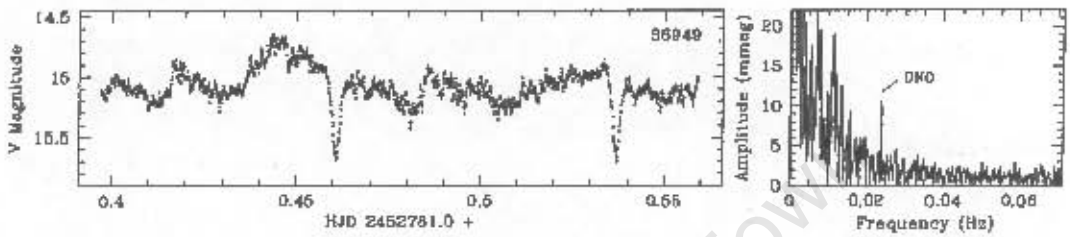

Figure 5.27: Left: The light curve of V893 Sco on 21 May 2003 (run S6949), showing the system at quiescence. Right: The Fourier transform of a 0.9 h section of the light curve (starting just after the first eclipse). A DNO with a period of 41.76 s is indicated.

my outburst light curves, but run S6949, taken at minimum, contains a DNO with a period of 41.76 s—a rare example of a DNO in quiescence. Fig. 5.27 shows the relevant light curve, together with a Fourier transform of a shorter section of the light curve. The DNO was present for only 0.9 h, and the signal-to-noise is too low to enable a more thorough investigation of its behaviour.

5.9 BR Lup

BR Lup is an SU UMa type DN (O'Donoghue 1987), with an orbital period of (probably) 1.909 h (O'Donoghue 1987; Mennickent & Sterken 1998). The outburst cycle lengths are not reliably known (Bateson 1998). O'Donoghue (1987) searched his outburst light curves for DNOs, but found none above an amplitude of 0.001 mag in the frequency range 5 to 100 mHz.

I observed BR Lup in April and July 2003; the April observations were during superoutburst, but it was not possible to determine whether the July bright state was a normal or superoutburst, the observations are listed in Table 5.8.

Fig. 5.28 shows the light curves of run S6911 (taken on the rise to maximum) and S6914. A DNO was detected in run S6911, the left hand panel of Fig. 5.29 is the Fourier transform of the first 1.3 h of this light curve, with the DNO at 21.65 s.

Table 5.8: Log of the observations of BR Lup. No filter was used.

Run No.	Date at start of night	Start time HJD = 2452000.0+	Length (h)	t_{int} (s)	Telescope	V (mag)
S6908	3 Apr. 2003	733.46996	1.17	6	30-in.	14.6:
S6911	4 Apr. 2003	734.41199	3.37	6	30-in.	14.5
S6914	7 Apr. 2003	737.42124	2.62	6	30-in.	14.3
S7015	22 Jul. 2003	843.20290	5.28	7, 8	40-in.	15.7
S7018	23 Jul. 2003	844.21386	2.83	8	40-in.	17.5

Notes: t_{int} is the integration time; ':' denotes an uncertain value.

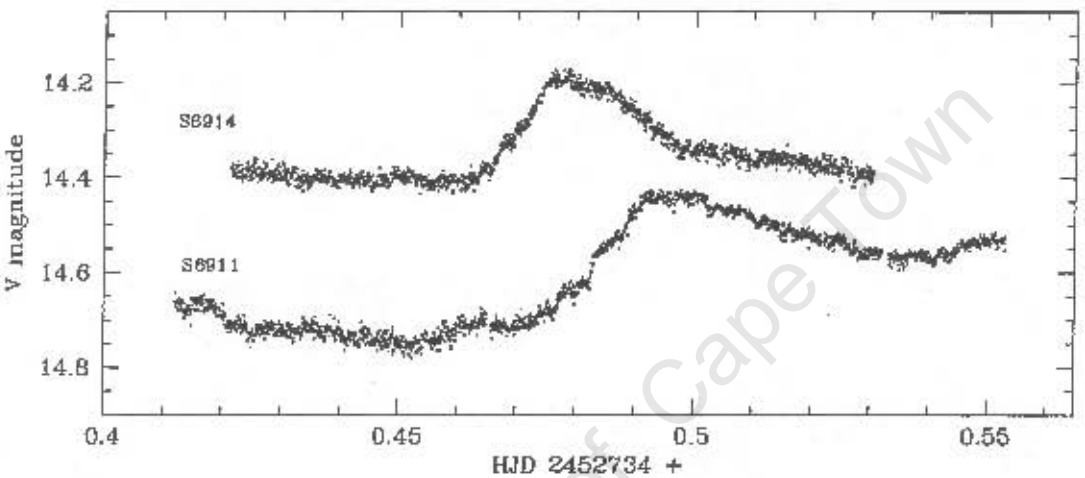

Figure 5.28: Light curves of BR Lup on 4 and 7 April 2003. On 4 April (run S6911) the system was clearly still rising into superoutburst. The 7 April data (S6914) are translated along the horizontal axis by −3.0 d; no vertical shift was applied. The large amplitude modulations are superhumps.

The Fourier transform of the central third of run S6914 (right hand panel of Fig. 5.29) shows the presence of a modulation at 25.04 s; since the system was brighter on this night than during run S6911, one would expect P_{DNO} to have decreased. However, the 25.04 s signal in S6914 is accompanied by a spike (only just visible above the noise) at the first harmonic (12.55 s). A non-sinusoidal profile is characteristic of a reprocessed DNO (Marsh & Horne 1998; WW02b) no QPO was seen in either of these light curves. Note that, depending on the geometry, it is possible to see the DNO reprocessed off a QPO structure, without the QPO itself being visible.

Run S7015, of the July 2003 outburst, contains a QPO with a period near 650 s, Fig. 5.30 shows the light curve at 21 s time resolution; the QPO is clearly visible.

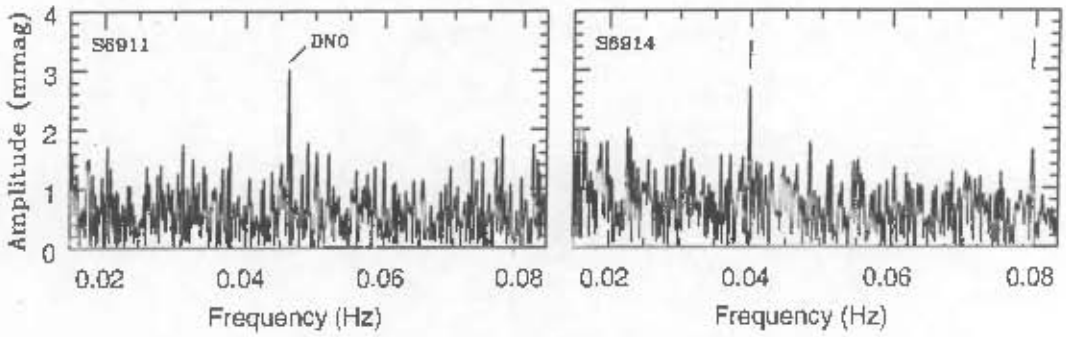

Figure 5.29: Left: The high frequency end of the Fourier transform of the first 1.3 h of run S6911, with a DNO at 21.65 s marked. Right: The high frequency end of the Fourier transform of the central third of run S6914. Vertical bars mark peaks at 25.038 s and 12.548 s (12.548 s is within 0.231% of where the first harmonic of 25.038 s is).

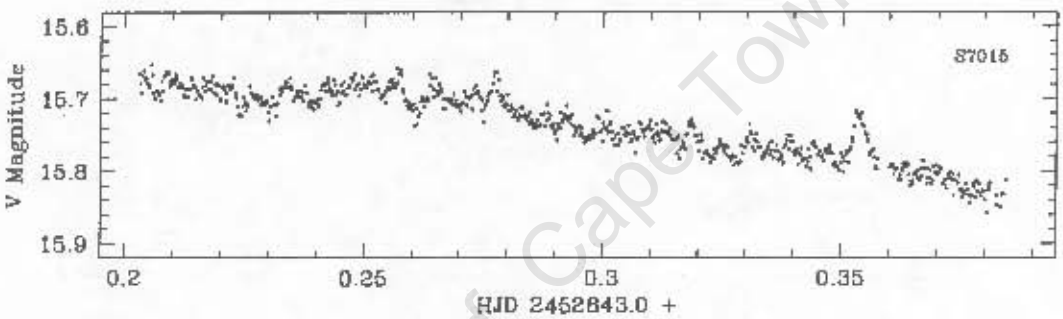

Figure 5.30: The light curve of BR Lup on 22 July 2003 (run S7015) binned to a third of its original time resolution. These data show a QPO with a period of ~650 s. The light curve contains no higher frequency signals.

5.10 CN Ori

Earlier believed to be a Z Cam star, CN Ori is more appropriately classified as a U Gem type DN (Bateson & Dodson 1984; Mantel et al. 1988), it has $P_{orb} = 3.91678$ h (Schoembs 1982a; Barrera & Vogt 1989). CN Ori varies from $V = 14.8$ to $V = 11.5$, with a cycle time of around 18 d, and is unusual in that it spends very little time in quiescence (Bateson 1979b; Bateson & Dodson 1984). DNOs with periods ranging from 24.3 s to 32.6 s have been detected in outburst observations of CN Ori (Warner & Robinson 1972a; Warner & Brickhill 1978; Schoembs 1982b).

I acquired 20.11 h of high speed photometry of CN Ori, spread over almost a year, without ever detecting an oscillation period in the range known for DNOs in this system (observations are listed in Table 5.9). Run S7174 however, contains a DNO at 45.94 s; the left hand panel of Fig. 5.31 is the Fourier transform of a 1 h section of the relevant light curve. It seems likely that this is simply a DNO at longer period,

Table 5.9: Log of the observations of CN Ori. A U filter was used in run S6702 and S6706, the V magnitudes given for these two nights are AAVSO visual estimates. The rest of the observations were made in white light.

Run No.	Date at start of night	Start time HJD = 2452000.0+	Length (h)	t_{int} (s)	Telescope	V (mag)
S6702	29 Dec. 2002	638.29558	1.92	4, 5	74-in.	12.1[a]
S6706	30 Dec. 2002	639.34296	2.37	5	74-in.	12.1[a]
S6774	19 Feb. 2003	690.25738	0.93	5	40-in.	12.7
S6779	20 Feb. 2003	691.26585	0.95	4, 5	40-in.	12.4
S6845	7 Mar. 2003	706.24954	3.13	4, 6	30-in.	12.8
S6849	8 Mar. 2003	707.26135	0.28	6	30-in.	12.7
S6853	9 Mar. 2003	708.24552	2.37	5, 6	30-in.	12.6
S6859	10 Mar. 2003	709.27726	1.32	6	30-in.	12.6
S7174	18 Dec. 2003	992.35155	2.10	5	40-in.	12.7
S7177	19 Dec. 2003	993.43358	1.32	5	40-in.	12.7
S7181	20 Dec. 2003	994.37195	1.20	5	40-in.	13.0:
S7189	23 Dec. 2003	997.43799	2.22	6	40-in.	14.0

Notes: t_{int} is the integration time; ':' denotes an uncertain value; [a]taken with a U filter.

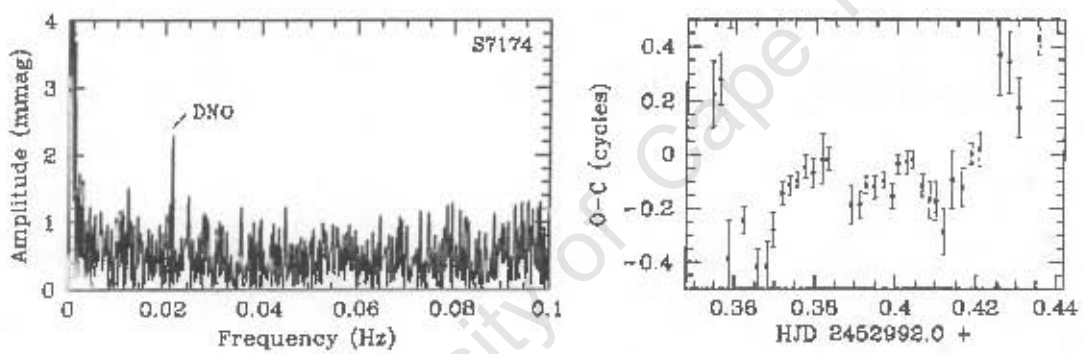

Figure 5.31: Left: The Fourier transform of the central half of run S7174 (CN Ori on 18 December 2003). Non-linear least squares gives a period of 45.94 s, and an amplitude of 2.269 mmag for the DNO. Right: The $O-C$ phase diagram of the DNO, calculated relative to a test period of 45.94 s.

rather than an instance of period doubling, or an lpDNO. Fig. 5.31 also shows the $O-C$ behaviour of the DNO. There does not appear to be any clearly systematic trend in the $O-C$ diagram; it only shows that the DNO has poor coherence.

5.11 HP Nor

HP Nor is a Z Cam star (Vogt & Bateson 1982) with a maximum brightness of $V = 12.6$, and minimum of $V = 16.4$ (Bruch & Engel 1994). The orbital period for this system is not known.

Table 5.10: Log of the observations of HP Nor; no photometric filter was used in any of these observations.

Run No.	Date at start of night	Start time HJD = 2452000.0+	Length (h)	t_{int} (s)	Telescope	V (mag)
S6766	16 Feb. 2003	687.49203	0.78	5	40-in.	13.1
S6832	4 Mar. 2003	703.56956	2.10	6	30-in.	13.7
S6837	5 Mar. 2003	704.46186	4.23	6	30-in.	14.0
S6844	6 Mar. 2003	705.54105	2.70	8	30-in.	14.3
S6966	28 May 2003	788.29731	1.52	6	30-in.	13.7:
S7028	26 Jul. 2003	847.20273	1.48	6	40-in.	13.1
S7032	27 Jul. 2003	848.20234	0.27	6	40-in.	13.0
S7033	28 Jul. 2003	849.20217	1.33	5	40-in.	13.1

Notes: t_{int} is the integration time; ':' denotes an uncertain value.

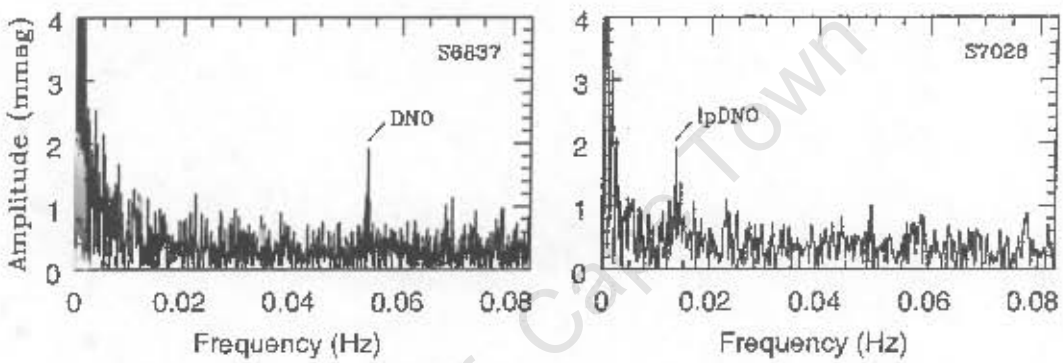

Figure 5.32: Left: The Fourier transform of the first 2.1 h of the light curve of HP Nor on 5 March 2003 (run S6837). The period determined from fitting a sine function to the DNO by non-linear least squares is 18.58 s. Right: The Fourier transform of a 0.76 h section of the light curve of HP Nor on 26 July 2003 (run S7028) showing an oscillation at 74.01 s, which I interpret as an lpDNO. The lpDNO was present only in this short section of data.

I observed HP Nor in outburst on eight different nights; the observing log is given as Table 5.10. Photometry of this object is complicated by a very crowded field—observing it photo-electrically would have been fairly awkward, but with a CCD the star crowding poses no serious problem, provided the seeing is not very bad. Both a DNO and an lpDNO were detected in HP Nor, but in separate outbursts[3].

Fig. 5.32 displays Fourier transforms of parts of the light curves of run S6837 and S7028, on these two nights a DNO and an lpDNO respectively were present. The DNO has a best-fit period of 18.58 s, and amplitude of 1.9 mmag; it persisted at detectable amplitude for the entire run. The lpDNO appeared only briefly; in the ~0.76 h section of data where it was most prominent, it has a period of 74.01 s, and an amplitude of 2.0 mmag. No QPOs were detected in any of my light curves.

[3]The 35.2 s DNO period listed in W04 is incorrect—my mistake.

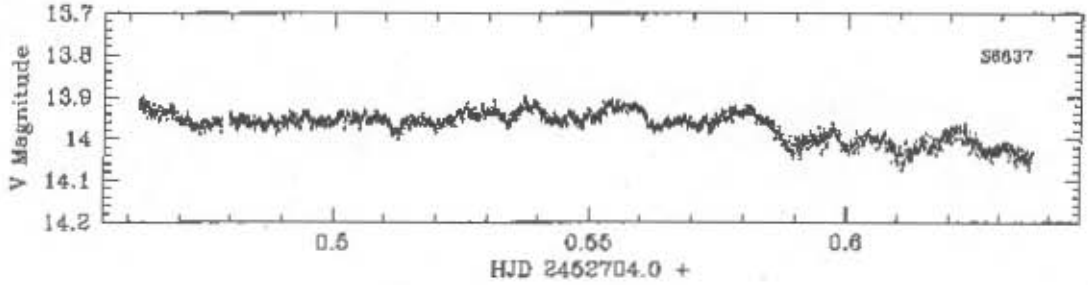

Figure 5.33: The light curve of HP Nor on 5 March 2003, corrected to first order for atmospheric extinction. The quality of photometry deteriorates towards the end of the run, despite decreasing airmass, because of worsening seeing.

I display the longest light curve in the data set (run S6837) as Fig. 5.33, since there is no high speed photometry of HP Nor published. None of the light curves showed any clear orbital modulation.

5.12 AG Hya

Very little is known about AG Hya; it is classified as a U Gem star (Vogt & Bateson 1982), and has been observed to vary in the range $V = 19.2$ to $V = 13.8$ (Szkody 1987; Echevarría, Costero & Michel 1993). There is no high speed photometry of this object in the literature, and the orbital period is not known.

I collected 13 h of high speed photometry of AG Hya (see Table 5.11). The data set did not reveal P_{orb}; run S6907, however, contains a QPO with a period of 683 s, as well as a 21.55 s DNO. Fig. 5.34 shows the light curve, in which the QPO is quite clear, together with the Fourier transform of a ~0.9 h section of the data. The DNO amplitude is sufficiently large for it to appear above the noise only in this short section of data, and it was never observed again. The low amplitude and brief presence make a more detailed investigation of the DNO impossible.

Table 5.11: The log of the observations of AG Hya; all observations were made in white light.

Run No.	Date at start of night	Start time HJD = 2452000.0+	Length (h)	t_{int} (s)	Telescope	V (mag)
S6907	3 Apr. 2003	733.29331	4.12	6	30-in.	14.7:
S6910	4 Apr. 2003	734.35400	1.25	6	30-in.	14.7:
S6913	7 Apr. 2003	737.33259	2.03	6	30-in.	14.7:
S6965	28 May 2003	788.19167	2.32	6, 7	30-in.	15.5:
S6969	29 May 2003	789.20833	2.32	6, 7	30-in.	16.0:
S6980	31 May 2003	791.19395	0.83	8, 10	30-in.	17.9

Notes: t_{int} is the integration time; ':' denotes an uncertain value.

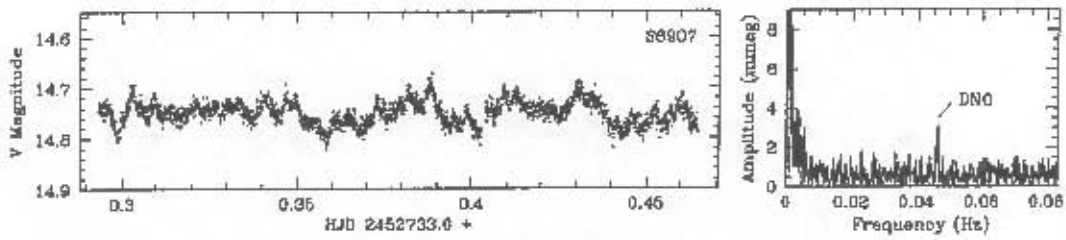

Figure 5.34: Left: The light curve of AG Hya on 3 April 2003, after being corrected for atmospheric extinction. Around 20 cycles of a QPO with a period of 683 s are directly visible in this light curve. Right: The Fourier transform of a ~0.9 h section of the light curve on the left, the DNO is at 46.40 mHz (21.55 s).

5.13 WX Hyi

WX Hyi is an SU UMa type DN, its normal outbursts have average maxima of $V = 12.7$ mag and recur roughly every 14 d; the average V magnitude at supermaximum is 11.4, and the supercycle is about 195 d. The system's visual magnitude varies in the range 15.0–14.2 at quiescence (Bateson & McIntosh 1986). Schoembs & Vogt (1981) spectroscopically measured the orbital period to be 1.7955 h. QPOs at ~1140 s and, on a different occasion, ~1560 s were observed during the decline from outburst by Kuulkers et al. (1991); WWP03 found a 185 s QPO present at the same time as a DNO with a period of 19.4 s, while WX Hyi was at $V = 14.5$.

WX Hyi was observed with the 30-, 40-, and 74-in. telescopes at Sutherland in outburst, as well as during quiescence. All observations were made in white light, and are listed in Table 5.12. No DNOs were found in any of the light curves, but two runs (S6463 and S7192) contained QPOs; they are displayed in Fig. 5.35. Run S7192 was made near quiescence, whereas S6463 was at minimum—only the second example of a QPO at quiescence. On both occasions the QPO period was near 190 s, which is similar to the 185 s QPO reported by WWP03.

Table 5.12: Log of the observations of WX Hyi.

Run No.	Date at start of night	Start time HJD = 2450000.0+	Length (h)	t_{int} (s)	Telescope	V (mag)
S6463	10 Jul. 2002	2466.48583	3.30	6	30-in.	15.0
S6700	28 Dec. 2002	2637.27838	1.40	4, 5	74-in.	12.8
S6979	30 May 2003	2790.58014	2.68	6	30-in.	14.1
S7192	24 Dec. 2003	2988.32532	1.62	5	40-in.	14.6
S7202	28 Dec. 2003	3001.30810	1.72	6	40-in.	15.0

Notes: t_{int} is the integration time; the final column lists the average nightly magnitudes.

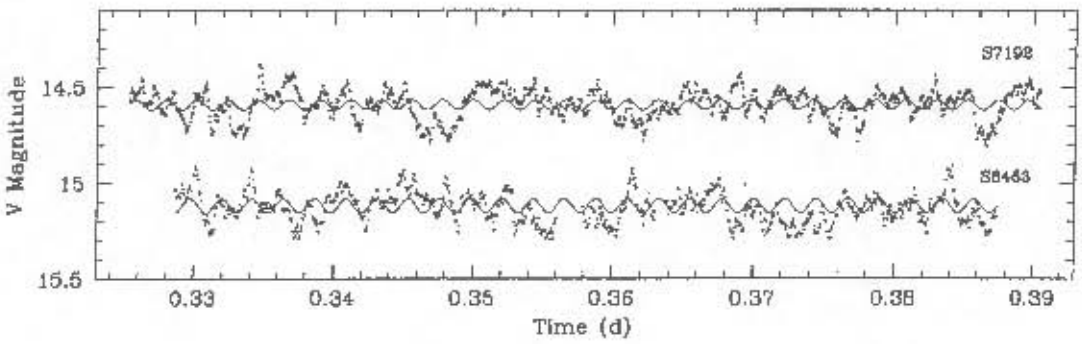

Figure 5.35: Sections of two of the WX Hyi light curves; slow variations were removed from both, and run S6463 is vertically shifted by +0.2 mag. The best-fit sine functions to the QPOs (for these sections) are over-plotted, the QPO periods are 193.5 s and 190.2 s for run S6463, and S7192 respectively.

Note that for the three ~100 s QPOs the period luminosity relation has the same sense as that for DNOs, although this may not mean much, since they were not observed during the same outburst cycle. The QPOs illustrated in Fig. 5.35 (especially the one in S6463), and also the WX Hyi QPO shown in WWP03, keep remarkably good phase.

5.14 TW Vir

TW Vir is a U Gem type DN, with a visual brightness of between 15.8 and 12.1 mag, an outburst recurrence time ranging from 15 to 44 d (Bateson, Jones & McIntosh 1993), and an orbital period of 4.3838 h (Shafter 1983).

TW Vir was observed from Sutherland on the decline from two different outbursts, in all cases with the 30-in. telescope in white light, see Table 5.13. Run S6948 contains a QPO, as well as a modulation at ~120 s, Fig. 5.36 shows this light curve. A large amplitude modulation is obvious to the eye, vertical bars at intervals of 1047 s along the bottom of Fig. 5.36 indicate the average QPO period. After a phase (or

Table 5.13: Log of the observations of TW Vir.

Run No.	Date at start of night	Start time HJD = 2452000.0 +	Length (h)	t_{int} (s)	Telescope	V (mag)
S6896	1 Apr. 2003	731.34857	3.60	6	30-in.	15.1
S6901	2 Apr. 2003	732.29515	2.38	6	30-in.	15.4
S6944	20 May 2003	780.31549	2.52	6	30-in.	13.6
S6948	21 May 2003	781.27655	2.65	6, 7	30-in.	15.1
S6952	23 May 2003	783.19448	4.35	7	30-in.	15.4

Notes: t_{int} is the integration time; the final column lists the average nightly magnitudes.

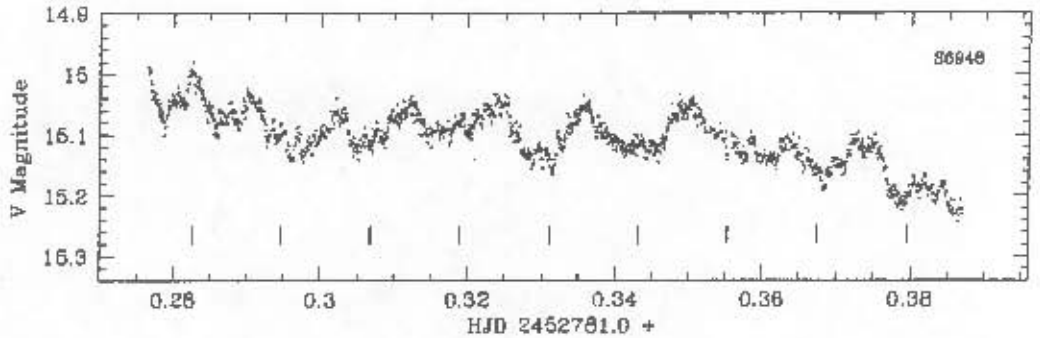

Figure 5.36: The light curve of TW Vir on 21 May 2003. Clearly visible is a prominent ~1000 s oscillation. The Fourier transform (left hand panel of Fig. 5.37) indicates that the period is 1047 s, bars along the bottom are equally spaced at this period.

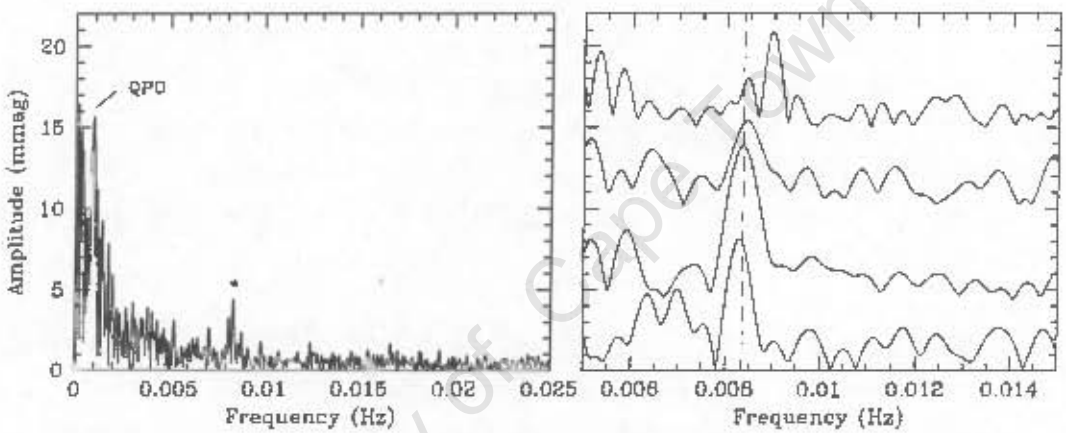

Figure 5.37: Left: The low frequency end of the Fourier amplitude spectrum of the light curve displayed in Fig. 5.36, the very large power centred on 0.9551 mHz (1047 s) is interpreted as a QPO. Another significant feature appears at 8.373 mHz (119.43 s; marked by an asterisk), this is possibly the telescope drive error, rather than an oscillation intrinsic to the star. Right: Fourier transforms of (bottom to top) the first, second, third and fourth quarter of run S6948, arbitrarily displaced along the vertical axis for display purposes. The dashed line indicates a period of 2 sidereal minutes (119.67 s). The amplitude maxima are at (bottom to top) 120.66, 119.70, 118.47, and 111.61 s.

perhaps period) change near the start of the light curve, the QPO minima roughly coincide with the bars. The best-fit amplitude for this modulation is 15.6 mmag.

The QPO shows up very clearly in the Fourier transform of run S6948 (see the left hand panel of Fig. 5.37) which also shows significant power close to the 30-in. telescope's known drive error of 2 sidereal minutes. Signals at around this period are usually dismissed as spurious (see Section A.1.2 for a more complete discussion of this problem), but in this case closer inspection hints that it may in fact be

intrinsic to the star. Dividing the light curve into four non-overlapping sections, and computing a Fourier transform of each of these parts individually, shows that the detected signal is not at constant period (right hand panel of Fig. 5.37). Guide corrections introduce phase changes to the the modulation caused by the telescope drive, which will broaden the peak in the Fourier transform, but should not shift the central frequency. Since the track rate is adjustable, the drive error need not be at exactly 2 sidereal minutes, but it is strictly constant (the track rate was not changed during the run). Fig. 5.37 shows a changing period. Nevertheless, this may result from a drive error, together with flickering. The ~120 s signal did not appear in the reference star (there is only one, relatively faint, reference star in the field of TW Vir). However, this does not conclusively demonstrate that the signal was real, since the position of a star on the CCD chip is a factor in determining whether its light curve will be contaminated by a drive error. Note that a real oscillation at the period in question is essentially undetectable with this telescope.

5.15 PU CMa

Judging by its orbital period of 1.3606 h (Thorstensen & Fenton 2003), the DN PU CMa is expected to be an SU UMa star; Kato et al. (2003) found some weak indications of superhumps during outburst, but the classification remains to be confirmed. There is no high speed photometry of this object published.

I observed it with the SAAO telescopes, once near minimum light, and on three other nights in outburst (see Table 5.14). PU CMa was found to flicker at large amplitude during all but one of the observations: the light curve of run S6762 is dominated by a quasi-coherent modulation, and does not seem to contain much flickering.

Fig. 5.38 displays this light curve, the average period is 119.1 s, and the oscillation has very low coherence, characteristic of a QPO. No shorter period oscillations could be in any of the PU CMa light curves.

Table 5.14: Log of the observations of PU CMa. No filter was used in any of the observations.

Run No.	Date at start of night	Start time HJD = 2452000.0+	Length (h)	t_{int} (s)	Telescope	V (mag)
S6701	28 Dec. 2002	637.35245	6.20	6	74-in.	16.1
S6758	15 Feb. 2003	686.26385	1.97	5	40-in.	14.4
S6762	16 Feb. 2003	687.25677	1.63	5	40-in.	14.7
S6768	17 Feb. 2003	688.26195	1.30	5, 6	40-in.	15.8

Note: t_{int} is the integration time.

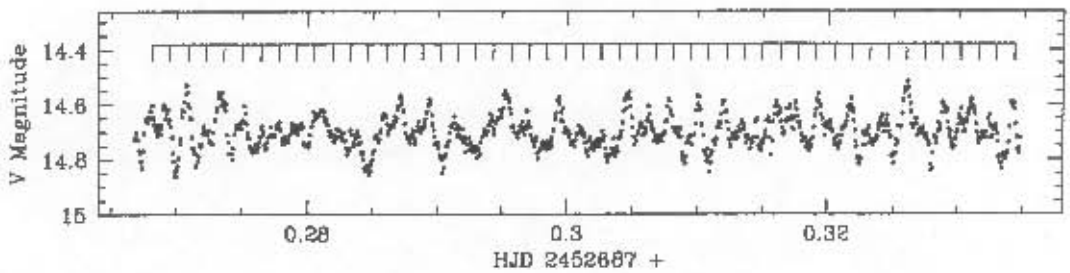

Figure 5.38: The light curve of PU CMa on 16 February 2003, with a long period modulation removed. The inset scale indicates the average QPO period of 119.1 s.

5.16 V426 Oph

V426 Oph is a Z Cam star with visual magnitude ranging from 10.9 to 13.4, an outburst cycle of about 22 d, and an orbital period of 6.847 h (Hessman 1988). Szkody (1986) detected a 1 h period in an *EXOSAT* X-ray observation, and proposed that this is the white dwarf spin period, and therefore, that V426 Oph is an IP. Norton & Watson (1989) and Hellier et al. (1990) reanalysed the *EXOSAT* data, and found that the 1 h period was, in fact, not statistically significant. Furthermore, in their optical photometry and spectroscopy, Hellier et al. (1990) find no evidence to suggest that V426 Oph is an IP. Szkody, Kii & Osaki (1990) report the presence of a ~28 min. QPO in *Ginga* data of this system, but a glance at their Fourier transforms (fig. 7) shows that any power present near 0.0006 Hz is no different from the red noise expected from random flickering. The latest addition to the confusion is the detection by Homer et al. (2004) of a 4.2 h modulation and its first harmonic in *Chandra* observations of V426 Oph; they also reanalysed *Ginga* (Szkody et al. 1990) and *ROSAT* (Rosen et al. 1994) data taken in 1988, and show that these data are just compatible with the 4.2 h or 2.1 h periods, but certainly do not demonstrate that "...the 4.2 h period or its harmonic are stable and persistent in X-ray/optical data from 1988 to 2003.". Homer et al. (2004) propose that the 4.2 h period may be identified with the rotation of the white dwarf, but point out that this interpretation is physically unreasonable.

I obtained high speed optical photometry of V426 Oph on eight nights in 2003, the observations are listed in Table 5.15. Weather conditions were unfavourable during all but two of the runs, but it was nevertheless possible to recover good quality differential photometry. Large amplitude flickering is present in every light curve, also, no single observation was long compared to any of the profusion of periods reported for this system. No sign of any persistent period was found in the data set, in fact, the only modulation to surface above the flickering was a signal at ~73 s in run S6935, taken on 18 May 2003. Fig. 5.39 shows the relevant light curve. A few

Table 5.15: Log of the observations of V426 Oph. All observations were made in white light.

Run No.	Date at start of night	Start time HJD = 2452000.0+	Length (h)	t_{int} (s)	Telescope	V (mag)
S6935	18 May 2003	778.49935	1.57	6	40-in.	12.1
S6962	27 May 2003	787.36622	0.80	6	30-in.	13.5:
S6967	28 May 2003	788.36347	0.95	6	30-in.	13.4:
S6973	29 May 2003	789.47237	2.12	6	30-in.	12.7:
S6978	30 May 2003	790.51931	1.52	6	30-in.	13.9:
S6983	31 May 2003	791.42537	2.22	6	30-in.	12.9:
S7083	4 Sept. 2003	887.21438	2.38	6	40-in.	12.6
S7086	5 Sept. 2003	888.21271	1.33	6	40-in.	12.6:

Notes: t_{int} is the integration time; ':' denotes an uncertain value.

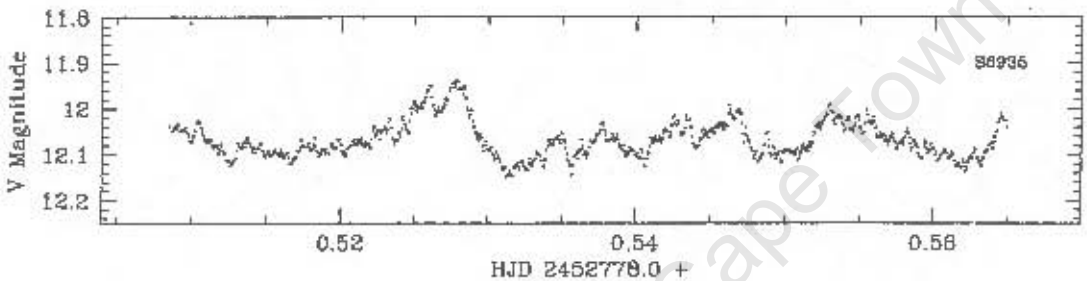

Figure 5.39: The light curve of V426 Oph on 18 May 2003 (run S6935), corrected to first order for atmospheric extinction. The rapid flickering disguises a quasi-coherent 73 s modulation—see Fig. 5.40.

of the most prominent cycles of the 73 s oscillation are directly visible but the the Fourier transform (left hand panel of Fig. 5.40) makes the signal more evident. Also displayed in Fig. 5.40 is the amplitude and phase variability of this modulation. The $O-C$ diagram shows that the 73 s oscillation has fairly high coherence, but is not strictly periodic (note that in this diagram only every third point is independent); from the amplitude diagram can be seen that the oscillation reached amplitudes as large as 10 mmag.

The 73 s oscillation appears unusually coherent for a QPO, but in the absence of more rapid oscillations, it is difficult to know whether to classify it as a DNO or an lpDNO. For the moment I will call the 73 s oscillation a DNO; the detection of a shorter period in V426 Oph may in the future change this classification. Until a similar time scale is observed in V426 Oph, one cannot have absolute confidence in the reality of the DNO. However, should the oscillation (and its quasi-periodic nature) be confirmed, the favoured model for DNOs (and lpDNOs) excludes V426 Oph from being an IP.

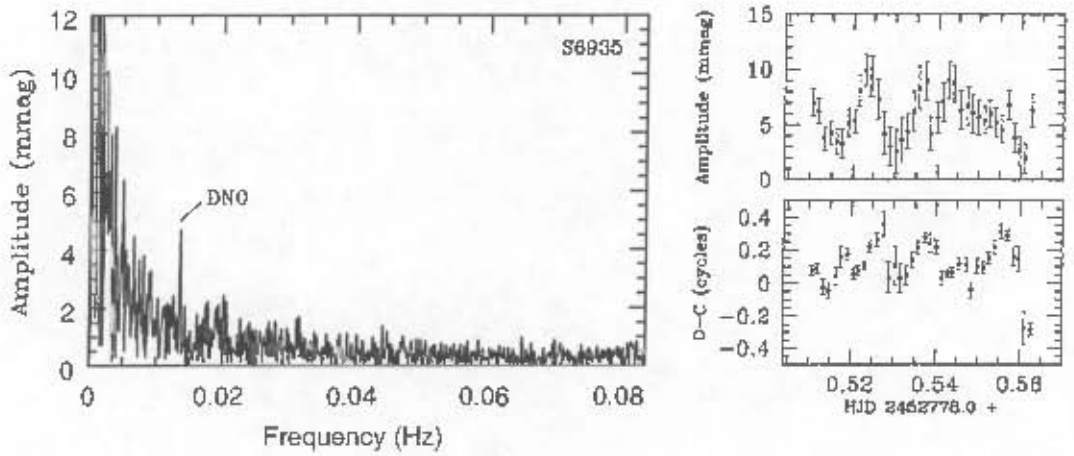

Figure 5.40: Left: The Fourier transform of the light curve shown in Fig. 5.39, the narrow spike at 0.01365 Hz (73.26 s) is interpreted as a DNO or lpDNO. Right: Amplitude and $O-C$ phase diagrams of the 73 s modulation. Each point represents a non-linear least squares fit of a sine function with period 73.26 s to ~5 cycles of the modulation; there is 67% overlap between consecutive points.

5.17 OY Car

OY Car was discovered to be an eclipsing DN by Vogt (1979), it is an SU UMa star (Bateson 1979c), with normal maxima of $V = 12.4$, and supermaxima of $V = 11.5$ (Bateson & Dodson 1983), and has $P_{orb} = 1.514902$ h (Vogt 1979; Vogt et al. 1981). This system has become one of the best studied DN, and has been observed to have the full set of DNOs, lpDNOs, and QPOs, including a DNO at quiescence (Schoembs 1986; Marsh & Horne 1998; Ramsay et al. 2001; WWP03); the 1500 s QPO listed by W04 is predicted in the model of WW02b, but has not been observed.

OY Car is also the only DN for which convincing evidence (independent of DNO or lpDNO models) for white dwarf magnetism exists—see Section 4.1.5. I present

Table 5.16: The observing log for OY Car; the final column lists the mean magnitude outside of eclipse for each night. The observations were made in unfiltered light.

Run No.	Date at start of night	Start time HJD = 2452000.0+	Length (h)	t_{int} (s)	Telescope	V (mag)
S6739	4 Feb. 2003	675.46915	1.97	5	40-in.	12.7
S6743	5 Feb. 2003	676.40368	2.47	5	40-in.	13.0
S6748	7 Feb. 2003	678.42970	1.57	5	40-in.	15.1:
S6752	9 Feb. 2003	680.31508	1.08	6	40-in.	15.1
S6754	9 Feb. 2003	680.42688	2.93	5	40-in.	15.0
S6755	10 Feb. 2003	681.46269	0.63	5, 6	40-in.	16.2:

Notes: t_{int} is the integration time; ':' denotes an uncertain value.

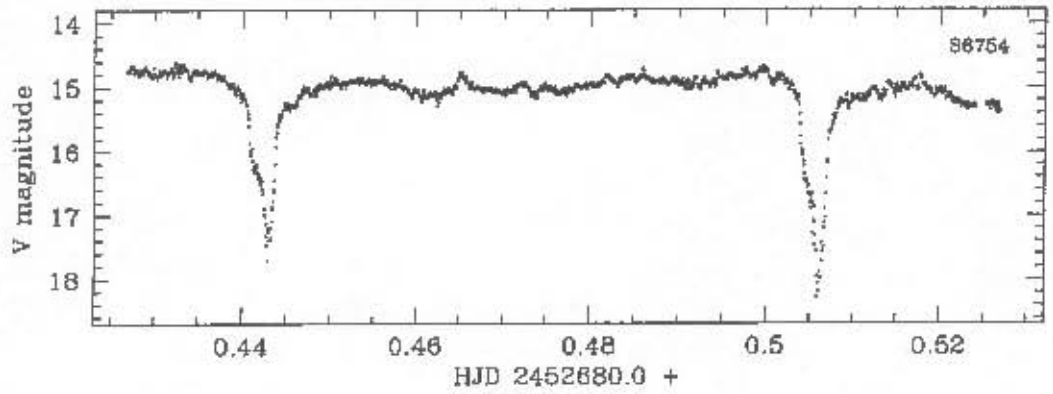

Figure 5.41: The second of the light curves of OY Car taken on 9 February 2003 (run S6754), taken during the late decline from superoutburst.

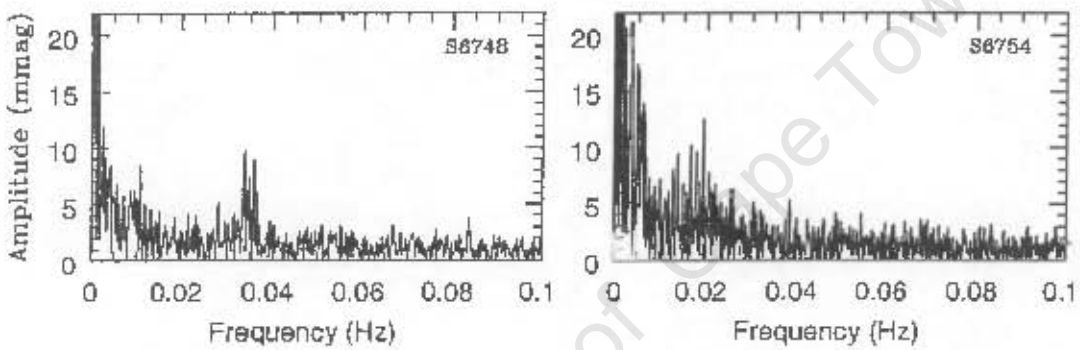

Figure 5.42: Fourier transforms of run S6748 (left panel) and S6754 (right panel; only the section of data between the two eclipses). The best-fit period to the DNO in run S6748 is 29.6 s; the excess power in the Fourier transform of run S6754 is centred on 0.0187 Hz (53.5 s).

here observations made later during the February 2003 superoutburst, in which DNOs at 17.62 s and 17.79 s, and QPOs between 281 s and 338 s were detected by WWP03 (see Table 5.16).

Fig. 5.41 displays the light curve of run S6754 (the second of two light curves obtained on 9 February 2003). DNOs were detected in this run, as well as in run S6748. Fig 5.42 gives Fourier transforms of these two light curves.

The broad, noisy appearance of the DNO in run S6748 is caused by an unstable period and amplitude. In run S6754 the DNO is very incoherent; a decrease in coherence of DNOs late in outburst is also seen in other systems (Hildebrand et al. 1981a; Córdova et al. 1984; WW02b), but it is not clear how the period of ~54 s fits in with the 48 s DNO found in OY Car in quiescence by WWP03.

5.18 VZ Pyx

Remillard et al. (1994) found VZ Pyx to be a DN, probably of SU UMa type, and report a 49 min. photometric period, which they suggest could be the white dwarf spin period, should it prove to be coherent on long time scales. VZ Pyx has $P_{orb} = 1.7597$ h (Remillard et al. 1994; Thorstensen 1997); its status as an SU UMa star was confirmed by Kato & Nogami (1997), but no evidence to support that it is an IP has since been published. WWP03 report a 112 s lpDNO, and, on a different night, a DNO at 23.86 s together with a QPO at a period of 390.5 s, with VZ Pyx at $V = 12.2$, and argue, based on their detection of DNOs, that VZ Pyx cannot be an IP.

I observed this system during three different outbursts (see Table 5.17). The February 2003 observations started with VZ Pyx on the decline from a normal outburst, which triggered a superoutburst, with superhumps appearing on 22 February.

Table 5.17: Log of the observations of VZ Pyx. A V filter was used in run S6791, the rest of the observations were made in white light.

Run No.	Date at start of night	Start time HJD = 2452000.0+	Length (h)	t_{int} (s)	Telescope	V (mag)
S6680	18 Dec. 2002	627.53220	1.93	6	40-in.	13.1
S6773	18 Feb. 2003	689.46641	1.10	5	40-in.	14.0
S6776	19 Feb. 2003	690.45966	1.78	5, 8	40-in.	15.0
S6781	20 Feb. 2003	691.45623	2.03	6	40-in.	15.3
S6786	21 Feb. 2003	692.47610	1.60	5	40-in.	12.8
S6791	22 Feb. 2003	693.36094	2.52	6	40-in.	12.1[a]
S6797	23 Feb. 2003	694.34161	2.03	5, 6	40-in.	11.7
S7170	16 Dec. 2003	990.47344	1.25	6	40-in.	15.4

Notes: t_{int} is the integration time; [a] taken with a V filter.

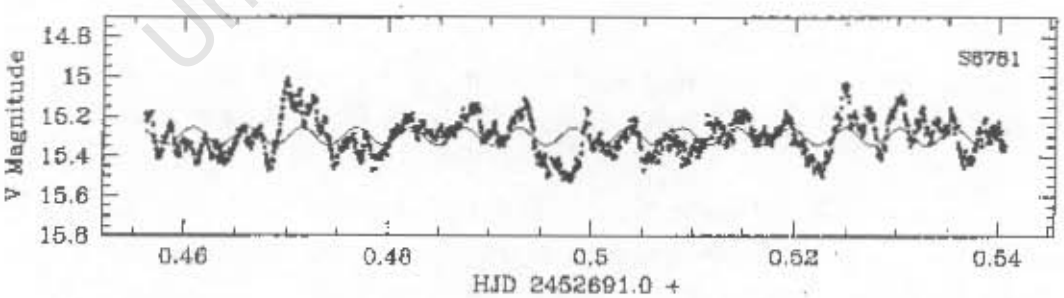

Figure 5.43: The light curve of VZ Pyx on 20 February 2003 (Run S6781); it was corrected for extinction, and prewhitened to remove a modulation with a period of 2 440 s. The light curve contains a QPO—non-linear least squares gives a best-fit period of 460 s and amplitude of 41.2 mmag. This fit is superimposed on the data.

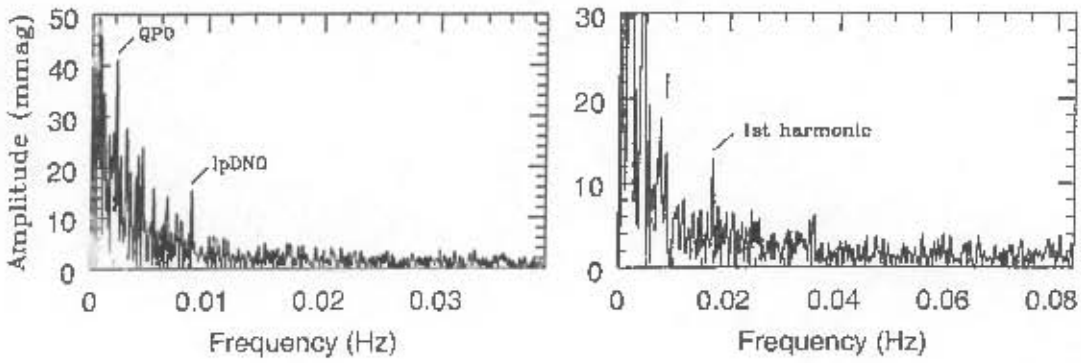

Figure 5.44: Left: The low frequency end of the Fourier transform of the whole of run S6781. QPO and lpDNO features at 2.16 mHz (463 s) and 8.64 mHz (116 s) are indicated. Right: The Fourier transform of the last third of the light curve displayed in Fig. 5.43. The lpDNO doubles in frequency during the run, and here appears at 17.3 mHz (57.8 s). A vertical bar marks the position of the fundamental.

Three significant periodicities were detected in run S6781. A QPO can be seen in the light curve of this run. Fig. 5.43 shows this light curve with a best-fit sine function to the QPO over-plotted. The QPO period is 460 s. The Fourier transform (left hand panel of Fig. 5.44) has a sharp spike above the red noise at 8.64 mHz (116 s). In light of the 112 s period reported by WWP03, I interpret this as an lpDNO. In the last third of run S6781, the lpDNO power shifts to the first harmonic (right hand panel of Fig. 5.44). Another example of frequency doubling of an lpDNOs may be a signal at 147 s in KT Per, which changed to 82 s (Robinson & Nather 1979).

5.19 V1159 Ori

There is a group of SU UMa type DN with unusually short recurrence times of normal and superoutbursts, sometimes referred to as ER UMa stars. V1159 Ori is such a system (Nogami et al. 1995; Robertson, Honeycutt & Turner 1995) it has a ~4 d recurrence period for normal outbursts (Jablonski & Cieslinski 1992), a ~45 d supercycle (Robertson et al. 1995), and $P_{orb} = 1.49227$ h (Jablonski & Cieslinski 1992; Thorstensen et al. 1997). The most comprehensive photometric study of this system is that by Patterson et al. (1995); they detected DNOs with a period evolving from 29 s to 34 s over 7 nights of the decline from superoutburst, and derive a period-luminosity relation $\frac{1}{P_{DNO}}\frac{dP_{DNO}}{dm} = 0.37 \pm 0.02$ mag^{-1} (or, equivalently, $\frac{d\log(P_{DNO}/s)}{d\log(I/I_{min})} = -0.40$).

I obtained two light curves of V1159 Ori during different superoutbursts (see Table 5.18) the observations were made in white light using the 40-in. reflector.

Table 5.18: Log of the observations of V1159 Ori.

Run No.	Date at start of night	Start time HJD = 2452000.0+	Length (h)	t_{int} (s)	Telescope	V (mag)
S6649	25 Nov. 2002	604.48413	3.07	4, 5	40-in.	12.9
S6784	21 Feb. 2003	692.25652	0.88	5	40-in.	12.9

Note: t_{int} is the integration time.

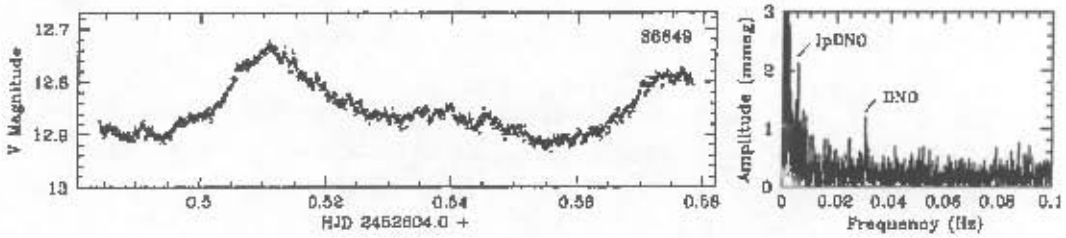

Figure 5.45: Left: The light curve of a 2.3 h section of run S6649, corrected to first order for atmospheric extinction. The large amplitude modulation is a superhump. Right: The Fourier transform of the light curve shown on the left. The DNO at 0.03097 Hz (32.28 s) and lpDNO at 0.00565 Hz (177 s) are indicated.

Rapid oscillations were detected on 25 November (run S6649), the left hand panel of Fig. 5.45 shows part of this light curve. The Fourier transform (right hand panel of Fig. 5.45) shows a DNO at 32.28 s with an average amplitude of 1.2 mmag; this really adds nothing to what was known from the work by Patterson et al. (1995). More interesting is the probable detection of an lpDNO. A spike at 177.0 s shows above the red noise, this is at $5.483 \times P_{DNO}$, and is probably an lpDNO.

5.20 SY Cnc

SY Cnc is a Z Cam star with a V magnitude of 12.2 at standstill, and outbursts taking it from $V = 14.5$ to $V = 11.1$ every $\sim$27 d (Vogt & Bateson 1982). The orbital period is 9.1 h (Shafter 1983). SY Cnc is known to have DNOs with periods in the range 20.20 s to 33.83 s (Robinson 1973b; Nevo & Sadeh 1978; Patterson 1981; Middleditch & Córdova 1982).

I observed SY Cnc on two nights of its December 2003 outburst (see Table 5.19). Robinson (1973b) remarks that the amplitude of flickering in SY Cnc is very low; this was noticeable in both of my light curves. Run S7178 was made under poor weather conditions and contained no short period oscillations above an amplitude of 1.5 mmag; five nights later, however (run S7194) a DNO at 24.87 s was detected—Fig. 5.46 shows the Fourier transform. Since DNOs in SY Cnc have been well studied, I will not describe my result in any more detail.

Table 5.19: Log of the observations of SY Cnc; white light was used on both nights.

Run No.	Date at start of night	Start time HJD = 2452000.0+	Length (h)	t_{int} (s)	Telescope	V (mag)
S7178	19 Dec. 2003	993.51959	0.88	5	40-in.	11.6:
S7194	24 Dec. 2003	998.55080	1.27	5	40-in.	13.3

Notes: t_{int} is the integration time; ':' denotes an uncertain value.

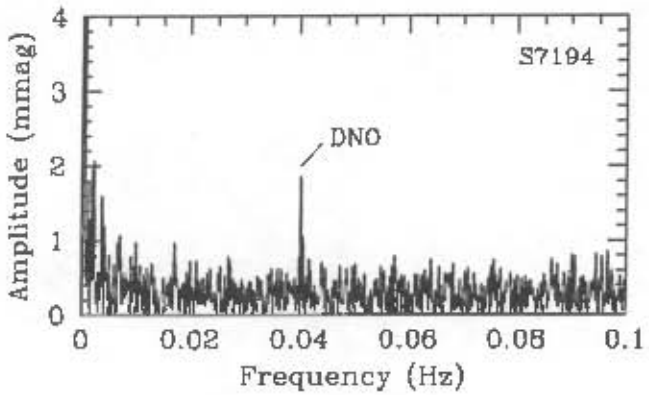

Figure 5.46: The Fourier transform of the light curve of SY Cnc on 24 December 2003 (run S7194). A clear DNO feature at 0.04020 Hz (24.87 s) is marked. The amplitude of the DNO (determined by non-linear least squares) is 1.86 mmag.

5.21 EC 21178-5417

EC 21178-5417 (hereafter abbreviated EC2117) is an eclipsing NL with P_{orb} = 3.708 h, and has been observed to have DNOs with periods in the range 10.82–25.46 s, lpDNOs in the range 79.9–195 s, and QPOs between roughly 330 s and 500 s (WWP03).

EC2117 was extensively observed during the 2002 season, and proved to be a prolific source of DNOs: in 14 out of 18 runs on this object taken during 2002 (including the first four listed in Table 5.20) DNOs were present for at least part of the time (WWP03). However, nine separate observations in 2003 (during which EC2117 was usually a few tenths of a magnitude fainter than in 2002) produced no DNO detections. The log of my observations of the system is given in Table 5.20.

lpDNOs and/or DNOs were found in three of my observations. Fig. 5.47 shows two light curves, together with their Fourier transforms. Run S6641 contains a DNO, and at the same time an lpDNO, while only a DNO was seen in S6666. Run S6660 was centred on an eclipse, and relatively short. A DNO at 23.17 s was nevertheless detected in the last ~20 min. These observations have already been thoroughly described in WWP03. Some evidence of an oscillation of low coherence at around 103 s was found in run S7077, but it was not very convincing. None of the other observations made during the 2003 season contained any quasi-coherent oscillations.

Table 5.20: Log of the observations of EC2117; the final column lists the nightly mean magnitude outside of eclipse. All the observations were made in unfiltered light.

Run No.	Date at start of night	Start time HJD = 2452000.0+	Length (h)	t_{int} (s)	Telescope	V (mag)
S6641	24 Nov. 2002	603.27788	1.77	6	40-in.	13.5
S6660	30 Nov. 2002	609.26322	1.03	6	40-in.	13.4
S6666	1 Dec. 2002	610.26547	1.07	6	40-in.	13.4
S6670	17 Dec. 2002	626.28606	0.82	6	40-in.	13.6
S6959	24 May 2003	784.52951	3.80	6	30-in.	13.8:
S6964	27 May 2003	787.56795	1.47	6	30-in.	13.8:
S6975	29 May 2003	789.61625	1.65	6	30-in.	13.9:
S7020	23 Jul. 2003	844.44374	1.27	5	40-in.	13.7
S7030	26 Jul. 2003	847.39234	3.05	5	40-in.	13.7
S7036	28 Jul. 2003	849.45274	2.23	5	40-in.	13.6
S7077	2 Sept. 2003	885.32688	2.62	5	40-in.	13.7
S7150	14 Oct. 2003	927.25266	2.77	5	40-in.	13.9:
S7153	16 Oct. 2003	929.23930	1.95	5	40-in.	13.9:

Notes: t_{int} is the integration time; ':' denotes an uncertain value.

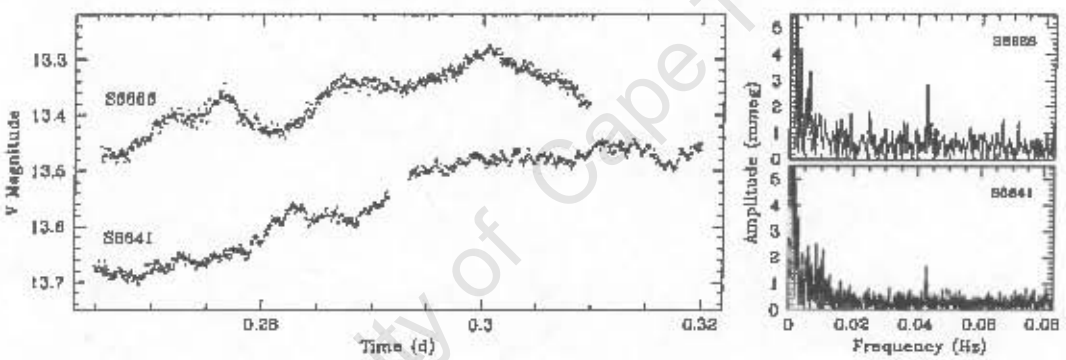

Figure 5.47: Left: Light curves of EC2117 on 24 November and 1 December 2002. An lpDNO is directly visible in the 24 November observations (run S6641), which is vertically translated by +0.02 mag. Right: Fourier transforms of these two light curves, with DNOs at 23.18 s (S6641) and 23.29 s (S6666). The lpDNO power in run S6641 is diluted in the Fourier transform, because it changes period from 95.82 s to 101.03 s during the run.

5.22 V1193 Ori

V1193 Ori was discovered as a rapidly varying blue star by Hamuy & Maza (1986), and classified as a UX UMa type NL by Bond et al. (1987); the spectroscopically determined orbital period is 3.96 h (Ringwald, Thorstensen & Hamwey 1994). What appears to be rapid, large amplitude flickering is evident in every published light curve of this object (Bond et al. 1987; Warner & Nather 1988; Papadaki et al. 2004). My light curves of V1193 Ori (see Table 5.21 for the observing log) are dominated by QPOs, rather than flickering, although they look very similar to those of Bond et al.

Table 5.21: Observing log for V1193 Ori; these observations were all made in white light. The final column lists the dominant period for each night.

Run No.	Date at start of night	Start time HJD = 2452000.0+	Length (h)	t_{int} (s)	Telescope	V (mag)	P_{QPO} (s)
S6648	25 Nov. 2002	604.41708	1.38	4, 8	40-in.	14.0	992
S6652	26 Nov. 2002	605.50435	2.70	6	40-in.	14.0	1255
S6655	28 Nov. 2002	607.40756	5.15	6	40-in.	14.0	1027
S6659	29 Nov. 2002	608.46563	3.47	5, 6	40-in.	13.8	780
S6663	30 Nov. 2002	609.47053	2.02	6	40-in.	14.0	1214
S6668	1 Dec. 2002	610.40801	3.12	5	40-in.	13.9	1321
S6675	17 Dec. 2002	626.54630	1.32	8	40-in.	14.8	934
S6689	23 Dec. 2002	632.32129	4.30	5	40-in.	13.9	707
S6692	24 Dec. 2002	633.48646	2.95	4, 5	74-in.	14.0	1151
S6694	25 Dec. 2002	634.32814	4.95	4, 5	74-in.	14.0	1468
S6696	26 Dec. 2002	635.48094	2.85	5	74-in.	14.0	1256
S6698	27 Dec. 2002	636.33502	3.55	5	74-in.	14.0	865

Note: t_{int} is the integration time.

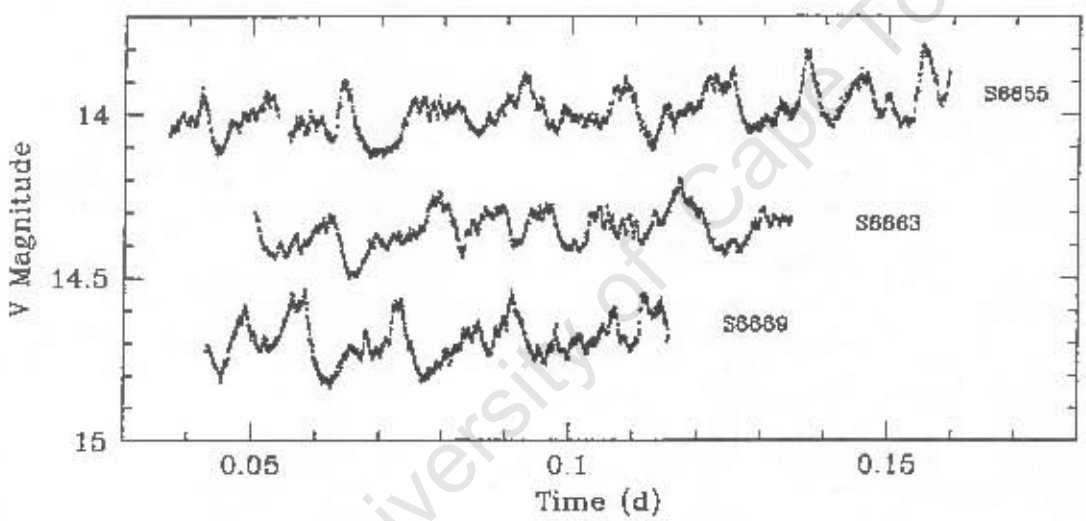

Figure 5.48: A sample of V1193 Ori light curves (the S6665 and S6689 light curves are not complete). The S6663 (S6689) data have been shifted vertically by +0.4 mag (+0.8 mag).

(1987) and Warner & Nather (1988). Fig. 5.48 shows sections of three of the light curves, all containing prominent QPOs. Despite a period that changes from night to night, the QPO stands out in the Fourier transform of the first six runs combined (see the left hand panel of Fig. 5.49), which implies unusually large coherence. At this point, in fact, we were wondering whether, given more observations, V1193 Ori might prove to be an IP. However, the QPO did not appear as strongly in Fourier transforms of other combinations of light curves in this data set. The average Fourier transform of all the observations of V1193 Ori shows power in excess of red noise at

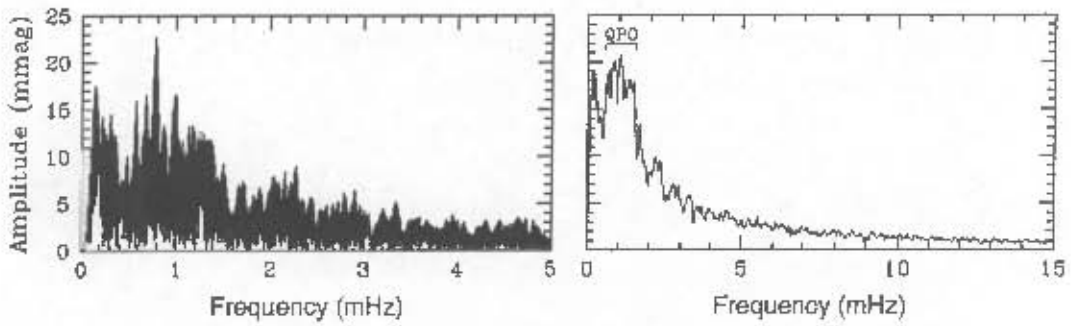

Figure 5.49: Left: The Fourier transform of the first six runs on V1193 Ori (taken over seven nights; see Table 5.21) combined. The data were prepared by subtracting a linear trend from each light curve individually before calculating the Fourier transform. The maximum amplitude is at 0.7834 mHz (1276 s). Right: The average Fourier transform of the whole V1193 Ori data set. The QPO appears as a hump of power at frequencies between 0.580 mHz (1720 s) and 1.54 mHz (649 s), superimposed on the smoothly rising red noise.

frequencies between 0.580 mHz (1720 s) and 1.54 mHz (649 s); this is displayed in the right hand panel of Fig. 5.49.

No shorter period oscillations (or, for that matter, persistent longer period modulations) were found in the data set.

The QPOs in V1193 Ori look very similar to kilosecond QPOs seen in V442 Oph, RX J1643.7+3402, and several more SW Sex stars, which have been interpreted as a low coherence manifestation of the underlying stable rotation of a magnetic white dwarf (Patterson et al. 2002; this is discussed in Section 3.2 and 4.2). However, V1193 Ori has none of the other characteristics of SW Sex stars.

5.23 CR Boo

CR Boo is an AM CVn star (Wood et al. 1987) with an orbital period of 1471.35 s (Provencal et al. 1991), it has high and low photometric states, similar to a DN outburst cycle, its B magnitude varying from 17.2 to 13.6 (Wood et al. 1987; Patterson et al. 1997). The high state light curve is dominated by a ~1490 s modulation (with considerable harmonic content) which is interpreted as a superhump (e.g. Patterson et al. 1997).

High state observations of this object were obtained on five nights, and are listed in Table 5.22. Harmonics of the familiar 1490 s modulation were present in almost all the light curves, run S6852 (taken on 8 March 2003) however, contains the full set of rapid oscillations. The light curve of this run is shown as Fig. 5.50; a QPO at ~291 s is clearly evident. The third and fourth harmonics of the superhump have periods in the range where QPOs could be expected, but the measured QPO period

Table 5.22: Log of the observations of CR Boo; white light was used throughout.

Run No.	Date at start of night	Start time HJD = 2452000.0+	Length (h)	t_{int} (s)	Telescope	V (mag)
S6848	7 Mar. 2003	706.44849	2.40	6, 7, 8	30-in.	15.1
S6852	8 Mar. 2003	707.42754	5.48	6	30-in.	14.6
S6856	9 Mar. 2003	708.41382	4.32	6, 7	30-in.	14.8
S6862	10 Mar. 2003	709.42319	5.53	6, 7, 8	30-in.	14.9
S6933	18 May 2003	778.31933	1.18	6, 7	40-in.	14.6

Notes: t_{int} is the integration time; the final column lists the average nightly magnitudes.

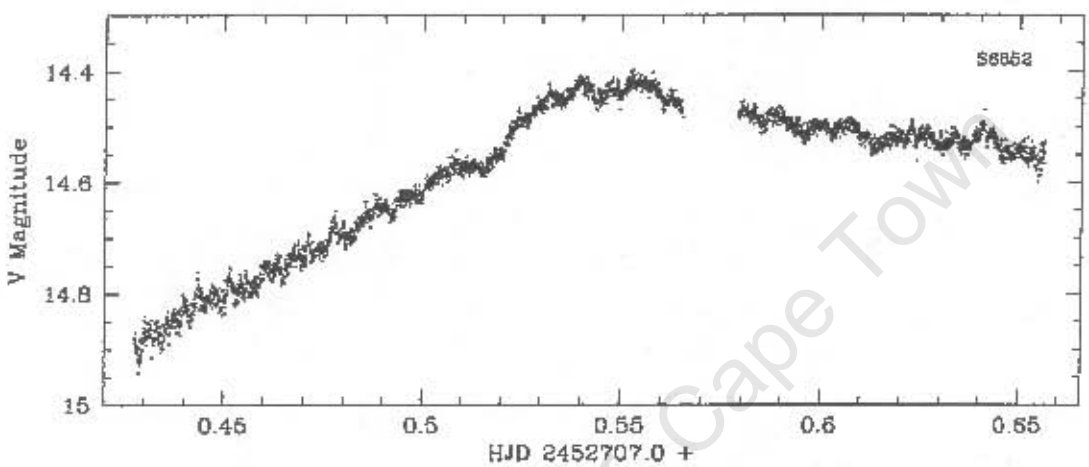

Figure 5.50: The light curve of CR Boo on 8 March 2003 (run S6852), corrected to first order for atmospheric extinction. A part of this light curve appeared as fig. 27 of WWP03.

(291 s) is far enough removed from the fourth harmonic of the superhump (298 s) to rule out any confusion.

The ~0.5 mag rise during the first ~2.9 h of the light curve is not unusual for this object; see e.g. fig. 1 of Patterson et al. (1997).

The Fourier transforms of shorter sections of the S6852 light curve (Fig. 5.51) shows that the run also contained an lpDNO (at 61.93 s) and a DNO (at 21.71 s). The DNO is rather less coherent than the lpDNO, and appears above the scintillation and photon counting noise only in Fourier transforms of short sections of light curve.

The presence of DNOs, QPOs and lpDNOs in the high $\dot{M}$ state of CR Boo is another parallel between this system and the DN. Accepting the magnetic models for DNOs and lpDNOs, it is also—together with the DNO and lpDNO in AM CVn (Warner & Robinson 1972a,b; Patterson et al. 1979, 1992) and the lpDNO in V803 Cen (see Section 5.24)—the only evidence for magnetism in AM CVn stars (WWP03).

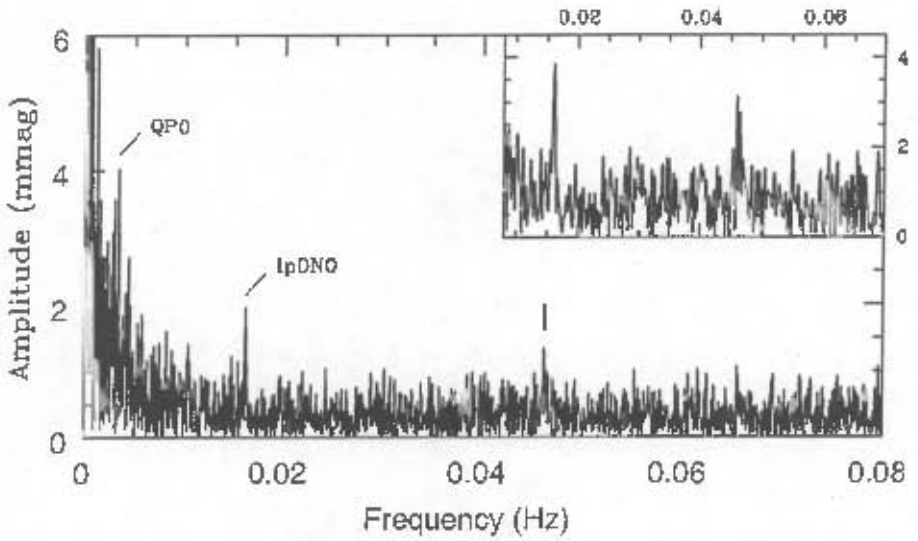

Figure 5.51: The Fourier transform of the first 3.31 h of the light curve shown in Fig. 5.50, with the QPO and lpDNO features indicated. A vertical bar marks the DNO frequency (46.05 mHz, corresponding to 21.71 s) but, because of its low coherence, the DNO does not really stand out above the noise in the Fourier transform of such a long section of data; the inset is the Fourier transform of only the first 0.89 h, here the DNO appears more clearly.

5.24 V803 Cen

V803 Cen was discovered by Elvius (1975) as a blue object with a V magnitude varying from 17 to 13, and a spectrum showing only HeI absorption features. O'Donoghue, Menzies & Hill (1987) identified it as an AM CVn star, and found photometric periods of 1611 s (together with harmonics) and 175 s. There is still no orbital period known for this object; the 1611 s modulation is believed to be a superhump (e.g. O'Donoghue & Kilkenny 1989; Patterson et al. 2000). Patterson et al. (2000) interpret the long term photometric behaviour of V803 Cen as the thermal limit cycle of a DN, making it one of only three Helium DN (see also Section 5.23).

The 175 s oscillation is very commonly observed in the high photometric state (O'Donoghue et al. 1987; O'Donoghue & Kilkenny 1989; Patterson et al. 2000) but is absent in the low state (O'Donoghue et al. 1990). O'Donoghue et al. (1987) found that a 2 mag reduction in brightness was accompanied by a period change from 175.2 s to 178.8 s, and noted that the dependence of period on luminosity has the same sense as that of DNOs, but is less sensitive (the implied gradient of $\frac{d\log(P/s)}{d\log(I/I_{min})} = -0.011$ differs by an order of magnitude from that found for DNOs; cf. Section 3.1 and 5.4). WWP03 argue that the 175 s oscillation is an lpDNO; if this interpretation is correct, it is the most persistent lpDNO yet identified, which (together with the oscillation's large amplitude) would make V803 Cen an ideal

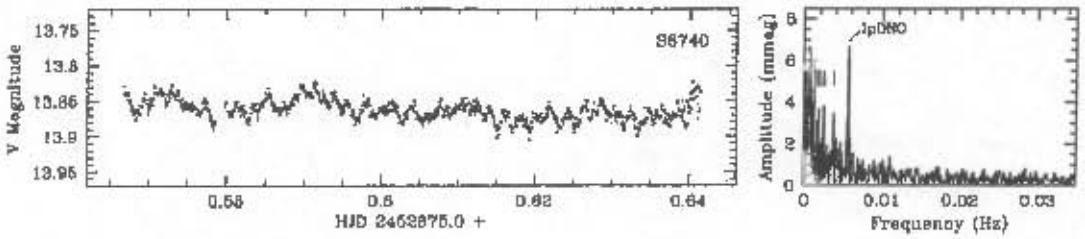

Figure 5.52: Left: The light curve of V803 Cen on 4 February 2003 (run S6740), corrected for atmospheric extinction, at 6 s time resolution. The ~175 s oscillation is directly visible. Right: The low frequency end of the Fourier transform of run S6740. There are no significant features at higher frequencies. Vertical bars mark the second, third, and fifth harmonics of the 1611-s modulation; the lpDNO at 176.3 s is indicated.

target for a detailed study of the properties of lpDNOs.

I obtained a single high speed photometry run on V803 Cen (using the 40-in. reflector, white light, and 6 s integration time) on 4 February 2003. The light curve, together with its Fourier transform, is displayed as Fig. 5.52. The lpDNO is clearly evident in the light curve; the best-fit period and amplitude are 176.3 s and 6.661 mmag respectively.

5.25 Summary

All periods detected in V1193 Ori are listed in Table 5.21; for easy reference, oscillation periods measured in the remaining objects discussed in this chapter are summarized here (together with the mean V magnitude for each run) as Table 5.23. I have tried to distinguish between DNO-related QPOs and kilosecond QPOs; the kilosecond QPO period is abbreviated P_{ksQPO}.

Table 5.23: Summary of detected rapid oscillation periods.

Object	Run no.	P_{DNO} (s)	P_{spDNO} (s)	P_{QPO} (s)	P_{beQPO} (s)	V (mag)
TU Men	S6695	20.55–22.20	—	304–420	—	15.0
	S7196	16.56	—	—	—	14.4
RU Peg	S7009	—	—	55.9	—	9.0[a]
	S7010	—	13.94	60.4	—	9.2[a]
	S7011	—	—	149	—	9.4[a]
	S7012		15.30	—	—	9.5[a]
	S7013	—	—	186	—	9.7[a]
	S7016	—	—	257	—	9.8[a]
	S7021	—	—	223	—	10.1[a]
	S7026	—	—	360	—	10.7[a]
WW Cet	S7082	23.1	103	263:	—	11.8
X Leo	S6742	—	114	—	—	14.0
	S6921	—	88.7	—	—	12.9
	S6923	—	91.3	—	—	12.9
	S6927	—	126	—	—	13.2
	S6931	—	146	—	—	14.5
	S6932	—	172	—	1600	14.9
	S7293	12.9	95.6	—	—	12.7
	S7295	—	98.8	—	—	13.2
	S7297	24.6	119	—	—	14.9
TY PsA	S7134	21.43–21.90	89–112	~357	—	12.7
HX Peg	S6471	—	114:	—	~1800	15.8:
	S6475	—	111.9	—	~1800:	15.9:
	S6646	16.19	—	—	—	12.7
	S6650	16.39	—	—	—	12.8
	S6656	—	83.4, 111.1	335:	—	13.0
	S6661	18.24	—	—	—	13.3
	S7162	—	—	347	746	14.8
V893 Sco	S6949	41.70	—	—	—	15.1[b]
8P Cra	S6912	38.64	—	—	—	14.3:
BR Lup	S6911	21.65	—	—	—	14.5
	S6914	25.04, 12.55	—	—	—	14.3
	S7015	—	—	~650	—	15.7
CN Ori	S7174	45.94	—	—	—	12.7
HP Nor	S6837	18.58	—	—	—	14.0
	S7028	—	74.01	—	—	13.1
AG Hya	S6907	21.53	—	683	—	14.7:
WX Hyi	S6463	—	—	193.5	—	13.0
	S7192	—	—	190.2	—	14.6
TW Vir	S6948	112: 121:	—	—	~1047	15.1

Notes: ':' denotes an uncertain value or detection; [a]U magnitude; [b]mean magnitude outside of eclipse.

Table 5.23: Continued: Summary of detected rapid oscillation periods.

Object	Run no.	P_{DNO} (s)	P_{lpDNO} (s)	P_{QPO} (s)	P_{ssQPO} (s)	V (mag)
PU CMa	S6762	- -	—	119.1	—	14.7
V426 Oph	S6935	73.26	—	—	—	12.1
OY Car	S6748	29.6	—	—	—	15.1:[b]
	S6754	~54	—	—	- -	15.0[b]
VZ Pyx	S6781	-	116, 57.8	460	—	15.3
V1159 Ori	S6649	32.28	177	- -	—	12.9
SY Cnc	S7194	24.87	—	—	—	13.3
EC2117	S6641	23.18	95.82–101.03	—	—	13.5[b]
	S6660	23.17	—	—	—	13.4[b]
	S6666	23.29	—	—	—	13.4[b]
CR Boo	S6852	21.71	61.93	291	—	14.6
V803 Cen	S6740	—	176.3	—	—	13.9

Notes: ':' denotes an uncertain value or detection; [a]U magnitude; [b]mean magnitude outside of eclipse.

Chapter 6

Discussion

Detections of rapid quasi-coherent oscillations in 24 CVs are presented in Chapter 5; 12 of these systems were not previously known to display rapid oscillations. I discuss here some of the more interesting recent results together with their implications, the exciting possibility of a connection between the phenomena in CVs and low-mass X-ray binaries (LMXBs), and future observations that may contribute to our understanding of rapid oscillations, and hence accretion in general.

6.1 Implications of Recent Results

The results presented in Chapter 5 followed from an extensive survey of high mass transfer rate CVs; an observing program like this could probably not have been executed anywhere other than Sutherland[1].

The QPO detected in RU Peg increased in coherence towards the end of outburst, furthermore, its period evolved over almost an order of magnitude; this may call into question the existence of two clearly separate sets of QPOs discussed in Section 3.2. In HX Peg, however, a QPO and kilosecond QPO have been simultaneously detected; implying that these are distinct phenomena.

An lpDNO in X Leo was found to follow a period-luminosity relation similar to what is observed for DNOs. Very little is presently known about lpDNOs; there are probably many features of their phenomenology that have not yet surfaced. Frequency doubling was observed for an lpDNO in VZ Pyx; there is as yet no certainty as to the cause of such behaviour in lpDNOs or DNOs. This dissertation was started at about the time that lpDNOs were first recognized as a phenomenon separate from DNOs and QPOs. As soon as lpDNOs were identified they were found to be fairly common—although not as common as DNOs—and have up until the present been seen in about 24 CVs (in around one half of these systems the

[1] I spent 139 nights (not excluding cloudy nights) at the telescope working on this program.

oscillations were at first reported as QPOs or DNOs). It is perhaps surprising that lpDNOs remained unrecognized for so long; however, there is nowhere in the earlier literature an amplitude spectrum that makes the existence of a third class of oscillations as clearly evident as e.g. the Fourier transform in Fig. 5.20.

DNOs and QPOs may be more commonly present in quiescent DN than is currently thought; it is certainly true that oscillations occur much more frequently in outburst than in quiescence, which means that they are not often looked for in quiescent light curves (see in this regard also Warner & Woudt 2004). Detections of DNOs, QPOs, and lpDNOs in DN at minimum light are mentioned in Chapter 3; to these can now be added a DNO in V893 Sco in quiescence, and QPOs in WX Hyi at minimum.

Many contradictory and confusing claims about periodic modulations in V426 Oph have been made. The detection of a DNO in this system casts further doubt on its status as an IP.

The kilosecond QPOs observed in V1193 Ori show some signs of an underlying periodic signal; this strengthens the interpretation of kilosecond QPOs offered by Patterson et al. (2002).

The detection of the full set of rapid quasi-coherent oscillations in the AM CVn star CR Boo shows that the system is also in this regard similar to hydrogen rich DN. Observations of DNOs, lpDNOs, and QPOs in AM CVn, V803 Cen, and CR Boo constitute the only existent (albeit model-dependent) evidence that the double degenerate systems may contain magnetic primaries (e.g. Warner & Robinson 1972a; Patterson et al. 1979; O'Donoghue et al. 1987; WWP03).

6.2 Similarities between CVs and LMXBs

The study of DNOs and QPOs in CVs took an exciting turn in recent years with the realization that they are in many respects comparable to QPOs in LMXBs. The properties of QPOs in LMXBs, as well as models to describe the oscillations, are reviewed by van der Klis (2000).

As for DNOs, the frequencies of kHz QPOs in LMXBs scale with inferred $\dot{M}$, and (in the case of neutron star binaries) are comparable to Keplerian frequencies in the inner disc. The $O-C$ phase diagrams of the 5 Hz QPO in the Rapid Burster illustrated in fig. 6 of Dotani et al. (1990) show systematic trends, as well as phase jitter—like the phase behaviour of DNOs. Furthermore, kHz QPOs sometimes occur in pairs, which may be compared to double DNOs. It is sometimes found that kHz QPOs in LMXBs occur in $1:2:3$ harmonic ratios (see e.g. Remillard et al. 2002); this has now also been observed for DNOs in VW Hyi (Warner & Woudt 2004).

Barret, Olive & Kluzniak (2004) analyze an 800 Hz QPO in a neutron star binary

and find that, rather than a modulation of $Q \sim 10$ which is persistently present, the signal consists of trains of ~100 cycles with $Q > 200$, occurring in bursts with a duty cycle of ~10%, and frequency changes of up to about 0.5% between different bursts. The high stability of the QPOs not only rules out a few of the models of kHz QPOs (see also Olive, Barret & Kluzniak 2004), but also makes them appear more similar to DNOs in CVs that grow and decay in amplitude, and undergo abrupt changes to different periods.

6.2.1 The Two-QPO Correlation

The most impressive apparent connection between the oscillating behaviour in CVs and LMXBs is the two-QPO correlation. The correlation for LMXBs emerged from the work of Psaltis, Belloni & van der Klis (1999) and Belloni, Psaltis & van der Klis (2002), who demonstrated that it is possible to find two classes of oscillations amongst the various types of QPOs and broad noise components observed in neutron star and black hole X-ray binaries, with frequencies that are tightly correlated in a way that seems to depend only weakly on the other properties of the sources, such as mass, magnetic field, or possibly the presence of a surface in the compact object. WW02b first pointed out that QPO and DNO frequencies in VW Hyi fit the same trend, and that this extends the two-QPO correlation shown as fig. 2 of Psaltis et al. (1999) to frequencies two orders of magnitude lower than seen in LMXBs. Mauche (2002) subsequently found that the DNO and QPO periods observed in SS Cyg place it between VW Hyi and the LMXBs on the same diagram—see fig. 4 of Mauche (2002).

Much of the motivation for this work has been to investigate the relation between QPO and DNO periods in CVs; considerable data now support the two-QPO correlation. The relation $\nu_{low} \approx \nu_{high}/16$ (where ν_{low} represents the QPO frequency in CVs, and the frequency of the horizontal branch oscillations—or the broad noise component identified with horizontal branch oscillations—in LMXBs, and ν_{high} represents CV DNO frequency and the lower frequency component of the pair of kHz QPOs in LMXBs) holds for accreting white dwarf, neutron star, and black hole binaries over nearly 6 orders of magnitude in frequency or period. There is no clear evidence of oscillations in CVs that do not fit the correlation.

Table 6.1 lists DNO, lpDNO, and QPO periods (only for CVs in which more than one class of rapid oscillations have been observed) using as far as possible simultaneous detections, and fundamental DNO or lpDNO frequencies, rather than QPO sidebands or harmonics of the frequencies. A few of these values are from observations presented in this dissertation, others are taken from W04, WWP03, and Warner (1995a), where more complete references may be found. Kilosecond QPOs are not included, since their periods do not seem to be related to the periods of the

other rapid oscillations; this necessarily introduces a bias to the periods selected for the correlation. Furthermore, the convenience of classifying basically any oscillation with a frequency somewhere between what is expected for a DNO and QPO leaves very little room for an oscillation period not to fit this scheme.

For the three IPs WZ Sge, V533 Her, and GK Per the periods given under P_{DNO} are thought to be their primary spin periods (or, in the case of GK Per, close to P_1).

Table 6.1: Oscillation periods for CVs that have more than one set of rapid oscillations. These are mostly only typical values; the observed ranges of the periods are given in table 1 of W04.

Object	P_{DNO} (s)	P_{spDNO} (s)	P_{QPO} (s)	References	Notes
RU Peg	2.97	13.94	~51, ~60	1, 2, 5	1
SS Cyg	7.7, 9.75	~32	83	3, 4	2
HX Peg	16.19-18.24	83.4	347	2	3
OY Car	17.79	116	338	5	
HP Nor	18.58	74.01	—	2	3
WX Hyi	19.4	—	186	5	
V436 Cen	19.6	..	~475	5, 6	
HT Cas	20.25-20.45	~100	—	7	
TU Men	20.91	—	304	2	4
AQ Eri	21.0	75.7	~296	5	
U Gem	21.15	79.9	~585	8, 9	5
AG Hya	21.55	—	683	2	6
TY PsA	21.57	110.4	~357	2	
BR Lup	21.65	—	~650	2	3, 6
CR Boo	21.71	61.23	291	2	
SW UMa	22.3	—	~300	10	
KT Per	22.4–29.3	~86, 147	—	3, 11, 12	3
WW Cet	23.1	103	263	2	
EC2117	23.27	94.21	480	5	
VZ Pyx	23.86	116	390.5, 460	2, 5	7
AH Her	24.0-38.8	~100	—	7	3
IX Vel	24.6-29.1	~77	~500	13, 14	8
X Leo	24.6	119	..	2	
Z Cha	25.15	—	585	5	
V893 Sco	25.2	—	375	5	
AM CVn	26.3	113–121	~290	15–17	3, 9
WZ Sge	27.87	—	742	18	
V2051 Oph	28.06	—	488	19	10
VW Hyi	29.08	88	444	20, 21	11
V3885 Sgr	29.08	—	~819	5, 22	12
V1159 Ori	32.28	177	—	2	
UX UMa	34.93	—	~650	5, 18, 23	13
RX And	35.7	..	~1020	5, 24	
V436 Car	~40	123	—	25	3
V533 Her	63.63	—	~1400	26, 27	14
GK Per	~380	—	~5000	7, 28	

References to Table 6.1: (1) Patterson et al. 1977; (2) This work; (3) Robinson & Nather 1979; (4) Mauche 2002; (5) WWP03; (6) Warner 1975b; (7) Patterson 1981; (8) Córdova & Mason 1984; (9) Eracleous et al. 1991; (10) Robinson et al. 1987; (11) Robinson 1973b; (12) Nevo & Sadeh 1976; (13) Williams & Hiltner 1984; (14) Warner et al. 1985; (15) Warner & Robinson 1972a,b; (16) Patterson et al. 1979, 1992; (17) Skillman et al. 1999; (18) WW02b; (19) Steeghs et al. 2001; (20) WW02a; (21) Haefner et al. 1977; (22) Hesser et al. 1974; (23) Nather & Robinson 1974; (24) Szkody 1976; (25) Woudt & Warner 2002b; (26) Patterson 1979a; (27) Rodríguez-Gil & Martínez-Pais 2002; (28) Morales-Rueda et al. 1999.

Notes to Table 6.1: (1) The lpDNO was present at the same time as the ∼60 s QPO; 2.97 s is the period of the DNO present together with the ∼51 s QPO, assuming that the observed period was a beat with the integration time. (2) The 7.7 s DNO was observed at the same time as the 83 s QPO; the 9.75 s DNO coexisted with the ∼32 s lpDNO. (3) These periods were detected in different light curves. (4) The QPO and DNO periods evolved during the observation, these are representative values. (5) The DNO and lpDNO, but not the QPO, were present in the same light curve. (6) The QPO is perhaps better classified as a kilosecond QPO. (7) The 390.5 s QPO was present at the same time as the DNO (run S6569), while the 460 s QPO coexisted with the lpDNO (run S6781). (8) The ∼77 and ∼500 s signals were of such poor coherence that they were seen only in autocorrelation functions; the DNOs were detected in different observations. (9) Patterson et al. (1992) suggest that the lpDNO may have been a telescope drive error, but Warner & Robinson (1972b) argue convincingly otherwise. (10) The QPO was not clearly visible in the light curve, but is inferred form the presence of a double DNO. (11) The QPO and DNO periods evolved during the observation, these are representative values; the lpDNO period is from a different outburst. (12) This QPO was not observed, but its existence is inferred from the presence of a QPO sideband at 30.25 s. (13) The QPO is a modulation of the phase of the DNO. (14) The QPO is a modulation of the equivalent width of the emission lines, and was not detected at the same time as the highly coherent 63.63 s photometric signal.

The fact that these fit on the same linear trend as the DNO periods in low magnetic field CVs is a bit of a contradiction, since the lpDNOs in these systems are thought to represent the white dwarf spin cycle. One may speculate that when the white dwarfs in these DN, NLs, and AM CVn stars reach equilibrium, solid body rotation, their spin periods will be what the DNO periods are now. Most IPs have $P_{orb} \approx 14 \times P_1$ (Barrett, O'Donoghue & Warner 1988). Therefore, if QPOs are excited at the inner disc edge of IPs by the same mechanism proposed for DN and NLs (which seems to be the case for GK Per; e.g. Hellier et al. 2004), there may be an observational bias against detecting them: typical values of P_1 are ∼1000 s, leading to $P_{QPO} \sim 4$ h; such long period QPOs are not easily detected, and may be masked by orbital modulations. Alternatively, IPs in their equilibrium, quiescent state may not have sufficient differential rotation between the magnetosphere and the disc to excite QPOs (Hellier 2004).

Fig. 6.1 shows the data for the 29 CVs in Table 6.1 that have both DNOs and QPOs graphically on the two-QPO diagram of Belloni et al. (2002); the dashed line is $\nu_{low} = \nu_{high}/16$. In Fig. 6.2 lpDNO frequencies are also shown; filled circles are lpDNO frequency as a function of QPO frequency for the CVs that have both lpDNOs and QPOs, while crosses represent lpDNO frequency as a function of DNO frequency; the dotted line marks $P_{lpDNO} = 4P_{DNO}$ and $P_{QPO} = 4P_{lpDNO}$. The inconsistency concerning IPs having $P_{QPO} \approx 16P_1$, whereas in the non-magnetic CVs $P_{QPO} \approx 4P_{lpDNO}$ is here clearly illustrated by the fact that the filled circles are compatible with the upper, rather than lower, line.

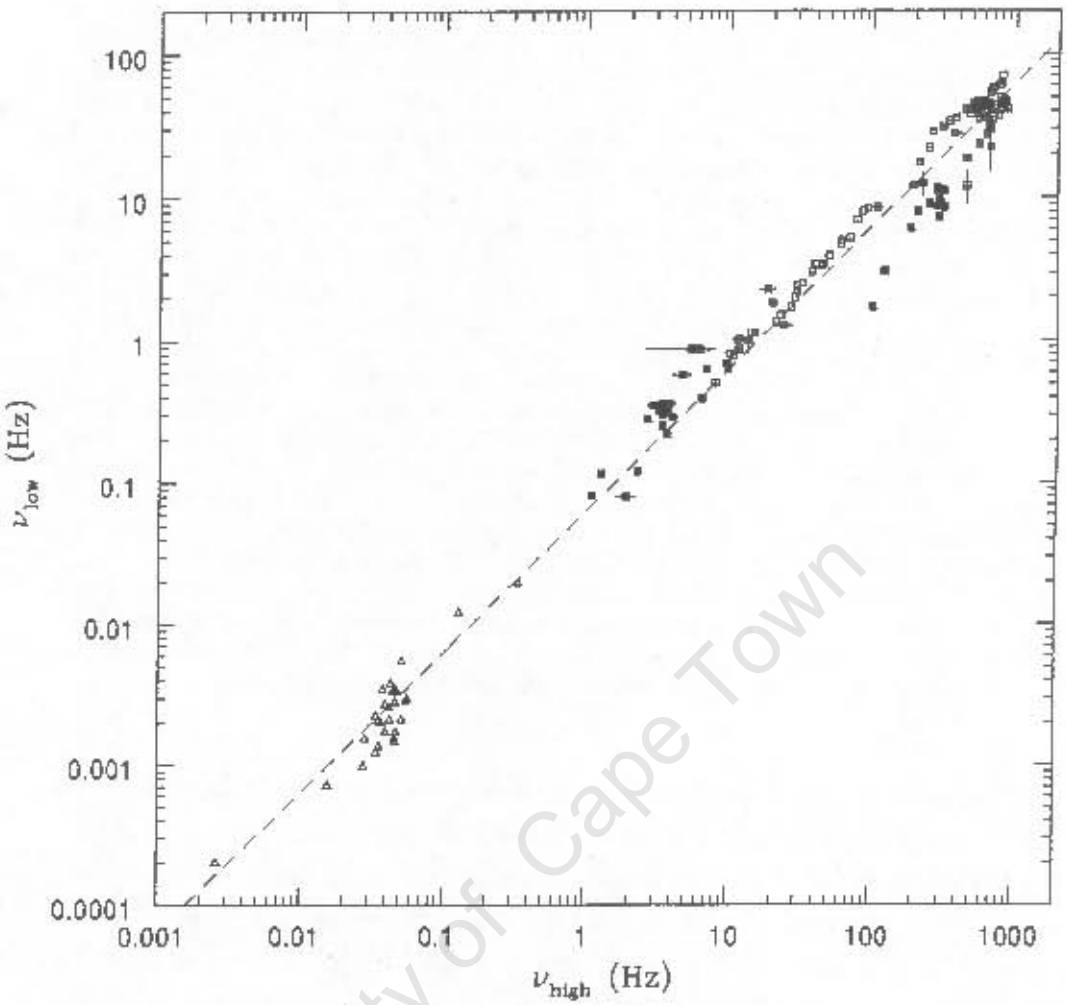

Figure 6.1: An extension of the two-QPO correlation of Belloni et al. (2002). Neutron star binaries are plotted as open squares; filled squares are black hole candidates. The open triangles represent QPO frequency as a function of DNO frequency, with values taken from Table 6.1. Whereas multiple points are plotted for the LMXBs, every CV is plotted only once. The dashed line indicates $P_{QPO} = 16P_{DNO}$, or more generally $\nu_{low} = \nu_{high}/16$.

W04 points out that there is a clear divide between rapidly rotating primaries with evidence of weak magnetic fields, and the more slowly rotating primaries in IPs where magnetic fields are stronger. The correlation between rotation period and magnetic field strength is in part caused by the fact that greater r_μ implies a longer equilibrium spin period, but $\dot{M}$ is also relevant, since r_μ is a function of not only μ_1, but also $\dot{M}$ (see equation 2.11). It seems likely that the long term average $\dot{M}$ is roughly the same in all CVs, and that the shorter spin periods of DN and NLs is a result only of their weaker magnetic fields (W04).

WWP03 discuss further similarities between oscillations in LMXBs and lpDNOs:

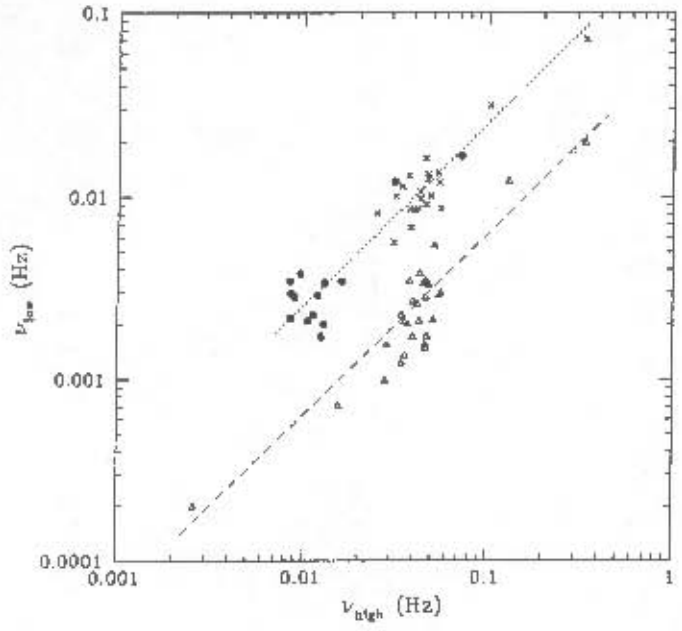

Figure 6.2: The region of Fig. 6.1 containing all the data points for CVs, with lpDNOs also plotted. The filled circles represent QPO frequency as a function of lpDNO frequency in the same system; crosses are lpDNO frequency plotted against DNO frequency. The dotted line marks $P_{lpDNO} = 4P_{DNO}$ and $P_{QPO} = 4P_{lpDNO}$. The open triangles and dashed line are repeated from Fig. 6.1.

During X-ray bursts in accreting neutron star binaries, pulsations with frequencies in the range 300–600 Hz are observed; these frequencies increase slightly during the burst. The oscillations are attributed to hot spots on the neutron star surface, where an outer layer of gas rotates differentially relative to the underlying atmospheric layers. If there are two hot spots on the neutron star, then the rotation frequencies would lie in the range 150–300 Hz, which puts them at $\sim 1/4$ times the frequency of the high frequency QPOs in the same systems (van der Klis 2000). This is the same relationship seen between lpDNOs (which represent the rotation of the white dwarf) and DNOs in CVs. The ratio of low frequency QPO periods to that of stellar rotation in the X-ray binaries is then also $\sim$4, which is matched by P_{QPO}/P_{lpDNO} in CVs. Furthermore, the phase behaviour of millisecond oscillations in type I X-ray bursts of neutron stars illustrated in fig. 6 and 7 of Muno, Chakrabarty & Galloway (2002) is similar to that of lpDNOs.

The two-QPO correlation suggests that similar physical mechanisms may be responsible for quasi-coherent oscillations in CVs and LMXBs; however, it is possible that the correlation is an artifact produced by the accidental line-up of multiple, independent correlations.

Assuming the correlation implies that the same oscillation mechanisms operate in the different systems, Mauche (2002) shows that most of the models that have been proposed for the QPOs in LMXBs are excluded; specifically, no model that requires the presence or absence of a stellar surface or magnetic field will be satisfactory.

There are some indications that the black hole candidates in LMXBs may in fact

be very similar to compact magnetic objects. This follows from the realization that the gravitational collapse of a magnetic star towards its event horizon can be slowed by the radiation pressure resulting from annihilation of electron-positron pairs that are produced by the compressed magnetic field—the collapsing object maintains an intrinsic magnetic moment outside its event horizon for orders of magnitude longer than a Hubble time (Robertson & Leiter 2003). The radio-IR correlation with mass and X-ray luminosity observed in neutron star and black hole binaries can be reproduced in models of the jets that arise from the interaction between the disc and magnetosphere of such an object (Robertson & Leiter 2004). Furthermore, in neutron star binaries the power-law part of the X-ray flux spectrum most likely originates in the stellar magnetosphere; the same model is successful when applied to black hole binaries (Robertson & Leiter 2002).

If the phenomena really do have the same origin, not only in neutron star and black hole binaries, but also in CVs, then further observations of CVs (where strong field general relativistic effects cannot be of significant importance) will contribute to the understanding of LMXBs.

6.3 Future Study of DNOs, QPOs, and lpDNOs

The study of rapid oscillations in CVs remains of value, not only because the oscillations hold important implications for disc-fed accretion in CVs, but also because of the many similarities shared with the QPOs in LMXBs. Accretion processes are more readily studied in CVs than in LMXBs (or any other objects). Amongst the reasons for CVs being the best laboratories for the study of accretion are that the accretion luminosity in CVs is well below the Eddington limit, radiation pressure and general relativistic effects are insignificant in CVs, and DN outburst cycles exhibit changes of $\sim 10^3$ in $\dot{M}$. Furthermore, optical observations can be obtained with modest-sized ground based telescopes. The combination of optical and EUV or soft X-ray data offers unique opportunities to study different aspects of the oscillation mechanisms. However, there does not seem to be any unequivocal observational test to establish the equivalence of CV and LMXB oscillations.

The LIMA model of DNOs and the unified model of DNOs and QPOs described in Chapter 4 are supported by a large amount of observational data, and these are certainly the most successful interpretations available. Some of the success of the magnetic models of DNOs and QPOs is probably owed to the complexity of these mechanisms. Note, however, that the observational behaviour of DNOs and QPOs is so complex and varied that no particularly simple model is likely to suffice.

The technology now exists to perform spectroscopic observations of the oscillations in CVs; such observations have been made in different wavelength regions by

Steeghs et al. (2001), Marsh & Horne (1998), Knigge et al. (1998), and Mauche (1997a). Time resolved spectroscopic observations of DNOs, lpDNOs, and QPOs in the future will likely overshadow the high speed photometry that has up until recently been the only means of studying rapid oscillations. Such studies could exploit the considerable diagnostic potential of emission lines in the optical and EUV. The Southern African Large Telescope (SALT; see e.g. Buckley & Stobie 2001) together with its Prime Focus Imaging Spectrograph (PFIS) will have unique time resolution capabilities, and will allow for spectroscopy as well as spectropolarimetry (e.g. Buckley et al. 2003; Kobulnicky et al. 2003).

Evidence for the presence of weak white dwarf magnetism in the conventionally non-magnetic CVs is mounting; furthermore, it is certainly reasonable to argue that magnetic field strengths in CV primaries extend to lower values than $\sim$1 MG inferred for the lowest field IPs. The most viable interpretation of DNOs and lpDNOs is that they are the signature of such magnetic fields, but all present evidence is indirect. The fact that not all high $\dot{M}$ CVs show DNOs or QPOs, and that the oscillations are not present in every outburst of DN known to display them sometimes, shows that there is a parameter that determines the presence or absence of oscillations. In the LIMA model this parameter is the strength of the primary magnetic field. An obvious next step is to attempt a measurement of circular polarization (ideally modulated at the DNO period) in a CV known to have DNOs; the whole matter could be clinched this way. VW Hyi is the most promising system for such an observation, since its DNOs appear at large amplitude in the late decline from outburst, when the disc has almost returned to quiescent brightness, so that the contribution of unpolarized flux should be smaller than in most systems. This observation will require the use of a large telescope, probably observing in the near IR. With its unusually high time resolution specifications PFIS on SALT should be better suited to such an experiment than most available instruments; however, PFIS will (at least initially) have no near IR capability. It is worth emphasizing in this context that not even for any DQ Her star does compelling direct observational evidence for white dwarf magnetism exist.

The wavelength dependence of QPO properties has not yet been investigated; also, it should be possible to demonstrate the obscuration aspect of QPOs spectroscopically. Eclipse mapping of edge-on systems to locate and study the sites of QPO production should be explored.

There is at present not very much known about lpDNOs, certainly in this area more observations are required. The phase behaviour of lpDNOs through eclipse in a suitable CV should be investigated. Such studies will be of particular use if the interpretation of lpDNOs as white dwarf rotation turns out to be correct, since this will then extend our knowledge of primary spin periods to conventionally non-

magnetic CVs.

More theoretical work on the LIMA model is required before it can be generally accepted; however, with variable M_b, a transient magnetic field of unknown geometry, variable ram pressure, and poorly understood interaction between the differentially rotating accretion belt and the degenerate core, it may be a long time before DNOs are satisfactorily modeled. The boundary between the disc and white dwarf magnetosphere is one of the most poorly understood regions in CVs. This complicates the theoretical investigation of the oscillations, but also implies that the rewards may be particularly valuable. DNOs, lpDNOs, and QPOs hold great potential for probing the structure of the inner accretion flow, and the interaction between the disc and magnetosphere; however, this potential will only be realized when the mechanisms responsible for the oscillations can be specified with more certainty.

Chapter 7

Concluding Remarks

Observations of rapid quasi-coherent oscillations in 24 CVs are presented; in the 12 systems TU Men, WW Cet, HX Peg, BP CrA, BR Lup, HP Nor, AG Hya, TW Vir, PU CMa, V426 Oph, V1193 Ori, and CR Boo oscillations are detected for the first time.

Amongst the results are detections in the same systems of DNOs and QPOs which strengthen the correlation, valid over nearly six orders of magnitude in frequency, between the ratio of time scales of different classes of oscillations in white dwarf, neutron star, and black hole binaries. This correlation may imply that the quasi-coherent oscillations in LMXBs arise from the same mechanism that operates in CVs, in which case models of the oscillations cannot appeal to significant general relativistic effects.

RU Peg is found to have a QPO period changing by 84% over ten nights of outburst. The recently recognized lpDNOs are seen to occur fairly frequently in high mass transfer rate CVs; however, they are not as commonplace as DNOs. A period-luminosity relation is seen for the lpDNO in X Leo—the first indication that some lpDNOs may scale with $\dot{M}_1$. Rapid oscillations are detected in the DN WX Hyi and V893 Sco in quiescence. Observations of rapid oscillations in the AM CVn stars CR Boo and V803 Cen show that the double degenerate binaries are, where rapid oscillations are concerned, similar to hydrogen rich CVs, and that the primaries in these systems may be weakly magnetic.

All observational data on DNOs can be accounted for in the LIMA model; this is certainly the most viable model of the oscillations presently available. However, the quantitative description of the processes involved is at present quite scant, and more theoretical work on the model is required.

Since rapid oscillations occur in a large fraction of CVs, the physical mechanisms producing DNOs, lpDNOs, and QPOs are likely to be of quite general significance to our understanding of accretion disc physics.

Observations to establish the presence of magnetic fields in DN and other supposedly non-magnetic CVs are required. Note, however, that even in the case of the best studied IP, DQ Her, there is still no convincing direct observational evidence of a white dwarf magnetic field. The photometric study of DNOs, lpDNOs, and QPOs is likely to be superseded in the future by high time resolution spectroscopy.

Appendix A

Discrete Fourier Analysis

In this appendix I discuss the discrete Fourier transform used for the analysis of data presented in Chapter 5, together with some of the difficulties encountered with Fourier analysis of finite and discrete data. This discussion is taken mostly from Deeming (1975); another useful paper on the subject is Brault & White (1971). Section A.1 is devoted to problems rooted in the photometer and telescopes used for my observations.

I limit the discussion of Fourier transforms to the special case of the brightness of a star as a function of time, denoted $f(t)$. The Fourier transform $F(\nu)$ of the function $f(t)$ is defined as

$$F(\nu) = \int_{-\infty}^{+\infty} f(t) e^{i2\pi\nu t} dt \ .$$

$F(\nu)$ is then simply another representation of the function $f(t)$ ($F(\nu)$ is the amplitude of oscillation as a function of time; the mean value or some low order polynomial trend is normally subtracted from $f(t)$ before transforming it to prevent the occurrence of very large power at low frequencies), in frequency instead of time, and no information is lost in transforming from $f(t)$ to $F(\nu)$. Since a real light curve is necessarily finite we define the finite Fourier transform $F_T(\nu)$ of $f(t)$ as

$$F_T(\nu) = \int_{-T/2}^{+T/2} f(t) e^{i2\pi\nu t} dt$$

where T is the length of a light curve (or the total base line, if light curves from different nights are combined). Furthermore, the brightness of a star is not recorded continuously, but only at discrete times t_k. In other words, a light curve is the discrete function $f(t_k) = f(t)w(t)$, where

$$w(t) = \begin{cases} 1 & \text{for } t = t_1, t_2, \cdots t_N \\ 0 & \text{otherwise.} \end{cases}$$

Actually, the values $f(t_k)$ are not instantaneous intensities, but instead the intensity of the star averaged over the integration time (t_{int}); these average intensities are assigned to discrete times t_k (the time at the middle of the kth integration, with $t_k - t_{k-1} = t_{int}$). Therefore the discrete Fourier transform

$$F_N(\nu_j) = \sum_{k=1}^{N} f(t_k) e^{i2\pi\nu_j t_k} \tag{A.1}$$

is applicable to the analysis of photometric data (note that F_N is dimensionally different from F and F_T). The definition of $F_N(\nu)$ places no restriction on the data spacing that may be used. Because $F_N(\nu)$ is complex, we are usually concerned with its magnitude $|F_N(\nu)|$ or magnitude squared $|F_N(\nu)|^2$. In my calculations, $|F_N(\nu)|$ is normalized to give amplitude directly.

As a practical point, when actually computing a Fourier transform, using equation A.1 is expensive in terms of CPU time. Since Euler's formula can be used to rewrite it to

$$F_N(\nu_j) = \sum_{k=1}^{N} f(t_k) cos(2\pi\nu_j t_k) + i \sum_{k=1}^{N} f(t_k) sin(2\pi\nu_j t_k) \ , \tag{A.2}$$

and a light curve typically consists of $\sim 10^3$ data points, the evaluation of equation A.2 for $\sim 10^4$ frequencies involves calculating $\sim 10^7$ sines and cosines. For equally spaced frequencies, $\nu_j = \nu_{j-1} + \Delta\nu$, one obtains from equation A.2

$$F_N(\nu_j) = \sum_{k=1}^{N} f(t_k) cos(2\pi\nu_{j-1} t_k + 2\pi\Delta\nu t_k) + i \sum_{k=1}^{N} f(t_k) sin(2\pi\nu_{j-1} t_k + 2\pi\Delta\nu t_k) \ ;$$

a few trigonometric identities then lead to the recursive formula

$$\begin{aligned} F_N(\nu_j) \ = \ & \sum_{k=1}^{N} f(t_k)[cos(2\pi\nu_{j-1} t_k) cos(2\pi\Delta\nu t_k) - sin(2\pi\nu_{j-1} t_k) sin(2\pi\Delta\nu t_k)] \\ & + \ i \sum_{k=1}^{N} f(t_k)[sin(2\pi\nu_{j-1} t_k) cos(2\pi\Delta\nu t_k) + cos(2\pi\nu_{j-1} t_k) sin(2\pi\Delta\nu t_k)] \ . \end{aligned} \tag{A.3}$$

The use of equation A.3 to calculate the discrete Fourier transform reduces the computation time by typically a factor of 4 to 6 depending on the the number of frequencies used and the number of data points (Kurtz 1985).

For a multiply periodic function $f(t)$ with frequencies ν_1, $\nu_2, \cdots$, the function $F(\nu)$ will be greater than zero at the frequencies $\pm\nu_1$, $\pm\nu_2 \cdots$. The presence of each of these frequencies will be independently detected, and their amplitudes will be determined. In the practically realizable case of $F_N(\nu)$ instead of $F(\nu)$ however, this is not always possible because $f(t_k)$ does not necessarily fully determine $f(t)$ (because of the discrete nature of $f(t_k)$, quite apart from such factors as photon statistics, variable sky transparency, and observational error). The calculated $F_N(\nu)$ can therefore differ from $F(\nu)$; in that case $F_N(\nu)$ is said to be aliased.

Aliasing arises when an oscillation is undersampled. What frequencies spurious power appears at (i.e. where $F_N(\nu)$ differs from $F(\nu)$) depends on the properties of the sampling. For an undersampled periodic signal at frequency ν_0, in the special case of equally spaced data, the function $f(t_k)$ is consistent with a periodic signal at the true frequency ν_0, as well as with its beats with the sampling frequency $1/t_{int}$. Thus the discrete Fourier transform of $f(t_k)$ will show peaks at ν_0, $1/t_{int} + \nu_0$, $1/t_{int} - \nu_0$, $2/t_{int} + \nu_0$, $2/t_{int} - \nu_0$, etc. The highest meaningful frequency is that at which ν_0 coincides with its lowest frequency alias, i.e. where $\nu_0 = 1/t_{int} - \nu_0$; this is called the Nyquist frequency $\nu_{Ny} \equiv 1/2t_{int}$. When signals are undersampled, the true frequency content of $f(t)$ cannot be determined from $f(t_k)$; no new information can be obtained by computing $F_N(\nu)$ at frequencies greater than ν_{Ny}.

Daily cycle count ambiguities occur when light curves from different nights are combined; this is not a concern in my work. The result of averaging the intensity over t_{int}, rather than measuring instantaneous intensities, is a reduction in the apparent amplitude of signals with frequencies near ν_{Ny}.

The observed Fourier transform $F_N(\nu)$ is the convolution[1] of the true Fourier transform $F(\nu)$ with the spectral window $\delta_N(\nu)$

$$F_N(\nu) = F(\nu) * \delta_N(\nu) \equiv \int_{-\infty}^{+\infty} F(\nu - \nu')\delta_N(\nu')d\nu'$$

(Deeming 1974), where $\delta_N(\nu)$ is defined as

$$\delta_N(\nu) = \sum_{k=1}^{N} e^{i2\pi\nu t_k} \quad ,$$

and is a function only of frequency and the times of observation t_k; it has no dependence on the observed intensities themselves. The function $\delta_N(\nu)$ completely specifies the effect that the way in which the light curve was sampled has on $F_N(\nu)$; for this reason $\delta_N(\nu)$ is a valuable aid in interpreting discrete Fourier transforms.

The convolution of $F(\nu)$ with $\delta_N(\nu)$ redistributes the Fourier amplitudes; this smearing effect is called spectral leakage. The frequency resolution ($d\nu$) of a Fourier transform is given by $d\nu = 1/T$ (but see Loumos & Deeming 1978 for the case of closely spaced frequencies).

For a sinusoidal oscillation, the signal-to-background ratio (r) in the Fourier amplitude spectrum depends (in addition, obviously, to the amplitude of the sinusoid) on the typical number of photons detected in each integration (n), as well as the length of the light curve: $r \propto \sqrt{nT}$ (Warner 1988). The result is that in long light curves, even very low amplitude signals can be detected, provided

[1]The convolution $(f * g)(x) \equiv \int_{-\infty}^{+\infty} f(x - x')g(x')dx'$ of two functions, f and g has the property that the Fourier transform of $f * g$ equals the product of the Fourier transforms of f and g, a proof of this theorem can be found in e.g. Edwards & Penney (2000).

that they are persistently present. In searching for DNOs, which may be present for only a short while, it is often advantageous to calculate Fourier transforms of different segments of a long light curve separately. Statistical significance of peaks in Fourier transforms of data composed of periodic functions together with noise, and criteria for accepting peaks as real, are discussed in e.g. Scargle (1981) and Horne & Buliunas (1986). Their arguments however, apply to periodic, rather than quasi-periodic oscillations, and depend on the mathematical model chosen to describe the noise present in the data. I have therefore resisted relying on such criteria in Chapter 5, and instead base decisions of whether to accept periods as real not only on the ratio r, but also on how long an oscillation persisted, and whether it was detected on more than one night.

A.1 Equipment Errors

Amongst the difficulties in finding short period, low amplitude signals are periodicities and limitations intrinsic to the equipment used to make the observations. Two such problems are described in this section.

A.1.1 Problems with the UCT CCD

A shortcoming of the UCT CCD, when operated in normal high speed photometry mode, is that when the observer starts a run, the instrument does not wait for the next minute or second pulse, but immediately opens the shutter to start the first integration. This creates problems because the time stamp that gets written to the fits header of every image is recorded only to the nearest second.

An example of the trouble this can cause is illustrated in Fig. A.1. On the left is a light curve of DH Aql in superoutburst, which was taken at 5 s time resolution. The high frequency end of the Fourier transform shows a broad hump of power centred on ~0.08 Hz (panel a of Fig. A.1). However, prewhitening the light curve at three much lower frequencies to remove the worst of the superhump (the sum of three sinusoids, which was subtracted, is shown superimposed on the light curve) resulted in the power at ~0.08 Hz disappearing. Panel b of Fig. A.1 shows this region of the Fourier transform of the prewhitened light curve. The explanation of this behaviour is found in the spectral window (panel c of Fig. A.1) which shows that the power around 0.08 Hz is an artifact of the way in which the light curve was sampled. The excess high frequency power in panel a of Fig. A.1 results from the very large power at a few low frequencies—caused by the superhump—showing up at ~0.08 Hz because of spectral leakage. If consecutive points had been spaced at equal intervals of 5 s, the spectral window would have been almost perfectly smooth and flat at frequencies between 0.02 and 0.1 Hz. Although the length of

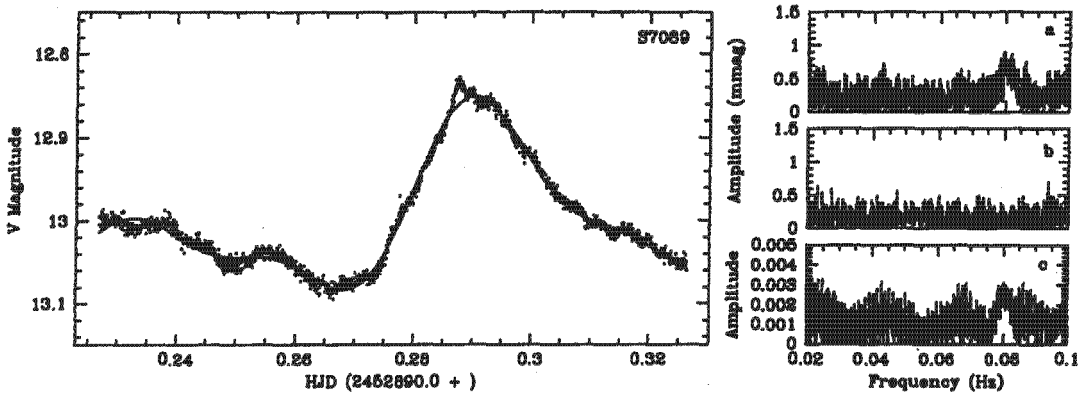

Figure A.1: Left: The light curve of DH Aql on 8 September 2003 with a sum of three sinusoids superimposed. Top right: The amplitude spectrum of the light curve on the left showing a broad hump of power around ~0.08 Hz caused by spectral leakage. Middle right: The amplitude spectrum of the same light curve, but after the sine fit over-plotted in the left hand panel was removed. Bottom right: The spectral window for the light curve shown on the left. Note that the scale in panel c is different from that used for the other two Fourier transforms, this is because the normalization is arranged to give amplitude (plotted here in mmag) for the Fourier transforms of data, whereas the spectral window is normalized to give a (dimensionless) amplitude of 1 at 0 Hz.

each integration really was 5 s, the first integration started between second pulses; this, coupled with the fact that the start time of every integration is recorded to only 1-s accuracy, resulted in the difference between the times written to consecutive images alternating irregularly between <5 s, and >5 s. This strobe effect leads to unexpected and unpredictable spurious signals (of course, the effect is worse when an integration time that is not an integer number of seconds is used).

A.1.2 Telescope Drive Errors

Although Fourier analysis is not ideally suited to the detection of oscillations of low coherence, it is very sensitive to truly periodic signals. For this reason, periodic errors in a telescope drive are sometimes detected by Fourier analysis of high time resolution light curves. This is likely to happen when too small an aperture is used with a photomultiplier tube, since an oscillation of the telescope may spill small fractions of the light outside the aperture. With a CCD, flat fielding should ensure a uniform sensitivity across the chip, so that it should not matter if the image of a star oscillates on the chip. However, the flat fielding is never really perfect. The UCT CCD chip, e.g., has a non-uniform response (with areas of higher and lower quantum efficiency forming striae across it), which is wavelength dependent. Flat fields taken in twilight, when the sky background differs in colour from a dark night

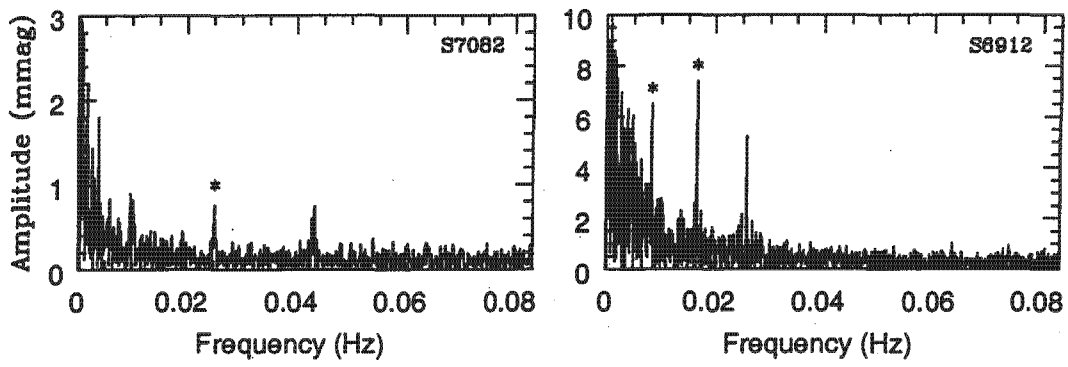

Figure A.2: Left: The amplitude spectrum of WW Cet on 3 September 2003 (run S7082); a Fourier transform of the same data, after prewhitening to remove the drive error, is shown in Fig. 5.13. An asterisk marks the 40-inch telescope drive error at 40 sidereal seconds. Right: An exceptionally large amplitude drive error and first harmonic (marked by asterisks at 120 and 60 sidereal seconds). A Fourier transform of the same light curve (BP Cra on 4 April 2003) after it was prewhitened to remove the drive error is shown in Fig. 5.21.

sky, therefore do not quite correct for the chip's non-uniform sensitivity.

A drive error is strictly periodic, but guiding interrupts its phase every so often, distributing some of the power in the Fourier transform over nearby frequencies, and giving the appearance of a quasi-coherent signal. The apparent amplitude of the drive error is proportional to the cosine of the declination at which the telescope is set (Warner 1988), and is typically very small.

The frequency of the telescope's drive error is usually known from experience (if not, it is easily determined by e.g. putting a reference star close to a defect on the CCD chip). Signals at frequencies close to the drive frequency or its harmonics are treated with special scepticism, and most often discarded as spurious. This makes real oscillations at these frequencies virtually undetectable, and confirmation of the reality of such an oscillation necessitates the use of a different telescope.

The SAAO 30-, 40-, and 74-inch telescopes have drive errors of 120, 40, and 90 sidereal seconds respectively. These periods were detected in several of my light curves, Fig. A.2 shows two examples. In the right hand panel (run S6912) the drive error and its first harmonic appear at uncommonly large amplitude. This happened because the position of the target on the frame coincided with a dust speck on the CCD window. Note that in both the Fourier transforms in Fig. A.2, DNOs are easily distinguished from the drive errors.

Appendix B

Null Results

In Table B.1 of this appendix I report null results, including only stars that I observed without ever detecting a DNO, lpDNO, or QPO. Note that many of the observing runs listed in Chapter 5 also produced no detections of rapid oscillations. The value of this record is that the truly non-magnetic DN and NLs are expected to be amongst those in which DNOs have never been seen. Some of these observations were of DN near minimum (run S6682, S6850, and S6847), in these cases detections of DNOs—rather than their absence—would have been surprising. The last object in Table B.1, SW Sex (together with the other members of its class) is suspected of being a strongly magnetic system (e.g. Patterson et al. 2002; see also Section 4.2.2).

For completeness, systems which have been known to have DNOs or QPOs, but in which I found none, are listed in Table B.2. For these systems DNOs and QPOs have been observed in V2051 Oph and TT Ari; only DNOs have been seen in RR Pic, SY Cnc, and HL Aqr; and only QPOs have been seen in TV Crv, V442 Oph, RW Sex, and V442 Cen. Also included in Table B.2 is a single observation of EX Hya, which, by the LIMA model, cannot produce DNOs, since it is an IP.

Except where otherwise noted, observations were made in white light. The upper limit on DNO or lpDNO amplitude (A_{max}) applies to the frequency range 0.01 Hz to ν_{Ny} (100 s to $2t_{int}$).

Table B.1: Objects observed without detecting rapid oscillations. The final column gives the upper limit on the DNO or lpDNO amplitude (A_{max}) for each run.

Object	Type	Run No.	Start time HJD = 2450000+	Length (h)	t_{int} (s)	Telescope	V (mag)	A_{max} (mmag)
BV Pup	DN	S6829	2703.29604	3.17	6	30-in.	13.6	1.8
		S6833	2704.25377	1.48	6	30-in.	13.8	1.7
		S7204	3001.43601	2.50	6	40-in.	14.2	1.9
		S7208	3002.43635	1.83	5	40-in.	14.1:	1.2
HL CMa	DN	S6828	2703.26635	0.92	6	30-in.	13.1[b]	1.3
		S6838	2705.25891	1.15	6	30-in.	12.1	1.8
		S7300	3085.22874	1.32	6	40-in.	11.9	1.6
AK Cnc	DN	S7205	3002.54607	1.52	6	40-in.	13.6	1.6
UZ Ser	DN	S6898	2731.56997	2.48	6	30-in.	13.0	0.9
		S6950	2781.56131	0.75	6	30-in.	13.1	2.0
		S6954	2782.51024	1.17	6	30-in.	13.2	1.1
CZ Ori	DN	S6737	2675.28554	1.20	5	40-in.	13.8:	1.0
		S6741	2676.28364	1.87	5	40-in.	13.0	0.9
		S6747	2678.34841	1.30	5	40-in.	14.2	1.0
		S6749	2679.27388	1.02	5	40-in.	14.6	2.0
V478 Sco	DN	S6919	2773.52674	2.40	5	40-in.	14.7	0.8
		S6925	2774.48373	1.90	6	40-in.	14.6	0.7
		S6928	2775.38140	2.40	5	40-in.	14.6	1.3
		S6972	2789.41505	1.32	8	30-in.	15.6	1.4
		S6982	2791.35458	0.63	8	30-in.	16.6	3.9
		S7019	2844.33389	2.48	6	40-in.	14.8	1.8
		S7022	2845.20918	2.37	5	40-in.	15.2	0.8
		S7024	2846.30624	0.98	5	40-in.	15.2	1.3
SDSS0407*	DN	S7157	2930.45407	2.35	6, 8	40-in.	15.2:[a]	1.8
		S7160	2931.48959	3.10	8	40-in.	15.3[a]	1.7
		S7164	2932.54966	1.65	8	40-in.	15.4[a]	1.1
		S7167	2933.50979	3.75	8	40-in.	15.7[a]	0.7
V730 Sgr	DN	S6968	2788.49467	0.97	6	30-in.	15.2:	2.2
		S6974	2789.56353	1.25	6	30-in.	14.6	1.1
		S7084	2887.32307	0.57	5	40-in.	14.6:	4.1
		S7155	2930.28078	0.45	5	40-in.	15.9	5.0
MM Sco	DN	S6963	2787.44515	0.68	7	30-in.	13.9:	2.1
FQ Sco	DN	S6971	2789.36750	1.07	6	30-in.	13.3	0.6
		S6977	2790.43541	1.38	6	30-in.	14.9	0.7
AD Men	DN	S6682	2628.35939	1.07	8, 10	40-in.	18.5	6.0
CU Vel	DN	S6943	2780.19671	2.00	6	30-in.	15.8:	2.0
		S6947	2781.19596	1.82	7	30-in.	17.3	3.3

Notes: t_{int} is the integration time; ':' denotes an uncertain value or classification; [a]average magnitude outside eclipse; [b]taken with a V filter; *SDSS J040714-064425.

Table B.1: Continued: Objects observed without detecting rapid oscillations. The final column gives the upper limit on the DNO or lpDNO amplitude (A_{max}) for each run.

Object	Type	Run No.	Start time HJD = 2450000+	Length (h)	t_{int} (s)	Telescope	V (mag)	A_{max} (mmag)
RY Ser	DN	S6918	2773.42663	2.27	5	40-in.	14.0	0.9
		S6924	2774.39861	2.08	5, 6	40-in.	14.2	1.0
UU Aql	DN	S6920	2773.67612	1.62	4, 5	40-in.	11.8	0.8
		S6937	2778.64186	1.22	6	40-in.	15.4	1.9
V373 Cen	DN	S6940	2779.31297	1.17	6	40-in.	15.0:	1.2
GZ Cnc	DN	S6704	2638.54807	1.53	5	74-in.	15.1	1.1
		S6842	2705.38806	2.67	8	30-in.	15.3	2.0
		S6847	2706.39907	1.12	8	30-in.	15.3	2.9
		S6850	2707.34165	1.82	8	30-in.	15.5	2.1
WZ CMa	DN	S6841	2705.33850	1.08	7	30-in.	14.8	1.4
		S6855	2708.35460	1.23	6	30-in.	14.8	1.9
SV CMi	DN	S6746	2678.29779	1.17	5	40-in.	13.7	1.0
		S6750	2679.32148	0.43	4	40-in.	13.9:	3.0
		S6751	2680.27192	0.95	5	40-in.	13.7	1.2
		S6790	2693.31658	0.97	6	40-in.	13.1	0.7
XZ Eri	DN	S7169	2990.41236	1.38	6	40-in.	15.5	1.8
		S7173	2991.42464	3.83	6	40-in.	15.7	1.3
		S7185	2996.31759	0.95	7	40-in.	16.3	2.4
BF Ara	DN	S6903	2733.43172	1.85	6	30-in.	15.2	1.9
		S7034	2849.26363	1.12	6	40-in.	14.2	0.7
AT Ara	DN	S6926	2774.58862	3.15	5, 6	40-in.	13.9	0.6
		S6929	2775.48401	5.05	6	40-in.	14.0	0.6
SY Vol	DN	S6756	2681.50508	0.70	5, 10	40-in.	15.4:	2.1
MU Cen	DN	S6760	2686.43847	2.22	5	40-in.	13.4	0.5
		S6765	2687.43823	1.10	5, 6	40-in.	12.4	0.7
		S6897	2731.49910	1.55	6	30-in.	13.8	0.7
		S6902	2732.39579	0.88	6	30-in.	13.9	1.8
NN Cen	DN	S6778	2690.60495	0.82	6	40-in.	13.5	1.9
		S6783	2691.59373	1.18	6	40-in.	13.8	0.9
		S6970	2789.31631	1.08	6, 10	30-in.	14.2:	1.0
UY Pup	DN	S6909	2734.26171	1.95	5	30-in.	14.3	1.8
BF Eri	DN	S7182	2994.42655	0.75	5	40-in.	13.0:	2.0
BI Ori	DN	S6789	2693.26090	1.13	8	40-in.	14.4	0.9
		S6796	2694.28742	1.12	5	40-in.	13.0	2.0
		S6801	2695.25526	1.37	6	40-in.	14.9	1.1

Notes: t_{int} is the integration time; ':' denotes an uncertain value or classification; [a]average magnitude outside eclipse; [b]taken with a V filter.

Table B.1: Continued: Objects observed without detecting rapid oscillations. The final column gives the upper limit on the DNO or lpDNO amplitude (A_{max}) for each run.

Object	Type	Run No.	Start time HJD = 2450000+	Length (h)	t_{int} (s)	Telescope	V (mag)	A_{max} (mmag)
DH Aql	DN	S7089	2890.22673	2.38	5	40-in.	12.9	0.6
QW Ser	DN	S6804	2695.58983	3.23	5	40-in.	12.8	0.8
V342 Cen	DN	S6836	2704.39279	1.57	7	30-in.	16.1	4.0
V383 Vel	DN	S6777	2690.53696	1.18	5	40-in.	13.0	0.5
		S6782	2691.54269	1.15	5	40-in.	13.4	0.8
		S6787	2692.54585	0.78	5	40-in.	14.0	1.0
		S6792	2693.46955	0.93	6	40-in.	14.6	0.9
		S6798	2694.48711	1.47	5	40-in.	15.4	1.7
OQ Car	DN	S6835	2704.33117	1.40	6, 8	30-in.	16.5	4.0
		S6900	2732.24883	0.78	6	30-in.	14.4	2.5
		S6976	2790.20882	2.23	7	30-in.	15.5	2.0
V1830 Sgr	DN	S6904	2733.51213	1.65	6	30-in.	13.8[b]	1.2
QU Car	NL	S6770	2688.38264	0.82	6	40-in.	8.6[c]	0.8
		S6788	2692.59813	0.42	5	40-in.	9.4[c]	1.2
		S6799	2694.56189	0.83	4	40-in.	8.9[c]	1.2
		S6956	2784.19713	2.20	6	30-in.	13.5[b]	1.1
		S6961	2787.27951	1.45	6	30-in.	13.4[b]	1.3
BPM 18764	NL	S6669	2610.54415	1.42	7, 8	40-in.	15.4	1.1
AH Pic	NL	S6673	2626.37055	1.00	5	40-in.	13.9	1.0
V395 Hya	NL	S6960	2787.19176	1.45	6	30-in.	13.3:	1.3
V391 Hya	NL	S6764	2687.38601	1.12	6	40-in.	14.1	1.4
Lib3	NL	S6843	2705.50249	0.87	6, 8	30-in.	14.6	1.3
		S6857	2708.62310	0.75	6	30-in.	14.6	1.9
BO Cet	NL	S6658	2608.38854	1.55	6	40-in.	14.1	1.2
		S6662	2609.39585	1.70	6	40-in.	14.2	1.0
HQ Mon	NL	S6644	2603.49628	1.08	6	40-in.	12.6	0.7
		S6665	2609.57036	0.90	6	40-in.	13.0	0.8
		S6683	2628.42801	1.28	6	40-in.	13.4[b]	0.7
KQ Mon	NL	S6759	2686.38617	0.75	5	40-in.	13.5	1.4
		S6763	2687.34042	0.52	5	40-in.	12.7	3.3
V617 Sgr	NL	S6936	2778.57524	2.50	6	40-in.	13.6	0.8
V345 Pav	NL	S6958	2784.44833	1.93	6	30-in.	13.5[a]	0.7
RZ Gru	NL	S7008	2836.64062	1.48	5	40-in.	12.5[b]	0.6

Notes: t_{int} is the integration time; ':' denotes an uncertain value or classification; [a]average magnitude outside eclipse; [b]taken with a V filter; [c]U magnitude.

Table B.1: Continued: Objects observed without detecting rapid oscillations. The final column gives the upper limit on the DNO or lpDNO amplitude (A_{max}) for each run.

Object	Type	Run No.	Start time HJD = 2450000+	Length (h)	t_{int} (s)	Telescope	V (mag)	A_{max} (mmag)
WX Cen	NL	S6761	2686.53529	2.13	5	40-in.	14.5	1.1
		S6934	2778.37174	2.95	6	40-in.	12.9	0.5
		S6957	2784.36076	2.02	6	30-in.	13.4	0.7
UU Aqr	NL	S6946	2780.64052	1.23	6	30-in.	13.8	1.8
		S6955	2783.55860	0.73	6	30-in.	14.1:	2.4
		S7007	2836.57438	1.48	5, 6	40-in.	13.4	2.2
FBS 0107-082	NL:	S6690	2633.29252	0.95	5	74-in.	14.8	1.0
SW Sex	NL	S6645	2602.55674	1.47	6	40-in.	12.9	0.7

Notes: t_{int} is the integration time; ':' denotes an uncertain value or classification; [a]average magnitude outside eclipse; [b]taken with a V filter.

Table B.2: Objects that have been reported to have DNOs and/or QPOs, but for which I was unsuccessful in detecting any rapid oscillations. The last two columns give the upper limit on the DNO or lpDNO amplitude (A_{max}) in my light curves, and references to earlier DNO and/or QPO detections in each object.

Object	Type	Run No.	Start time HJD = 2450000+	Length (h)	t_{int} (s)	Telescope	V (mag)	A_{max} (mmag)	References
V2051 Oph	DN	S6767	2687.53032	2.57	6	40-in.	14.9[a]	2.6	1, 2
		S6771	2688.56846	1.28	6	40-in.	15.6:	3.1	
RR Pic	NL	S6678	2627.41940	1.56	6	40-in.	12.4[b]	1.6	3, 4
		S6684	2629.52022	2.02	5	40-in.	12.4[b]	1.4	
		S6860	2709.33419	1.82	6	30-in.	12.4	2.1	
HL Aqr	NL	S6642	2603.37524	0.40	6	40-in.	13.1	2.0	5
V442 Cen	DN	S6895	2731.28961	1.32	6	30-in.	12.3	1.0	6
		S6916	2773.24376	0.88	5	40-in.	15.3:	3.8	
		S6939	2779.24543	1.38	7	40-in.	15.8	1.7	
RW Sex	NL	S6769	2688.32907	0.62	5	40-in.	11.0[b]	0.7	7, 8
		S6840	2705.32508	0.27	6	30-in.	12.0[b]	2.1	
TV Crv	DN	S6917	2773.34211	1.87	5	40-in.	14.0	1.4	9
		S6922	2774.26121	1.43	6	40-in.	14.1	1.0	
V442 Oph	NL	S6794	2693.54299	0.77	4	40-in.	14.3	2.2	10
		S6800	2694.59949	0.88	5	40-in.	14.1	2.0	
		S7076	2885.21592	2.28	6	40-in.	13.8	1.1	
		S7079	2886.23713	1.13	6	40-in.	13.9	1.2	
TT Ari	NL	S6643	2603.41082	1.80	6	40-in.	10.9[b]	0.5	11 – 19
EX Hya	IP	S6981	2704.39279	1.78	6	30-in.	16.0	3.1	

Notes: t_{int} is the integration time; ':' denotes an uncertain value or classification; [a]average magnitude outside eclipse; [b]taken with a V filter.

References: (1) Steeghs et al. 2001; (2) Warner & O'Donoghue 1987; (3) Warner 1981; (4) Schoembs & Stolz 1981; (5) Haefner & Schoembs 1987; (6) Marino & Walker 1984; (7) Hesser, Lasker & Osmer 1972; (8) Córdova & Mason 1984; (9) Uemura et al. 2001; (10) Patterson et al. 2002; (11) Smak & Stepien 1969; (12) Mardirossian et al. 1979, 1980; (13) Sztajno 1979; (14) Jensen et al. 1983; (15) Semeniuk et al. 1987; (16) Udalski 1988; (17) Hollander & van Paradijs 1992; (18) Tremko et al. 1996; (19) Kraicheva et al. 1999.

References

Aznar Cuadrado R., Jordan S., Napiwotzki R., Schmid H.M., Solanki S.K., Mathys G., 2004, A&A, in press (astro-ph/0405308)

Bailey J., 1980, MNRAS, 190, 119

Balbus S.A., Hawley J.F., 1991, ApJ, 376, 214

Baptista R., Bortoletto A., 2004, AJ, 128, 411

Barrera L.H., Vogt N., 1989, A&A, 220, 99

Barret D., Olive J.-F., Kluzniak W., 2004, ApJL, submitted

Barrett P., O'Donoghue D., Warner B., 1988, MNRAS, 233, 759

Barwig H., Hunger K., Kudritzki R.P., Vogt N., 1982 A&A, 114, L11

Bateson F.M., 1979a, Publ. Var. Star Sect. R. Astron. Soc. New Zealand, 7, 5

Bateson F.M., 1979b, Publ. Var. Star Sect. R. Astron. Soc. New Zealand, 7, 29

Bateson F.M., 1979c, in Bateson F.M., Smak J., Urch I.H., eds, Proc. IAU Coll. 46, Changing Trends in Variable Star Research. p.89

Bateson F.M., 1982a, Publ. Var. Star Sect. R. Astron. Soc. New Zealand, 10, 12

Bateson F.M., 1982b, Publ. Var. Star Sect. R. Astron. Soc. New Zealand, 10, 24

Bateson F.M., 1998, Publ. Var. Star Sect. R. Astron. Soc. New Zealand, 23, 1

Bateson F.M., Dodson A.W., 1983, Publ. Var. Star Sect. R. Astron. Soc. New Zealand, 11, 1

Bateson F.M., Dodson A.W., 1984, Publ. Var. Star Sect. R. Astron. Soc. New Zealand, 12, 69

Bateson F.M., McIntosh R., 1986, Publ. Var. Star Sect. R. Astron. Soc. New Zealand, 14, 1

Bateson F.M., Jones A.F., McIntosh R., 1993, Publ. Var. Star Sect. R. Astron. Soc. New Zealand, 19, 39

Bath G.T., 1969, ApJ, 158, 571

Bath G.T., 1972, ApJ, 173, 121

Bath G.T., 1973, Nature Phys. Sci., 246, 84

Bath G.T., Evans W.D., Papaloizou J., 1974b, MNRAS, 167, 7P

Bath G.T., Evans W.D., Pringle J.E., 1974a, MNRAS, 166, 113

Bath G.T., Evans W.D., Papaloizou J., Pringle J.E., 1974c, MNRAS, 169, 447

Belloni T., Psaltis D., van der Klis M., 2002, ApJ, 572, 392

Bergeron P., Saffer R.A., Liebert J., 1992, ApJ, 394, 228

Bond H.E., Grauer A.D., Burnstein D., Marzke R.O., 1987, PASP, 99, 1097

Brault J.W., White O.R., 1971, A&A, 13, 169

Brickhill A.J., 1975, MNRAS, 170, 405

Bruch A., 1992, A&A, 266, 237

Bruch A., Engel A., 1994, A&AS, 104, 79

Bruch A., Steiner J.E., Gneiding C.D., 2000, PASP, 112, 237

Buckley D.A.H., Stobie R.S., 2001, in Clowes R.G., Adamson A.J., Bromage G.E., eds, The New Era of Wide Field Astronomy. ASP Conf. Ser., 232, Astron. Soc. Pac., San Francisco, p. 380

Buckley D.A.H., Sekiguchi K., Motch C., O'Donoghue D., Chen A.-L., Schwarzenberg-Czerney A., Pietsch W., Harrop-Allin M.K., 1995, MNRAS, 275, 1028

Buckley D.A.H., Haberl F., Motch C., Pollard K., Schwarzenberg-Czerney A., Sekiguchi K., 1997, MNRAS, 287, 117

Buckley D.A.H., Hearnshaw J.B., Nordsieck K.H., O'Donoghue D., 2003, in Guhathakurta P., ed, Discoveries and Research Prospects from 6- to 10-meter Class Telescopes II. Proc. *SPIE*4834, p. 264

Cannizzo J.K., 1993, ApJ, 419, 318

Cannizzo J.K., Gosh P., Wheeler J.C., 1982, ApJ, 260, L83

Carrol B.W., Cabot W., McDermott P.N., Savedoff M.P., Van Horn H.M., 1985, ApJ, 296, 529

Chanan G.A., Nelson J.E., Margon B., 1978, ApJ, 226, 963

Chanmugam G., 1972, Nature Phys. Sci., 236, 83

Cheng F.H., Sion E.M., Horne K., Hubeny I., Huang M., Vrtilek S.D., 1997, AJ, 114, 1165

Chester T.J., 1979, ApJ, 230, 167

Collins T.J.B., Helfer H.L., van Horn H.M., 2000a, ApJ, 534, 934

Collins T.J.B., Helfer H.L., van Horn H.M., 2000b, ApJ, 534, 944

Córdova F.A., 1979, in van Horn H.M., Weidemann V., eds., Proc. IAU Coll. 53, White Dwarfs and Variable Degenerate Stars. University of Rochester, Rochester, p. 398

Córdova F.A., Mason K.O., 1982, in Cox J.P., Hansen C.J., eds, Pulsations in Classical and Cataclysmic Variable Stars. p. 23

Córdova F.A., Mason K.O., 1984, MNRAS, 206, 879

Córdova F.A., Chester T.J., Tuohy I.R., Garmire G.P., 1980, ApJ, 235, 163

Córdova F.A., Chester T.J., Mason K.O., Kahn S.M., Garmire G.P., 1984, ApJ, 278, 739

Cox J.P., 1981, ApJ, 247, 1070

Cox J.P., Everson B.L., 1982, in Cox J.P., Hansen C.J., eds, Pulsations in Classical and Cataclysmic Variable Stars. p. 42

Cox J.P., Everson B.L., 1983, ApJS, 52, 451

Cropper M.S., 1986, MNRAS, 222, 225

Deeming T.J., 1975, Ap&SS, 36, 137

Dhillon V.S., Jones D.H.P., Marsh T.R., Smith R.C., 1992, MNRAS, 258, 225

Dotani T., Mitsuda K., Inoue H., Tanaka Y., Kawai K., Tawara Y., Makishima K., van Paradijs J., Penninx W., van der Klis M., Tan J., Lewin W.H.G., 1990, ApJ, 350, 395

Downes R.A., Webbink R.F., Shara M.M., Ritter H., Kolb U., 2001, PASP, 113, 764

Durisen R.H., 1973, ApJ, 183, 215

Echevarría J., Costero R., Michel R., 1993, A&A, 275, 201

Edwards C.H., Penney D.E., 2000, Elementary Differential Equations. Prentis Hall, Upper Saddle River

Elsner R.F., Lamb F.K., 1977, ApJ, 215, 897

Elvius A., 1975, A&A, 44, 117

Eracleous M., Patterson J., Halpern J., 1991, ApJ, 370, 330

Faulkner J., Flannery B.P., Warner B., 1972, ApJ, 175, L79

Flannery B.P., 1975, MNRAS, 170, 325

Frank J., King A.R., Raine D.J., 1985, Accretion Power in Astrophysics. Cambridge Univ. Press, Cambridge

Fu H., Li Z.-Y., Leung K.-C., Zhang Z.-S., Li Z.-L., Gaskell C.M., 2004, Chinese Journal of Astronomy & Astrophysics, 4, 88

Ghosh P., Lamb F.K., 1978, ApJ, 223, L83

Ghosh P., Lamb F.K., 1979a, ApJ, 232, 259

Ghosh P., Lamb F.K., 1979b, ApJ, 234, 296

Godon P., Livio M., Lubow S., 1998, MNRAS, 295, L11

Godon P., Sion E.M., Cheng F.-H., Szkody P., Long K.S., Froning C.S., 2004, ApJ, in press (astro-ph/0405263)

Goodson A.P., Winglee R.M., 1999, ApJ, 524, 159

Goodson A.P., Böhm K.-H., Winglee R.M., 1999, ApJ, 524, 159

Groot J.P., Rutten R.G.M., van Paradijs J., 2001, A&A, 368, 183

Haefner R., Schoembs R., 1987, MNRAS, 224, 231

Haefner R., Schoembs R., Vogt N., 1977, A&A, 61, L38

Haefner R., Schoembs R., Vogt N., 1979, A&A, 77, 7

Hameury J.-M., Lasota J.-P., 2002, A&A, 394, 231

Hamuy M., Maza J., 1986, IBVS, 2867

Harvey D., Skillman D.R., Patterson J., Ringwald F.A., 1995, PASP, 107, 551

Hassall B.J.M., Pringle J.E., Schwarzenberg-Czerny A., Wade R.A., Whelan J.A.J., Hill P.W., 1983, MNRAS, 203, 865

Hellier C., 2000, New Astronomy Rev., 44, 131

Hellier C., 2001a, PASP, 113, 469

Hellier C., 2001b, Cataclysmic Variable Stars: How and why they vary. Springer-Praxis, Chichester

Hellier C., 2004, in Tovmassian G., Sion E.M., eds, Proc. IAU Coll. 194, Compact Binaries in the Galaxy and Beyond. in press (astro-ph/0402103)

Hellier C., Harmer S., Beardmore A.P., 2004, MNRAS, 349, 710

Hellier C., Mukai K., Beardmore A.P., 1997, MNRAS, 292, 397

Hellier C., O'Donoghue D., Buckley D., Norton A., 1990, MNRAS, 242, 32P

Herbst W., Hesser J.E., Ostriker J.P., 1974, ApJ, 193, 679

Hesser J.E., Lasker B.M., Osmer P.S., 1972, ApJ, 176, L31

Hesser J.E., Lasker B.M., Osmer P.S., 1974, ApJ, 189, 315

Hessman F.V., 1988, ApJS, 72, 515

Hessman F.V., Hopp U., 1990, A&A, 228, 387

Hessman F.V., Mantel K.-H., Barwig H., Schoembs R., 1992, A&A, 263, 147

Hildebrand R.H., Spillar E.J., Steining R.F., 1981a, ApJ, 243, 223

Hildebrand R.H., Spillar E.J., Steining R.F., 1981b, ApJ, 248, 268

Hildebrand R.H., Spillar E.J., Middleditch J., Patterson J.J., Stiening R.F., 1980, ApJ, 238, L145

Hirose M., Osaki Y., 1990, PASJ, 42, 135

Hoard D.W., Thorstensen J.R., Szkody P., 2000, ApJ, 539, 936

Hoard D.W., Szkody P., Froning C.S., Long K.S., Knigge C., 2003, AJ, 126, 2473

Hollander A., van Paradijs J., 1992, A&A, 265, 77

Homer L., Szkody P., Raymond J.C., Fried R.E., Hoard D.W., Hawley S.L., Wolfe M.A., Tramposch J.N., Yirak K.T., 2004, ApJ, 610, 991

Honeycutt R.K., Robertson J.W., Turner G.W., Mattei J.A., 1998, PASP, 110, 676

Horne J.H., Buliunas S.L., 1986, ApJ, 302, 757

Horne K., 1999, in Hellier C., Mukai K., eds, ASP Conf. Ser. Vol. 157, Annapolis Workshop on Magnetic Cataclysmic Variables. Astron. Soc. Pac., San Francisco, p. 349

Horne K., Gomer R., 1980, ApJ, 237, 845

Hoshi R., 1979, Progress of Theoretical Physics, 61, 1307

Huang M., Sion E.M., Hubeney I., Cheng F.H., Szkody P., 1996, ApJ, 458, 355

Ivanova N., Taam R.E., 2003, ApJ, 599, 516

Jablonski F.J., Cieslinski D., 1992, A&A, 259, 198

Jensen K.A., Córdova F.A., Middleditch J., Mason K.O., Grauer A.D., Horne K., Gomer R., 1983, ApJ, 270, 211

Jones M.H., Watson M.G., 1992, MNRAS, 257, 633

Kato S., 1978, MNRAS, 185, 629

Kato T., 2002, PASJ, 54, 87

Kato T., Nogami D., 1997, PASJ, 49, 481

Kato T., Hirata R., Mineshige S., 1992, PASJ, 44, L215

Kato T., Matsumoto K., Uemura M., 2002, IBVS, 5262

Kato T., Santallo R., Bolt G., Richards T., Nelson P., Monard B., Uemura M., Kiyota S., Stubbings R., Pearce A., Watanabe T., Schmeer P., Yamaoka H., 2003, MNRAS, 339, 861

Katz J.I., 1975, ApJ, 200, 298

Kemp J.C., Swedlund J.B., Wolstencroft R.D., 1974, ApJ, 193, L15

Kim S.-W., Wheeler J.C., Mineshige S., 1992, ApJ, 384, 269

King A.R., 1985, Nature, 313, 291

Kley W., 1991, A&A, 247, 95

Knigge C., Drake N., Long K.S., Wade R.A., Horne K., Baptista R., 1998, ApJ, 499, 429

Knigge C., Long K.S., Hoard D.W., Szkody P., Dhillon V.S., 2000, ApJ, 539, L49

Kobulnicky H.A., Nordsieck K.H., Burgh E.B., Smith M.P., Percival J.W., Williams T.B., O'Donoghue D., 2003, in Iye M., Moorwood A.F., eds, Instrument Design and Performance for Optical/Infrared Ground-based Telescopes. Proc. *SPIE*4841, p. 1634

Koen M.C., 1976, M.Sc. thesis, University of Cape Town

Kraicheva Z., Stanishev V., Genkov V., Illiev L., 1999, A&A, 351, 607

Krzeminski W., 1965, ApJ, 142, 1051

Kuijpers J., Pringle J.E., 1982, A&A, 114, L4

Kurtz D.W., 1985, MNRAS, 213, 773

Kuulkers E., Hollander A., Oosterbroek T., van Paradijs J., 1991, A&A, 242, 401

Lamb D.Q., 1974, ApJ, 192, L129

Lamb D.Q., 1988, in Coyne et al., eds, Polarized Radiation of Circumstellar Origin. Vatican Observatory, Vatican p. 151

Lamb F.K., Aly J.-J., Cook M.C., Lamb D.Q., 1983, ApJ, 274, L71

Lamb F.K., Shibazaki N., Alpar M.A., Shaham J., 1985, Nature, 317, 681

Langer S.H., Chanmugam G., Shaviv G., 1981, ApJ, 245, L23

Lasota J.-P., 2004, in Tovmassian G., Sion E.M., eds, Compact Binaries in the Galaxy and Beyond. in press (astro-ph/0402190)

Livio M., 1993, in Wheeler J.C., ed, Accretion Discs in Compact Stellar Systems. Advanced Series in Astophysics and Cosmology, Vol. 9, World Sci. Publ., Singapore p. 243

Livio M., Pringle J.E., 1992, MNRAS, 259, 23P

Long K.S., Blair W.P., Bowers C.W., Davidsen A.F., Kriss G.A., Sion E.M., Hubeny I., 1993, ApJ, 405, 327

Loumos G.L., Deeming T.J., 1978, Ap&SS, 56, 285

Lubow S.H., Pringle J.E., 1993, ApJ, 409, 360

Lynden-Bell D., 1969, Nature, 223, 690

Lynden-Bell D., Pringle J.E., 1974, MNRAS, 163, 603

Mantel K.H., Marschhäusser H., Schoembs R., Haefner R., La Dous C., 1988, A&A, 193, 101

Mardirossian F., Mezzetti M., Pucillo M., Santin P., Sedmak G., Cester B., Giuricin G., 1979, IBVS, 1622

Mardirossian F., Mezzetti M., Pucillo M., Santin P., Sedmak G., Giuricin G., 1980, A&A, 85, 29

Marino B.F., Walker W.S.G., 1984, South. Stars, 30, 389

Marsh T.R., Horne K., 1998, MNRAS, 299, 921

Mauche C.W., 1996, ApJ, 463, L87

Mauche C.W., 1997a, ApJ, 476, L85

Mauche C.W., 1997b, in Wickramasinghe D.T., Bicknell G.V., Ferrario L., eds, Proc. IAU Coll. 163, Accretion Phenomena and Related Outflows. Astron. Soc. Pac., San Francisco, p. 251

Mauche C.W., 2002, ApJ, 580, 423

Mauche C.W., Robinson E.L., 2001, ApJ, 562, 508

Mauche C.W., Mattei J., Bateson F., 2001, in Podsiadlowski P. et al., eds, Evolution of Binary & Multiple Star Systems. Bormio, Italy

Mazeh T., Tal Y., Shaviv G., Bruch A., Budell R., 1985, A&A, 149, 470

McDermott P.N., Taam R.E., 1989, ApJ, 342, 1019

Mennickent R.E., 1995, A&A, 294, 126

Mennickent R.E., Sterken C., 1998, PASP, 110, 1032

Meyer F., Meyer-Hofmeister E., 1981, A&A, 104, L10

Middleditch J., 1982, ApJ, 257, L71

Middleditch J., Córdova F., 1982, ApJ, 255, 585

Mineshige S., Osaki Y., 1985, PASJ, 37, 1

Morales-Rueda L., Marsh T.R., Billington I., 2000, MNRAS, 313, 454

Morales-Rueda L., Still M.D., Roche P., 1999, MNRAS, 306, 753

Mumford G.S., 1966, ApJ, 46, 411

Mumford G.S., 1967, PASP, 79, 283

Muno M.P., Chakrabarty D., Galloway D.K., 2002, ApJ, 580, 1048

Murray J.R., 1996, MNRAS, 279, 402

Murray J.R., Warner B., Wickramasinghe D.T., 2000, MNRAS, 315, 707

Nather R.E., Robinson E.L., 1974, ApJ, 190, 637

Nather R.E., Warner B., 1971, MNRAS, 152, 209

Nevo I., Sadeh D., 1976, MNRAS, 177, 167

Nevo I., Sadeh D., 1978, MNRAS, 182, 595

Nogami D., Kato T., Masuda S., Hirata R., 1995, IBVS, 4155

North R.C., Marsh T.R., Moran C.K.J., Kolb U., Smith R.C., Stehle R., 2000, MNRAS, 313, 383

Norton A.J., Watson M.G., 1989, MNRAS, 237, 853

Nousek J.A., Baluta C.J., Corbet R.H.D., Mukai K., Osborne J.P., Ishida M., 1994, ApJ, 436, L19

O'Donoghue D., 1987, Ap&SS, 136, 247

O'Donoghue D., 1995, Baltic Astron., 4, 519

O'Donoghue D., Kilkenny D., 1989, MNRAS, 236, 319

O'Donoghue D., Soltynski M.G., 1992, MNRAS, 254, 9

O'Donoghue D., Menzies J.W., Hill P.W., 1987, MNRAS, 227, 347

O'Donoghue D., Wargau W., Warner B., Kilkenny D., Martinez P., Kanaan A., Kepler S.O., Henry G., Winget D.E., Clemens J.C., Grauer A.D., 1990, MNRAS, 245, 140

Olive J.-F., Barret D., Kluzniak W., 2004, in Combes F., Barret D., Contini T., Meynadier F., Pagani L., eds, EdP-Sciences, Conference Series, p. 63

Osaki Y., 1974, PASJ, 26, 429

Osaki Y., 1989, PASJ, 41, 1005

Osaki Y., 1996, PASP, 108, 39

Osaki Y., Hansen C.J., 1974, ApJ, 185, 277

Osaki Y., Hirose M., Ichikawa S., 1993, in Wheeler J.C., ed, Accretion Discs in Compact Stellar Systems. Advanced Series in Astophysics and Cosmology, Vol. 9, World Sci. Publ. Singapore p. 272

Paczynski B., 1977, ApJ, 216, 822

Paczynski B., 1978, in Zytkow A., ed, Nonstationary Evolution of Close Binaries. Polish Scientific Publ., Warsaw, p. 89

Pandel D., Córdova F.A., Howell S.B., 2003, MNRAS, 346, 1231

Papadaki C., Boffin H.M.J., Cuypers J., Stanishev V., 2004, in Hilditch R.W., Hensberge H., Pavlovski K., eds, ASP Conf. Ser., Spectroscopically and Spatially Resolving the Components of Close Binary Stars. Astron. Soc. Pac., San Francisco, in press (astro-ph/0312477)

Papaloizou J.C., Pringle J.E., 1978, MNRAS, 182, 423

Papaloizou J.C., Pringle J.E., 1980, MNRAS, 190, 43

Papaloizou J.C.B., Stanley G.Q.G., 1986, MNRAS, 220, 593

Parker E.N., 1970, in Habing H.J., ed, Interstellar Gas Dynamics. Reidel, Dordrecht, p. 168

Patterson, J., 1978, ApJ, 219, 168

Patterson, J., 1979a, ApJ, 233, L13

Patterson, J., 1979b, ApJ, 234, 978

Patterson, J., 1980, ApJ, 241, 235

Patterson, J., 1981, ApJS, 45, 517

Patterson, J., 1984, ApJS, 54, 443

Patterson, J., 1991, PASP, 103, 1149

Patterson, J., 1994, PASP, 106, 209

Patterson, J., 1999, in Mineshige S., Wheeler J.C., eds, Frontiers Science Series 26, Disk Instabilities in Close Binary Systems. Universal Academy Press, Tokyo, p. 61

Patterson, J., Raymond J.C., 1985, ApJ, 292, 535

Patterson J., Richman H., Kemp J., 1998, PASP, 110, 403

Patterson J., Robinson E.L., Kiplinger A.L., 1978a, ApJ, 226, L137

Patterson J., Robinson E.L., Nather R.E., 1977, ApJ, 214, 144

Patterson J., Robinson E.L., Nather R.E., 1978b, ApJ, 224, 570

Patterson J., Robinson E.L., Nather R.E., Handler F., 1979, ApJ, 232, 819

Patterson J., Sterner E., Halpern J.P., Raymond J.C., 1992, ApJ, 384, 234

Patterson J., Jablonski F., Koen C., O'Donoghue D., Skillman D.R., 1995, PASP, 107, 1183

Patterson J., Kemp J., Shambrook A., Thomas E., Halpern J.P., Skillman D.R., Harvey D.A., Vanmunster T., Retter A., Fried R., Buckley D.A.H., Nogami D., Kato T., Baba H., 1997, PASP, 109, 1100

Patterson J., Walker S., Kemp J., O'Donoghue D., Bos M., Stubbings R., 2000, PASP, 112, 625

Patterson J., Fenton W.H., Thorstensen J.R., Harvey D.A., Skillman D.R., Fried R.E., Monard B., O'Donoghue D., Beshore E., Martin B., Niarchos P., Vanmunster T., Foote J., Bolt G., Rea R., Cook L.M., Butterworth N., Wood M., 2002, PASP, 114, 1364

Penning W.R., Schmidt G.D., Liebert J.E., 1986, ApJ, 301, 885

Petterson J.A., 1979, in Van Horn H.M., Weidemann V., eds., Proc. IAU Coll. 53, White Dwarfs and Variable Degenerate Stars. University of Rochester, Rochester, p. 412

Petterson J.A., 1980, ApJ, 241, 247

Pojmanski G., 1986, Acta Astronomica, 36, 69

Ponman T.J., Belloni T., Duck S.R., Verbunt F., Watson M.G., Wheatley P.J., Pfeffermann E., 1995, MNRAS, 276, 495

Popham R., 1999, MNRAS, 308, 979

Pringle J.E., 1977, MNRAS, 178, 195

Pringle J.E., 1981, ARA&A, 19, 137

Pringle J.E., Savonije G.J., 1979, MNRAS, 187, 777P

Provencal J.L., Winget R.E., Nather J.C., Clemens J.C., Hine B.P., Henry G., Kepler S.O., Vauclair G., Chevreton M., O'Donoghue D., Warner B., Grauer D.A., Ferrario L., 1991, in Vauclair G., Sion E., eds, White Dwarfs. Kluwer, Dordrecht, p. 449

Psaltis D., Belloni T., van der Klis M., 1999, ApJ, 520, 262

Ramsay G., Poole T., Mason K., Córdova F., Priedhorsky W., Breeveld A., Much R., Osborne J., Pandel D., Potter S., West J., Weatley P., 2001, A&A, 365, L288

Rappaport S., Joss P.C., Verbunt F., 1983, ApJ, 275, 713

Remillard R.A., Bradt H.V., Brissenden R.J.V., Buckley D.A.H., Schwartz D.A., Silber A., Stroozas B.A., Tuohy I.R., 1994, ApJ, 428, 785

Remillard R.A., Muno M.P., McClintock J.E., Orosz J.A., 2002, ApJ, 580, 1030

Ringwald F.A., 1994, MNRAS, 270, 804

Ringwald F.A., Thorstensen J.R., Hamwey R.M., 1994, MNRAS, 271, 323

Ringwald F.A., Thorstensen J.R., Honeycutt R. K., Smith R.C., 1996, AJ, 111, 2077

Robertson J.W., Honeycutt R.K., Turner G.W., 1995, PASP, 107, 443

Robertson S.L., Leiter D.J., 2002, ApJ, 565, 447

Robertson S.L., Leiter D.J., 2003, ApJ, 596, L203

Robertson S.L., Leiter D.J., 2004, MNRAS, 350, 1319

Robinson E.L., 1973a, ApJ, 180, 121

Robinson E.L., 1973b, ApJ, 183, 193

Robinson E.L., 1974, ApJ, 193, 191

Robinson E.L., 1976, ARA&A, 14, 119

Robinson E.L., Nather R.E., 1979, ApJS, 39, 461

Robinson E.L., Warner B., 1984, ApJ, 277, 250

Robinson E.L., Barker E.S., Cochran A.L., Cochran W.D., Nather R.E., 1981, ApJ, 251, 611

Robinson E.L., Shafter A.W., Hill J.A., Wood M.A., 1987, ApJ, 313, 772

Rodríguez-Gil P., Martinez-Pias I.G., 2002, MNRAS, 337, 209

Rodríguez-Gil P., Potter S.B., 2003, MNRAS, 342, L1

Rodríguez-Gil P., Casares J., Martínez-Pais I.G., Hakala P., Steegs D., 2001, ApJ, 548, L49

Rodríguez-Gil P., Casares J., Martínez-Pais I.G., Hakala P., 2002, in Gänsicke B.T., Beuermann K., Reinsch K., eds, ASP Conf. Ser. Vol. 261, The Physics of Cataclysmic Variables and Related Objects. Astron. Soc. Pac., San Francisco, p. 533

Rolfe J.D., Haswell C.A., Patterson J., 2001, MNRAS, 324, 529

Romanova M.M., Ustyugova G.V., Koldoba A.V., Wick J.V., Lovelace R.V.E., 2003, ApJ, 595, 1009

Romanova M.M., Ustyugova G.V., Koldoba A.V., Lovelace R.V.E., 2004, ApJ, 610, 920

Rosen S.R., Clayton K.L., Osborne J.P., McGale P.A., 1994, MNRAS, 269, 913

Ryu D., Goodman J., 1992, ApJ, 388, 438

Sawada K., Matsuda T., Hachisu I., 1986, MNRAS, 224, 307

Scargle J.D., 1981, ApJS, 45, 1

Schecter P., Mateo M., Saha A., 1993, PASP, 105, 1342

Schoembs R., 1977, in Kippenhahn R., Rahe J., Strohmeier W., eds, Proc. IAU Coll. 42, The Interaction of Variable Stars with their Environment. Schadel Druck, Bamberg, p. 218

Schoembs R., 1982a, IBVS, 2116

Schoembs R., 1982b, A&A, 115, 190

Schoembs R., 1986, A&A, 158, 233

Schoembs R., Stolz B., 1981, IBVS, 1986

Schoembs R., Vogt N., 1980, A&A, 91, 25

Schoembs R., Vogt N., 1981, A&A, 97, 185

Schreiber M.R., Hameury J.-M., Lasota J.-P., 2004, A&A, in press (astro-ph/0408179)

Semeniuk I., Schwarzenberg-Czherny A., Duerbeck H., Hoffmann M., Smak J., Stepien K., Tremko J., 1987, Acta Astronomica, 37, 197

Shafter A.W., 1983, IBVS, 2377

Shafter A.W., Harkness R.P., 1986, AJ, 92, 658

Shakura N.I., Sunyaev R.A., 1973, A&A, 24, 337

Sion E.M., Urban J., 2002, ApJ, 572, 456

Sion E.M., Cheng F.-H., Huang M., Hubeny I., Szkody P., 1996, ApJ 471, L41

Skillman D.R., Patterson J., Kemp J., Harvey D.A., Fried R.E., Retter A., Lipkin Y., Vanmunster T., 1999, PASP, 111, 1281

Smak J., 1967, Acta Astronomica, 17, 255

Smak J., 1971, Acta Astronomica, 21, 15

Smak J., 1987, Ap&SS, 131, 479

Smak J., 1989, Acta Astronomica, 39, 217

Smak J.I., 2001, Acta Astronomica, 51, 295

Smak J., Stepien K., 1969, Commun. Konkoly Obs., 65, 355

Spruit H.C., Ritter H., 1983, A&A, 124, 267

Spruit H.C., Taam R.E., 1993, ApJ, 402, 593

Steeghs D., Harlaftis E.T., Horne K., 1997, MNRAS, 290, L28

Steeghs D., O'Brien K.O., Horne K., Gomer R., Oke J.B., 2001, MNRAS, 323, 484

Stiening R.F., Dragovan M., Hildebrand R.H., 1982, PASP, 94, 672

Stiening R.F., Hildebrand R.H., Spillar E.J., 1979, PASP, 91, 384

Stockman H.S., Berriman G., Liebert J., Moore R.L., Whickramasinghe D.T., 1992, ApJ, 401, 628

Stolz B., Schoembs R., 1981, IBVS, 1955

Stolz B., Schoembs R., 1984, A&A, 132, 187

Stover R.J., 1981, ApJ, 249, 673

Stover R.J., Robinson E.L., Nather R.E., 1981, ApJ, 248, 696

Swank J.H., 1979, in van Horn H.M., Weidemann V., eds., Proc. IAU Coll. 53, White Dwarfs and Variable Degenerate Stars. University of Rochester, Rochester, p. 135

Swedlund J.B., Kemp J.C., Wolstencroft R.D., 1974, ApJ, 193, L11

Szkody P., 1976, ApJ, 207, 190

Szkody P., 1986, ApJ, 301, L29

Szkody P., 1987, ApJS, 63, 685

Szkody P., Mattei J.A., 1984, PASP, 96, 988

Szkody P., Kii T., Osaki Y., 1990, AJ, 100, 546

Szkody P., Hoard D.W., Sion E.M., Howell S.B., Cheng F.H., Sparks W.M., 1998, ApJ, 497, 928

Sztajno M., 1979, IBVS, 1710

Tajima T., Gilden D., 1987, ApJ, 320, 741

Tassoul J.-P., 1988, ApJ, 324, L71

Thorstensen J.R., 1997, PASP, 109, 1241

Thorstensen J.R., Fenton W.H., 2003, PASP, 115, 37

Thorstensen J.R., Ringwald F.A., Wade R.A., Schmidt G.D., Nosworthy J.E., 1991, AJ, 102, 272

Thorstensen J.R., Taylor C.J., Becker C.M., Remillard R.A., 1997, PASP, 109, 477

Tout C.A., Pringle J.E., 1992a, MNRAS, 256, 269

Tout C.A., Pringle J.E., 1992b, MNRAS, 259, 604

Tremko J., Andronov I.L., Chinarova L.L., Kumsiashivili M.I., Luthardt R., Pajdosz G., Patkos L., Roessiger S., Zola S., 1996, A&A, 312, 121

Tylenda R., 1981, Acta Astronomica, 31, 276

Udalski A., 1988, Acta Astronomica., 38, 315

Uemura M. et al., 2001, vsnet-campain, 786

Uzdensky D.A., 2002, ApJ, 572, 432

Uzdensky D.A., Königl A., Litwin C., 2002, ApJ, 565, 1208

van der Klis M., 2000, ARA&A, 38, 717

van der Woerd H., Heise J., Paerels F., Beuermann K., van der Klis M., Motch C., van Paradijs J., 1987, A&A, 182, 219

van Horn H.M., Wesemael F., Winget D.E., 1980, ApJ, 235, L143

van Teeseling A., 1997, A&A, 324, L73

Vogt N., 1974, A&A, 36, 369

Vogt N., 1979, IAU Circ. No. 3357

Vogt N., 1982, ApJ, 252, 653

Vogt N., 1983, A&A, 118, 95

Vogt N., Bateson F.M., 1982, A&AS, 48, 383

Vogt N., Schoembs R., Krzeminski W., Pedersen H., 1981, A&A, 94, L29

Wade R.A., Ward M.J., 1985, in Pringle J.E., Wade R.A., eds, Interacting Binary Stars. Cambridge Univ. Press, Cambridge, p. 129

Walker M.F., 1956, ApJ, 123, 68

Walker M.F., 1957, Proc. IAU Symp. 3, p. 46

Wang Y.-M., 1996, ApJ, 465, L111

Warner B., 1973, MNRAS, 163, 25P

Warner B., 1974, MNRAS, 168, 235

Warner B., 1975a, MNRAS, 170, 219

Warner B., 1975b, MNRAS, 173, 37P

Warner B., 1976, in Eggleton P., Mitton S., Whelan J., eds, Proc. IAU Symp. 73, Structure and Evolution of Close Binary Systems. Reidel, Dordrecht, p. 85

Warner B., 1981, MNRAS, 195, 101

Warner B., 1983, in Livio M., Shaviv G., eds, Proc. IAU Coll. 72, Cataclysmic Variables and Related Objects. Reidel, p. 155

Warner B., 1986, MNRAS, 219, 347

Warner B., 1987a, MNRAS, 227, 23

Warner B., 1987b, in Cox A.N., Sparks W.M., Starrfield S.G., eds, Lecture Notes in Physics 274, Springer-Verlag, p. 384

Warner B., 1987c, MNRAS, 227, 23

Warner B., 1988, High Speed Astronomical Photometry. Cambridge Univ. Press, Cambridge

Warner B., 1995a, Cataclysmic Variable Stars. Cambridge Univ. Press, Cambridge

Warner B., 1995b, in Buckley D.A.H., Warner B., eds, ASP Conf. Ser. Vol. 85, Cape Workshop on Magnetic Cataclysmic Variables. Astron. Soc. Pac., San Francisco, p. 343

Warner B., 1995c, Ap&SS, 225, 249

Warner B., 1997, Ap&SS, 241, 263

Warner B., 2004, PASP, 116, 115 (W04)

Warner B., Brickhill A.J., 1974, MNRAS, 166, 673

Warner B., Brickhill A.J., 1978, MNRAS, 182, 777

Warner B., Harwood J.M., 1973, IBVS, 756

Warner B., Nather R.E., 1971, MNRAS, 152, 219

Warner B., Nather R.E., 1972, MNRAS, 159, 429

Warner B., Nather R.E., 1988, IBVS, 3140

Warner B., O'Donoghue D., 1987, MNRAS, 224, 733

Warner B., Robinson E.L., 1972a, Nature Phys. Sci., 239, 2

Warner B., Robinson E.L., 1972b, MNRAS, 159, 101

Warner B., van Citters G.W., 1974, Observatory, 94, 116

Warner B., Woudt P.A., 2002, MNRAS, 335, 84 (WW02b)

Warner B., Woudt P.A., 2004, in Hamuery J.-M., Lasota J.-P., eds, The Astrophysics of Cataclysmic Variables and Related Objects. ASP Conf. Ser., Astron. Soc. Pac., San Francisco, in preparation

Warner B., O'Donoghue D., Allen S., 1985, MNRAS, 212, 9P

Warner B., O'Donoghue D., Wargau W., 1989, MNRAS, 238, 73

Warner B., Woudt P.A., Pretorius M.L., 2003, MNRAS, 344, 1193 (WWP03)

Warner B., Peters W.L., Hubbard W.B., Nather R.E., 1972, MNRAS, 159, 321

Welsh F.W., Sion E.M., Godon P., Gänsicke B.T., Knigge C., Long K.S., Szkody P., 2003, ApJ, 599, 509

Wheatley P.J., West R.G., 2003, MNRAS, 345, 1009

Wheatley P.J., Mauche C.W., Mattei J.A., 2003, MNRAS, 345, 49

Wheatley P.J., Verbunt F., Belloni T., Watson M.G., Naylor T., Ishida M., Duck S.R., Pfeffermann E., 1996, A&A, 307, 137

White N.E., Marshall F.E., 1981, ApJ, 249, L25

Whitehurst R., 1988a, MNRAS, 232, 35

Whitehurst R., 1988b, MNRAS, 233, 529

Wickramasinghe D.T., Wu K., 1994, Ap&SS, 211, 61

Wickramasinghe D.T., Wu K., Ferrario L., 1991, MNRAS, 249, 460

Williams G.A., Hiltner W.A., 1984, MNRAS, 211, 629

Wood M.A., Winget D.E., Nather R.E., Hessman F.V., Liebert J., Kurtz D.W., Wesemael F., Wegner G., 1987, ApJ, 313, 757

Woudt P.A., Warner B., 2002a, MNRAS, 333, 411 (WW02a)

Woudt P.A., Warner B., 2002b, MNRAS, 335, 44

Woudt P.A., Warner B., 2003, MNRAS, 340, 1011

Wu K., Wickramasinghe D.T., Warner B., 1995a, PASA, 12, 60

Wu K., Wickramasinghe D.T., Warner B., 1995b, in Bianchini A., della Valle M., Orio M., eds, Cataclysmic Variables. Kluwer, Dordrecht, p. 315

Wynn G.A., King A.R., Horne K., 1997, MNRAS, 286, 436

Zhang E., Robinson E.L., Stiening R.F., Horne K., 1995, ApJ, 454, 447